SAINT-PETERSBURG UNIVERSITY

Nefedov Denis Yurievich

NMR of Ca-In and Ga-In-Sn alloys under nanoconfinement

Scientific specialty
1.3.8. Condensed matter physics

Dissertation for the degree of
Candidate of Physical and Mathematical Sciences

Translation from Russian

Scientific advisor:
Doctor of Physico-mathematical Sciences, Professor
Charnaya Elena Vladimirovna

Saint Petersburg - 2024

Contents

Introduction

The study of nanocomposite materials is one of the priority areas of research in modern condensed matter physics. Interest in nanocomposites is due to the growing use of these materials in microelectronics, biotechnology, engineering, optics, electrochemistry, and many other areas of science and technology [1; 2]. Nanocomposite materials are characterized by a number of new properties and advantages compared to their macrocomposite counterparts [1], which is primarily due to the occurrence of dimensional effects and the large surface area of the components. Therefore, nanocomposites are becoming increasingly popular in the creation of mechanically reinforced lightweight structures, various sensors, nanocontacts, multicomponent electronics and other functional materials. A special place is occupied by nanostructured materials in the elements and devices of information technology, the efficiency and speed of which is achieved, among other things, due to a significant reduction in size. In view of the need to meet the growing demands of modern applied science, the study of the physical properties of nanostructured substances, as well as the study of nanocomposites themselves as a separate type of materials, is an urgent and important task.

In particular, considerable attention is paid to nanocomposites based on porous matrices, into which solids and liquids, such as ferroelectrics, semiconductors, organic liquids, ferromagnets, metals and metal alloys, are introduced [3; 4; 5; 6; 7]. At the same time, the central issue of nanocomposite physics is the identification of changes in the properties of substances under nanoconfinement conditions compared to the bulk case. Recently, there has been a significant increase in the number of studies of nanoporous matrices with various fillers [8].

The transition of the particle sizes of the substance under study to the nanoscale can be manifested in the displacement and blurring of the temperatures of the phase transitions, in the change in the sequence and types of phase transitions, in the appearance of new phase transformations that are not present in the bulk case, in the formation of new crystalline modifications of the substance under study that are absent in the volume. Nanoconfinement also affects atomic mobility in both the liquid and crystalline phases, which entails changes in the rate of diffusion processes.

At the forefront of modern applied physics and technology is the development and use of micro- and nanoelectronic devices, the element base of which includes nanostructured metal alloys in liquid and solid states. The ultra modern application of metal nanostructures in this field includes the creation of flexible and deformable electronic elements, wearable electronics, flexible displays, self-healing electrical circuits, biocompatible robotics, etc. [9; 10]. Liquid gallium-containing alloys are considered promising substances for creating flexible contacts [11]. Liquid metal nanoparticles injected into the elastomer serve as triboelectric nanogenerators for wearable electronics [12]. For use in microelectronics, in communication systems, in devices for transmitting and storing information, a va-

riety of metal-organic systems are being actively developed, which are nanocomposites based on metals and polymers. Metal nanoparticles are used to create non-volatile memory [13; 14], which are also used for plasmon memory [15], and when introduced into porous matrices – for the manufacture of sensors in biology and medicine [16]. A technology for the production of metal nanodendritic systems is being developed [17]. Recently, the use of surface plasmons in metallic structures in optical coupling elements has been proposed [18; 19]. The use of metallic nanoscale objects in medicine is part of a new field called nanomedicine, in which metal-containing nanocomposites and nanoparticles are used in various fields, from the production of new types of biosensors and methods of drug delivery to the desired organ in cancer to accelerating tissue regeneration [2]. Despite the rapid development of the technique of obtaining and using nanostructures with metal alloys, the features of the phase diagrams of eutectic metal alloys that arise during nanostructuring, and the relationship between the morphology of nanosystems and the atomic structure of metal alloys, remain practically unexplored. Changes in low-dimensional systems involving metal alloys are of utmost importance to ensure the high quality and stability of conductive micro- and nanoelements and compounds.

Metal-containing nanocomposites prepared by introducing pure metals and metal alloys into the pores of nanoporous matrices have a number of advantages, including the ability to provide a given size, shape and relative arrangement of metal particles determined by the characteristic size and geometry of the pores, to create ordered ensembles of particles through the use of matrices such as artificial opal, molecular sieves or porous alumina, and disordered ensembles of particles under the use of nanoporous glasses and polymer matrices, which are characterized by irregular pore arrangement. In addition, in nanocomposites based on porous matrices, the particles in the pores are protected from environmental influences. Such nanocomposites attract a lot of attention as a separate class of nanostructures that have great prospects for application in various fields of science and technology. On the other hand, they are unique model systems for studying the physical properties of substances under nanoconfinement conditions.

For metals and alloys introduced into nanoporous matrices, changes in structural and dynamic characteristics induced by nanoconfinement are observed. It should be noted that when studying substances under nanoconfinement conditions, it is possible to use the same experimental methods as for bulk samples. This fact makes it possible to compare the measurement results for nano-sized particles and bulk substances, being sure that the observed changes are not due to the difference in experimental methods, but exclusively to the differences in the physical properties of the substance during the transition to the nanoscale.

One of the most informative experimental methods for studying nanocomposites created by injecting metal particles into various nanoporous matrices is the nuclear magnetic resonance (NMR) method. An important advantage of NMR is its high sensitivity to local changes in matter [5; 20]. It should be emphasized that the NMR method is sensitive to changes in atomic mobility in individual pores of

nanocomposites, in contrast to the gradient NMR method, which tracks changes in atomic mobility between pores.

Despite a large number of studies on the physical properties of nanocomposites, many problems remain open. These include the effect of nanoconfinement on structural changes in liquids, particularly in liquid metals and alloys. In works [21; 22; 23; 24; 25; 26; 27; 28; 29; 30; 31; 32] a phase transition between fluid structures of the same composition is described for such substances as water, phosphorus, carbon, SiO_2, Al_2O_3-Y_2O_3. It was expected that pure gallium, which compares favorably with the liquids mentioned above in that it is capable of forming a large number of polymorphic phases in its solid state [33; 34; 35] and is prone to hypothermia [36; 37], will also demonstrate the presence of a liquid-liquid phase transition, but this phase transition has not been detected for bulk gallium. However, under nanoconfinement conditions, a liquid-liquid phase transition is observed in liquid gallium, which was demonstrated by NMR [37]. Later, in [38], the existence of a first-order phase transition from high-density liquid gallium to low-density liquid gallium was predicted using the molecular dynamics method. A review of studies on liquid-liquid phase transition in various metal alloys is presented in the paper [39]. Structural changes in the liquid eutectic alloy Ga-In at temperatures of 400-550 K were detected experimentally and then confirmed theoretically using the ab initio method of molecular dynamics in operation [40]. Investigations [41; 42] showed that under conditions of increased pressure at room temperature and at high temperatures up to 673 K, the liquid-liquid phase transition is not observed. It is of considerable interest to find out whether a liquid-liquid phase transition is possible in a eutectic Ga-In melt under conditions of nanoconfinement below room temperature. It can be assumed that the answer to this question will be provided by studies conducted by the NMR method.

Bulk gallium crystallizes on cooling into a stable phase of α-Ga [43], the NMR signal from which in polycrystals and powders cannot be observed due to the significant broadening of the resonance line. However, under certain conditions, gallium can form metastable structural modifications, the most common of which is β-Ga [43]. Under nanoconfinement conditions, gallium can crystallize both in the β phase and in modifications not observed in bulk metal [44]. At the same time, it was found that the β phase stabilizes in gallium in the pores of the nanometer range [44]. It is important to identify the formation of the β phase in the gallium Ga-In alloy introduced into nanoporous matrices.

Recently, it has been discovered that liquid metals introduced into nanoporous matrices undergo significant changes in electronic properties and atomic mobility, manifested in a decrease in the Knight shift and an acceleration of nuclear quadrupole relaxation [6; 45; 46; 47]. Later, similar changes were also observed for a number of binary gallium metal alloys under nanoconfinement conditions [48; 49]. For triple alloys, such studies have not been carried out before. Taking into account the prospects of practical applications of liquid gallium-containing alloys, the study of the features of liquid gallium ternary alloys in a limited geometry is important both in applied and fundamental terms. This applies, in particular, to the triple alloy of gallium, indium and tin. In industry, a Ga-In-Sn alloy with small

impurities of eutectic composition called "Gallinstan" (The trademark belongs to a German company Geratherm Medical AG.[50]). Due to its non-toxicity and low vapor pressure, gallinstan in liquid state is widely used and is beginning to replace mercury in such applications as thermometers, electromechanical relays, coolants, etc. [51; 52; 53; 54]. In addition to being used as a substitute for mercury, galinstan is used in micromechanical systems [55; 56; 57; 58]. The prospects for the use of gallium ternary alloy in nanocomposites require the study of the influence of nano-confinement conditions on the physical properties of this alloy, in particular, on the change in atomic diffusion. It should be noted that methods of measuring spin echo attenuation under an applied magnetic field gradient [59], which is used to study the velocity of fluids flowing through porous media, is not applicable to liquid alloys that have a short spin-lattice relaxation time. A technique using measurements of the spin-lattice relaxation rate for nuclei with spin I>1/2 [60; 61], is an alternative and consists in the extraction of a quadrupole contribution to relaxation, which is due to the interaction of the nuclear quadrupole moment with the dynamic gradients of electric fields that arise during movement in a liquid. In addition, atomic mobility can affect NMR spectra. A change in the displacement of the resonance line due to dynamic effects in the substance under study is called a dynamic shift [62; 63; 64; 65; 66; 67]. Dynamic shift is observed in the NMR spectra of viscous liquids with a long correlation time of atomic motion [68; 69; 70; 71; 72] and solids with high atomic mobility [73]. The use of data obtained from line position and shape measurements, in addition to information obtained from spin-lattice relaxation measurements, should allow for a more accurate determination of atomic mobility in the substance under study.

The purpose of this dissertation is to study the features of the physical properties of gallium-containing alloys under conditions of nanoconfinement by the NMR method: liquid-liquid phase transition in a binary Ga-In alloy introduced into the pores of an opal matrix, deceleration of atomic mobility in a liquid ternary alloy Ga-In-Sn in nanoporous matrices and the effect of nanoconfinement on the magnitude of displacement of NMR resonance lines, the formation of an opal matrix in a hard eutectic alloy in the pores of the opal matrix crystalline phase with β-Ga structure.

To achieve the goals of the dissertation, it is necessary to solve **the following tasks**:

1. To investigate by NMR the possibility of the existence of a liquid-liquid phase transition in a supercooled binary alloy Ga-In introduced into the pores of artificial opal. If a transition is detected, study its main characteristics and relationship with the phase diagram of the nanostructured alloy.
2. To investigate the deceleration of atomic mobility in a triple liquid alloy Ga-In-Sn introduced into the pores of an opal matrix and porous glasses by the change in the velocity of quadrupole spin-lattice relaxation of gallium and indium isotope isotopes in various magnetic fields in comparison with a bulk Ga-In-Sn melt.
3. To investigate the shape and displacement of NMR lines for two gallium isotopes in a ternary liquid alloy Ga-In-Sn introduced into an opal matrix

and porous glasses in various magnetic fields. Interpret the results using a dynamic quadrupole shift model. To detect a decrease in the Knight shift of resonant lines with a decrease in pore size.

4. To identify NMR signals of gallium isotopes from crystalline modification of a binary Ga-In alloy with a β-gallium structure. Find the temperature domain of this modification and determine the value of the quadrupole constant as a function of temperature.

To solve these problems, it is necessary to conduct the following **experiments**:

1. Measurement of the shape and displacement of resonance lines for two isotopes of gallium ^{69}Ga and ^{71}Ga and the isotope ^{115}In in the binary alloy Ga-In introduced into the pores of artificial opal in magnetic fields of 9.4, 11.7 and 17.6 T in the temperature range of 155 – 294 K.
2. Measurement of spin-lattice relaxation time T_1 for two gallium isotopes ^{69}Ga and ^{71}Ga in a binary Ga-In alloy introduced into the pores of artificial opal in the temperature range 155 – 294 K.
3. Measurement of spin-lattice relaxation time, shape and displacement of NMR lines for two isotopes of gallium ^{69}Ga and ^{71}Ga and isotope ^{115}In in bulk triple melt Ga-In-Sn and melt injected into the pores of artificial opal and porous glasses with pore diameters of 7, 18 and 25 nm, at room temperature in magnetic fields of 9.4, 11.7 and 17.6 T.
4. Detection of NMR signals of gallium isotopes ^{69}Ga and ^{71}Ga from the solid phase with a β-Ga structure in a binary Ga-In alloy introduced into an opal matrix in the temperature range from 100 to 294 K and study of the temperature dependence of the shape and position of resonance lines.

Scientific novelty

1. For the first time, the liquid-liquid phase transition in a binary Ga-In melt injected into the pores of artificial opal was discovered and studied in detail. A phase transition was found in a supercooled melt by anomalies in the temperature dependence of the Knight shift of NMR lines for gallium isotopes. For the first time, it was revealed that the phase diagram of the Ga-In binary alloy under nanoconfinement conditions has significant differences from the phase diagram of the Ga-In bulk alloy. A shift in the concentration of the position of the eutectic point was observed.
2. For the first time, the change in the Knight shift of NMR lines of gallium isotopes ^{69}Ga and ^{71}Ga and indium isotope ^{115}In was investigated for a triple liquid alloy Ga-In-Sn injected into the pores of artificial opal with a diameter of amorphous silica balls equal to 210 nm and porous glasses with a pore diameter of 7, 18 and 25 nm. compared to bulk melt. It is shown that the decrease in the Knight shift correlates with the size of the pores.
3. For the first time, for a triple Ga-In-Sn melt introduced into nanoporous glasses with a pore size of 7 nm, a difference in the frequency shift of the NMR resonant line for two gallium isotopes and the dependence of the

frequency shift on the value of the constant magnetic field was observed. For the first time, these features were interpreted within the framework of the dynamic quadrupole shift model of the NMR line.

4. For the first time, the effect of nanoconfinement on atomic mobility in a Ga-In-Sn melt introduced into nanoporous matrices with different pore sizes and geometries was investigated. With the help of measurements of the spin-lattice relaxation rate, it was found that for the Ga-In-Sn alloy injected into the pores of artificial opal with a characteristic silicate ball size of 210 nm and into porous glasses with a pore diameter of 7 and 18 nm, atomic diffusion is significantly slowed down and its deceleration increases with a decrease in the characteristic pore size. The self-consistency of the mobility data obtained from the study of spin relaxation and resonance line shifts is demonstrated.
5. For the first time, direct evidence of the formation of a crystal phase with a β-Ga structure in a hard binary alloy Ga-In introduced into an opal matrix was obtained, and the stability of this phase under nanoconfinement conditions was demonstrated. The temperature region of its existence in the pores of the opal matrix has been revealed, and the values of the quadrupole constant in this temperature region have been found.

Scientific and practical significance

From a practical point of view, the information obtained can be useful in the design of new and improvement of existing technical devices in which Ga-In and Ga-In-Sn alloys are used. In particular, in the improvement of simple non-toxic thermometers, solar cells, the improvement of the qualities of liquid refrigerants and heat transfer fluids, as well as in the development of flexible and deformable electronic components in such state-of-the-art applications as the creation of artificial muscles and tactile sensors, in liquid robotics, in 3D printing, nanomedicine and much more.

The results of this work expand knowledge about the effect of nanoconfinement on the physical properties of liquid and solid metal eutectic alloys and can be used in the educational process in the training of specialists in the field of nanophysics.

Personal contribution

The author personally carried out the main part of the work. The author completely obtained experimental data, carried out data processing and analysis, prepared material for publications and wrote draft versions of articles and theses of reports. E.V. Charnaya carried out the formulation of the thesis objectives and general supervision of the work, as well as editing of publications. A.V. Uskov, D.Y. Podorozhkin, and A.O. Antonenko assisted in the measurements and carried out studies of the liquid-liquid phase transition in the ternary alloy, the results of which were not included in the thesis. Y.A. Kumzerov, A.V. Fokin, and M.I. Samoilovich provided samples for research. M.K. Lee, J.L. Chang, J. Haase, D. Michel, and A.S. Bugaev participated in the discussion of the results and theoretical models.

Structure and scope of the thesis

The dissertation consists of an introduction, five chapters, a conclusion and a list of references consisting of 141 titles. The total volume of the work is 87 pages and includes 37 figures and 5 tables.

The introduction describes the relevance of the topic of the dissertation work and reviews the existing research results in this scientific topic at the moment, formulates the goal of the work and sets tasks to achieve the goal, describes the experiments that were necessary to solve the problems, describes the scientific novelty of the results presented in the dissertation work, the scientific and practical significance of the results obtained, personal contribution and a summary of the dissertation work with information about the volume and structure of the dissertation are presented, the main scientific results are presented and the scientific provisions submitted for defense are formulated.

In the first chapter a brief theoretical review of the basic concepts and methods used for research and analysis of experimental results in this dissertation is carried out. Section 1.1 provides a brief theoretical description of the Knight shift of the NMR resonance line in metals and alloys and its behavior under nanoconfinement conditions. Section 1.2 discusses the function of the NMR line shape. In the third part, the basic concepts of nuclear spin-lattice relaxation are introduced and the magnetic and quadrupole mechanisms of spin-lattice relaxation are described. Section 1.4 provides a brief description of the dynamic quadrupole shift model of NMR lines.

Chapter two is devoted to the study of the phenomenon of liquid-liquid phase transition found in a supercooled eutectic Ga-In melt injected into the pores of artificial opal with an average diameter of amorphous silica balls of 260 nm, as well as to the features of the phase diagram under nanoconfinement conditions. This chapter presents the temperature evolution of the shape and position of the NMR line and the temperature dependencies of the NMR signal intensity for the gallium isotope ^{71}Ga and the isotope of indium ^{115}In, indicating the stratification of the melt in the temperature range of 165 – 175 K into almost pure gallium with a very small admixture of indium and the Ga-In melt with a higher concentration of indium. In the indium-depleted part of the melt, a liquid-liquid phase transition occurs. The temperature dependencies of the Knight shift and the spin-lattice relaxation time T_1 are given for isotope ^{71}Ga. The NMR line was also decomposed for ^{71}Ga by two lorentzian lines in the temperature range where a complex line structure was observed. The decomposition was used to find the Knight shifts of both phases of the fluid and to calculate the spin-lattice relaxation times. The temperature dependencies of the Knight shift and the spin-lattice relaxation time T_1 are provided for both components of the decomposition of NMR signal of isotope ^{71}Ga. The temperature dependence of the nuclear spin-lattice relaxation rate for the ^{71}Ga isotope showed that in the temperature range from 215 to 240 K the relaxation is due to two main mechanisms: quadrupole and magnetic. Also in this chapter, the dependence of the correlation time of atomic motion on temperature was obtained and the activation energy was calculated.

In chapter three the results of observation of resonance lines due to the formation of a crystal phase with a β-Ga structure during the solidification of a binary Ga-In alloy in the pores of an opal matrix are considered. Stabilization of this phase under nanoconfinement conditions was demonstrated, in contrast to bulk alloy, where it is metastable. A single-stage melting-crystallization hysteresis loop was obtained, which made it possible to conclude that there was no phase with the α-Ga structure and only a phase with the β-Ga structure was formed. The dependencies of the isotropic shift of the NMR line were measured δ_{iso} and quadrupole constants C_q for isotopes ^{71}Ga and ^{69}Ga on the temperature. It was found that the melting point of the eutectic Ga-In alloy in the pores of artificial opal was close to the solidus temperature in the bulk alloy for segregated β-Ga. Temperature measurements of the spin-lattice relaxation time in the Ga−In solid alloy with the β-Ga structure were also carried out, as a result of which it was found that in the temperature range from 215 K to 240 K, two main mechanisms contribute to spin-lattice relaxation: the mechanism of interaction of quadrupole moments with dynamic gradients of electric fields and the mechanism of interaction of magnetic moments with conduction electrons. It was found that the correlation time of atomic motion decreased from 7.9 to 0.27 μs. The activation energy of atomic motion was also calculated E_a = 7200 K = 0.62 eV.

In chapter four a study of atomic mobility in a triple Ga-In-Sn melt introduced into the pores of artificial opal with an average diameter of amorphous silica spheres of 210 nm and porous glasses with a characteristic pore size of 7 and 18 nm in various magnetic fields is described. The experimental results obtained were compared with the results for the bulk case. Broadening of the NMR resonance line of gallium isotopes was demonstrated ^{71}Ga and ^{69}Ga and the isotope of indium ^{115}In, which grows as the pore size decreases. Experimental results of measurements of the NMR line shape and spin-lattice relaxation rate are presented. Quadrupole and magnetic contributions to spin-lattice relaxation for gallium isotopes were evaluated ^{71}Ga and ^{69}Ga and the isotope of indium ^{115}In. At the same time, for gallium isotopes, the quadrupole and magnetic contributions to relaxation were taken into account in the spin-lattice relaxation analysis, taking into account the fact that these isotopes have different gyromagnetic ratios and quadrupole moments. It was assumed that the quadrupole constant and the magnetic spin-lattice relaxation time remained unchanged when the melt was introduced into different pores. The results obtained revealed that as the pores decrease, the dominance of the magnetic mechanism in spin-lattice relaxation decreases, and the main contribution to spin-lattice relaxation is made by the quadrupole mechanism. The correlation time of atomic motion was also estimated, and based on the results of this assessment, it was concluded that in the triple Ga-In-Sn melt under nanoconfinement conditions, there is a significant decrease in the atomic diffusion rate compared to the bulk case, and as the pore diameter decreases, the diffusion slowdown progresses.

In chapter five a description of NMR studies of a bulk triple melt of Ga-In-Sn, as well as a melt of the same composition injected into the pores of an opal matrix and nanoporous glasses in various magnetic fields, is given. The results of the

Knight shift measurement for gallium isotopes for porous matrices with different pore sizes are presented. It is shown that for a melt in porous glass with a pore size of 7 nm, the shifts of the resonance lines of the two gallium isotopes differ and a change in the shifts in various quantizing magnetic fields is observed. Such anomalous behavior of frequency shifts of NMR lines was absent in porous matrices with large pore sizes. Later in this chapter, an interpretation of the results obtained based on the model of dynamic quadrupole shift of the NMR line is given. With the help of this model, the correlation time of atomic motion τ_c was obtained. In the final part of the chapter, it is shown that the results of the calculation τ_c using a dynamic quadrupole shift model, the NMR lines and the spin-lattice relaxation time method are consistent.

In the final part of the work the main results are formulated. This is followed by a list of references.

Main scientific results.

1. NMR studies of temperature evolution of the line shape, temperature dependence of spin-lattice relaxation time, size dependence of the Knight shift, dependence of the Knight shift on the strength of a constant magnetic field for Ga-In and Ga-In-Sn alloys introduced into the pores of various nanoporous matrices have been carried out. The results and interpretation of the results of these studies are presented in works: [74] (pp. 169 – 173), [75] (pp. 255101-1 – 255101-7), [76] (pp. 1675 – 1679), [77] (pp. 1721 – 1727), [61] (pp. 351 –356), [78] (pp. 2452 – 2456).
2. A significant difference between phase diagrams of binary Ga-In alloy under nanoconfinement and in the bulk case, consisting in the shift of the eutectic point in the direction of decreasing indium concentration, has been found. The data indicating that a liquid-liquid phase transition occurs in a part of $Ga_{94}In_6$ binary melt introduced into opal pores have been obtained. (see [74] pp. 169 – 173, [75] pp. 255101-1 – 255101-7).
3. In the process of crystallization, the formation of a solid phase of $Ga_{94}In_6$ alloy with the β-Ga structure was found. It was found that in this phase with β-Ga structure in the temperature range 215-240 K spin-lattice relaxation is due to two main mechanisms: quadrupole, consisting in the interaction of nuclear quadrupole moments with dynamic gradients of electric fields produced by the motion of atoms, and magnetic, consisting in the interaction of magnetic moments of nuclei with conduction electrons. The activation energy of atomic motion E_a = 7200 K = 0.62 eV was also calculated. (see [76] pp. 1675 – 1679, [77] pp. 1721 – 1727).
4. A decrease of the Knight shift for ^{69}Ga, ^{71}Ga, and ^{115}In isotopes in Ga-In-Sn melt in the pores of various nanoporous matrices as the characteristic pore size decreases is revealed. Also, for this melt the correlation times of atomic motion are calculated and the slowing down of atomic diffusion, which correlates with the decrease of characteristic pore size, is revealed. (see [61] pp. 351 –356).
5. Using the dynamic quadrupole shift model, the difference of the Knight shift

for ^{69}Ga and ^{71}Ga isotopes in the same magnetic field and dependence of the Knight shift on the magnetic field strength for each of the gallium isotopes observed for the Ga-In-Sn liquid alloy introduced into the pores of nanoporous glass with an average pore diameter of 7 nm have been interpreted. The atomic motion correlation time calculated in the framework of this model agrees with the data obtained by measuring the spin-lattice relaxation time. (see [78] pp. 2452 – 2456).

Provisions to be defended.

1. The phase diagram of the Ga-In binary alloy introduced into the opal matrix changes compared to the bulk Ga-In alloy. In the pores of the opal matrix, during the crystallization of the Ga-In alloy, a phase with a β-Ga structure is formed and stabilized. The eutectic point shifts towards a lower concentration of indium.
2. In the Ga-In binary alloy injected into the pores of the opal matrix, a liquid-liquid phase transition is observed. The phase transition takes place in a supercooled melt below the crystallization temperature of the main part of indium. The difference in Knight shifts of NMR signals for the two gallium isotopes in different melt phases reaches 20 ppm. The spin-lattice relaxation times of gallium also differ for the two phases of the liquid alloy.
3. The Knight shift of the resonant NMR lines of the isotopes ^{71}Ga, ^{69}Ga and ^{115}In in the liquid ternary alloy Ga-In-Sn injected into the pores of artificial opal and nanoporous glasses with an average pore diameter of 7, 18 and 25 nm is reduced compared to the bulk alloy. The decrease of Knight shift correlates with pore size.
4. The spin-lattice relaxation rate for the isotopes ^{71}Ga, ^{69}Ga and ^{115}In in the liquid triple alloy Ga-In-Sn of eutectic composition injected into the pores of opal and nanoporous glasses is significantly increased compared to the bulk alloy Ga-In-Sn. The increase in the rate of spin-lattice relaxation is due to an increase in the efficiency of the quadrupole relaxation mechanism and correlates with a decrease in the characteristic pore size. In the Ga-In-Sn melt under nanoconfinement atomic diffusion is significantly slowed down.
5. The NMR lines of gallium isotopes ^{71}Ga and ^{69}Ga in the liquid ternary alloy Ga-In-Sn introduced into porous glass with a pore size of 7 nm have different frequency shifts that depend on the magnitude of the constant magnetic field. The difference in the shifts of the resonance lines is due to the dynamic quadrupole shift associated with the slowing down of atomic mobility.

Chapter 1. Review

In this work, the research was carried out by the method of nuclear magnetic resonance. In addition to being a non-destructive method of quantitative and structural analysis of matter, NMR is also sensitive to local changes and allows you to study the mobility of atoms in the sample under study. The disadvantages of the method include lower sensitivity compared to other experimental methods (electron paramagnetic resonance (EPR), fluorescence, optical spectroscopy), but this is solved by a large number of NMR signal accumulations. The year 1945 is considered to be the year of the discovery of NMR. This year, Felix Bloch of Stanford and Harvard's Edward Purcell and Robert Pound discovered the NMR signal on protons in liquids and solids for the first time. (Bloch and Purcell were awarded the Nobel Prize in Physics in 1952 for this discovery.) At that time, the NMR phenomenon itself had already been predicted and several attempts had been made to detect it experimentally. In addition, a year earlier in Kazan, Evgeny Zavoisky discovered the phenomenon of EPR. He also observed the NMR signal in 1941, but he had a magnet with poor field uniformity and so these results were poorly reproduced and not published. Also, before the "official" discovery, the NMR phenomenon was observed by the American scientist Isidore Rabi in 1938. He detected the NMR signal in molecular beams and was awarded the Nobel Prize in Physics in 1944.

1.1 Knight Shift

The Knight shift is named after Professor W.D. Knight, who first observed it in 1949 [79]. Knight discovered that the resonant frequency of the core ^{63}Cu in metallic copper is 0.23% higher than in the diamagnetic salt CuCl in the same magnetic field. This shift is one of the important characteristics of metals and it is an order of magnitude higher than chemical shifts in various diamagnetic substances [80]. The Knight shift occurs as a result of the interaction of the magnetic moments of the nuclei with the resulting magnetization of the ensemble of conduction electrons, the direction of the spins of which is ordered in a constant magnetic field. Let's denote ω_m and ω_d resonant frequencies in the same nucleus in metals and diamagnets in the same constant magnetic field, and for $\Delta\omega$ the difference in resonant frequencies. Then the resonant frequency of the nucleus in metals will be determined by the following equation: $\omega_m = \omega_d + \Delta\omega$. The main properties of the Knight shift include:

1) The value of $\Delta\omega$ is positive except in a few cases.
2) When the constant magnetic field changes, the relative shift $\Delta\omega/\omega_d$ does not change.

3) The relative shift is weakly dependent on temperature and generally increases with the charge of the Z nucleus.

As reported in the [80], to explain the Knight shifts, we consider the magnetic fields on the nuclei due to the ultrafine interaction of the nuclei with conduction electrons in the S-state. With an external magnetic field of zero, the spins of the electrons are directed chaotically and the magnetic field on the nucleus is zero. When magnetic field B_0 is applied the spins of the electrons are oriented, and the nucleus, in addition to the magnetic field B_0, is affected by the magnetic field resulting from the ultrafine interaction. Since the field resulting from the ultrafine interaction is parallel to the electron magnetic moment, and the total magnetic moment of the metal's electrons is oriented parallel to the external magnetic field B_0, the resulting magnetic field acting on the nucleus will actually be greater than B_0. The frequency shift is proportional to the degree of polarization of the electron spins, which in turn is proportional to B_0. As a result, this means that the frequency shift is proportional to the resonant frequency of the nucleus in diamagnetic substances ωd. Since the spin paramagnetism of a highly pronounced electron gas is weakly dependent on temperature, the Knight shift proportional to the degree of polarization of the electron spins is also weakly dependent on temperature. The increase in shift with an increase of the charge of the nucleus Z is due to the fact that the density of the wave function on the nucleus increases with an increase in the value of Z due to the attraction of electrons by the nucleus. The superfine interaction has all the properties necessary to explain the properties of the Knight shift. According to conventional approximations [81], the Knight shift for metals with filled inner electron shells is defined by the following expression:

$$K_s = \frac{8}{3}\pi\chi_s\Omega\langle|\Psi_F(0)|^2\rangle,$$

where χ_s is the electron susceptibility, Ω is the volume associated with one atom, $\langle|\Psi_F(0)|^2\rangle$ is the density of the wave function averaged over the ensemble of electrons at the Fermi surface, at the location of the nucleus. In view of the dependence of the magnitude of the Knight shift on the electron susceptibility, it is possible to study how the nanoconfinement affects the electronic properties of the substance from the changes in the Knight shift for a substance introduced into the pores of different nanoporous matrices with different characteristic pore sizes, compared to the bulk case.

Work [82] is devoted to one of the first studies of the Knight shift in metals injected into the pores of nanoporous matrices. Most of the NMR studies of the electronic properties of metals in the form of small isolated particles or thin films, which have been carried out before, have been carried out for the solid phase [83; 84; 85; 86; 87; 88; 89; 90; 91; 92; 93], with dimensional effects creating an inhomogeneous broadening of the NMR line, which complicates the shape of the line and deflects the center of mass of the line from the amplitude maximum. It is known that the Knight shift is anisotropic for solid metals with a non-cubic crystal lattice and depends on the orientation of the external magnetic field B_0 relative to the crystallographic axes [80]. For isolated particles, powdered samples, or solid metals in the pores, the orientation of the crystallographic axes of the particles is

disordered, resulting in the anisotropy of the Knight shift also resulting in a broadening of the NMR line. The broadening described above greatly complicates the study of the dimensional dependence of the Knight shift in solid metals. In work [82] for the first time, the Knight shift was investigated for liquid pure gallium injected into the pores of nanoporous glasses with different pore sizes and opal pores. A decrease in Knight shift with a decrease in pore size was found, as demonstrated in Table 1.1.

Table 1.1 - Change of Knight shift ΔK relative to a bulk sample for gallium introduced into porous glasses with pore sizes of 3.5, 4, 5, 8 nm, porous glass with two pore sizes of 8 and 200 nm, Vycor glass with a pore size of 6 nm and opals with silica sphere sizes of 100 and 250 nm (size marked with the letter a).

Sample	Bulk	Porous glasses						Vycor glass	Opals	
Pore size (nm)		3.5	4	5	8	200 (8 nm)	200 (200 nm)	6	100[a]	250[a]
ΔK (ppm)	0	192	137	74	54	74	17	143	71	14

Later, the Knight shift was investigated in other liquid metals, and alloys introduced into nanoporous matrices [6; 46; 48; 49; 94; 95]. In [94] liquid indium injected into the pores of opals with silica ball diameters of 210 and 240 nm and porous glass with a pore diameter of 7 nm were studied. Figure 1.1 shows the resonant lines ^{115}In in bulk specimen and specimens injected into opals described above at room temperature. The inset to figure 1.1 shows the resonance line corresponding to the liquid ^{115}In in porous glass with a pore diameter of 7nm. As can be seen from Figure 1.1 and its insert, the position of the resonant line for indium in opal matrices does not differ from the position corresponding to indium in a bulk sample within the margin of error, and the position corresponding to the sample in porous glass is 100 ppm smaller than for the bulk case, which is equal to about 1% of the shift in the bulk sample.

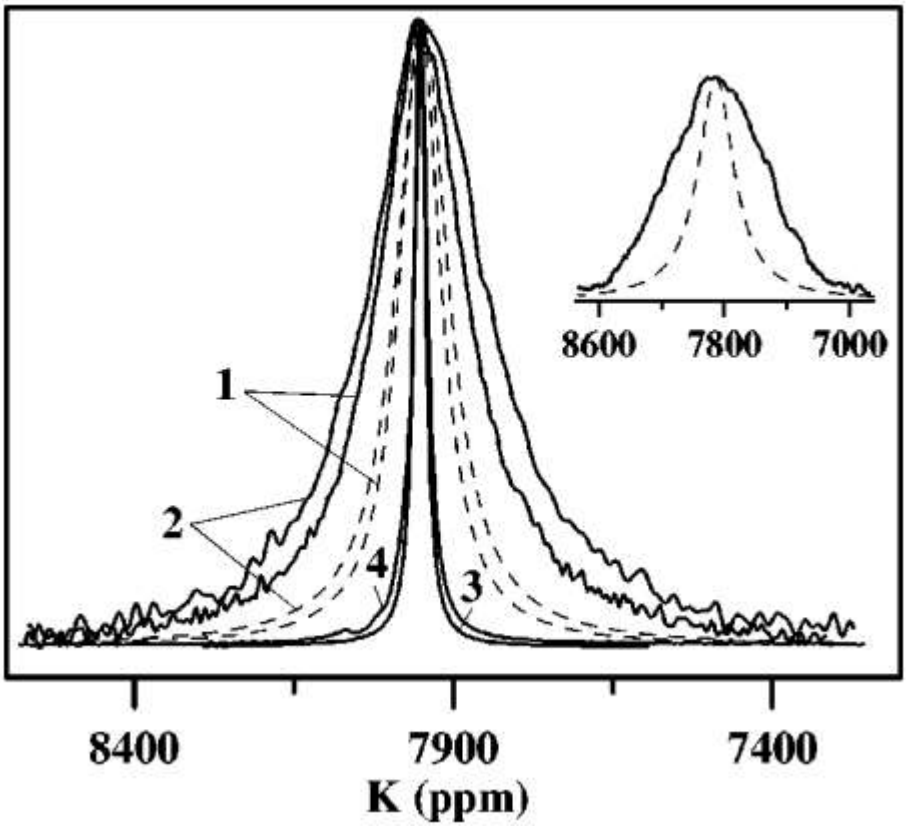

Figure 1.1 - NMR isotope lines ^{115}In in liquid indium injected into the pores of opals with a ball size of 210 nm (1) and 240 nm (2), in a bulk sample (3) and on the surface of opal with a ball size of 240 nm (4). The insert to the figure shows the NMR line of isotope ^{115}In in liquid indium injected into the pores of nanoporous glass with an average pore diameter of 7 nm. Solid lines denote experimental data, dashed lines are calculated theoretically taking into account the equality of $T_2 = T_1$ [94].

In [46] isotopes ^{119}Sn and ^{199}Hg were studied in liquid tin and mercury injected into the pores of artificial opal with an average silica ball diameter of 210 nm and an average radius of tetrahedral and octahedral pores of 18 and 30 nm, respectively. Porous glasses with an average pore radius of 4 and 3 nm were also used as nanoporous matrices. Figures 1.2 and 1.3 show that relative to bulk samples for both mercury and tin, the resonant line shifts towards lower frequencies with a decrease in pore size, and the line itself is widened.

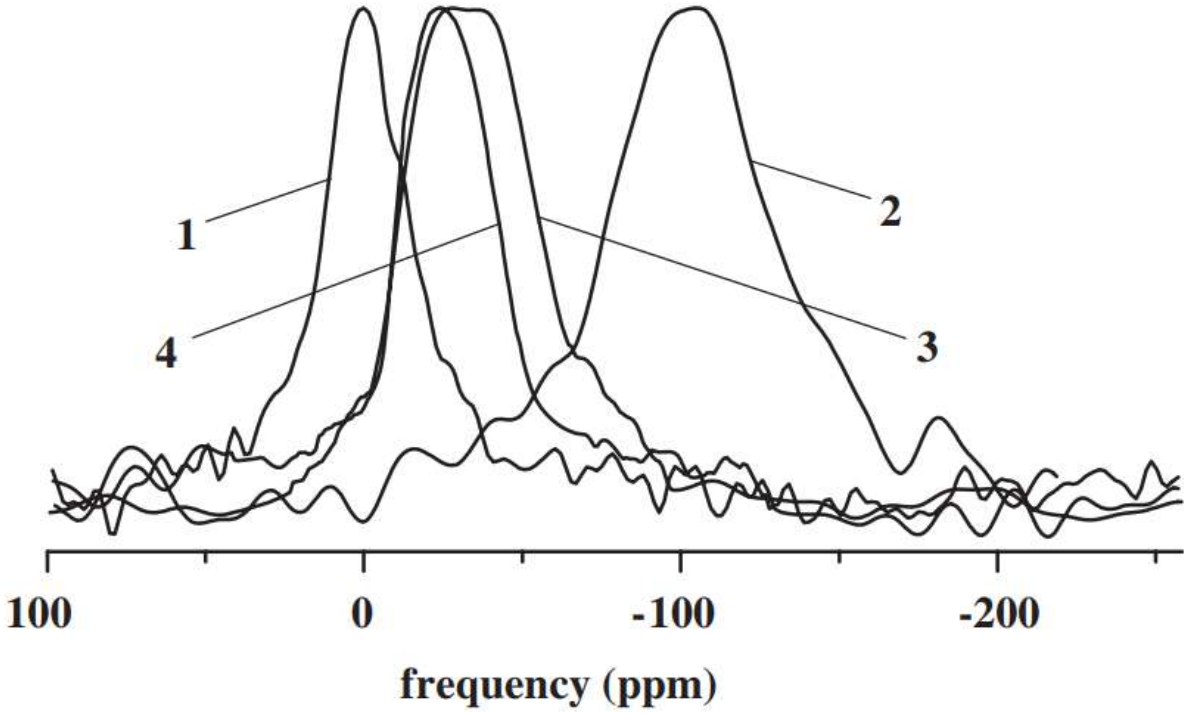

Figure 1.2 - NMR isotope lines ^{119}Sn in liquid tin in bulk sample (1) injected into the pores of nanoporous glass with an average pore radius of 4 nm (2) injected into the pores of artificial opal with an average silica sphere diameter of 210 nm and a filling factor of 85% (3) and 40% (4) [46].

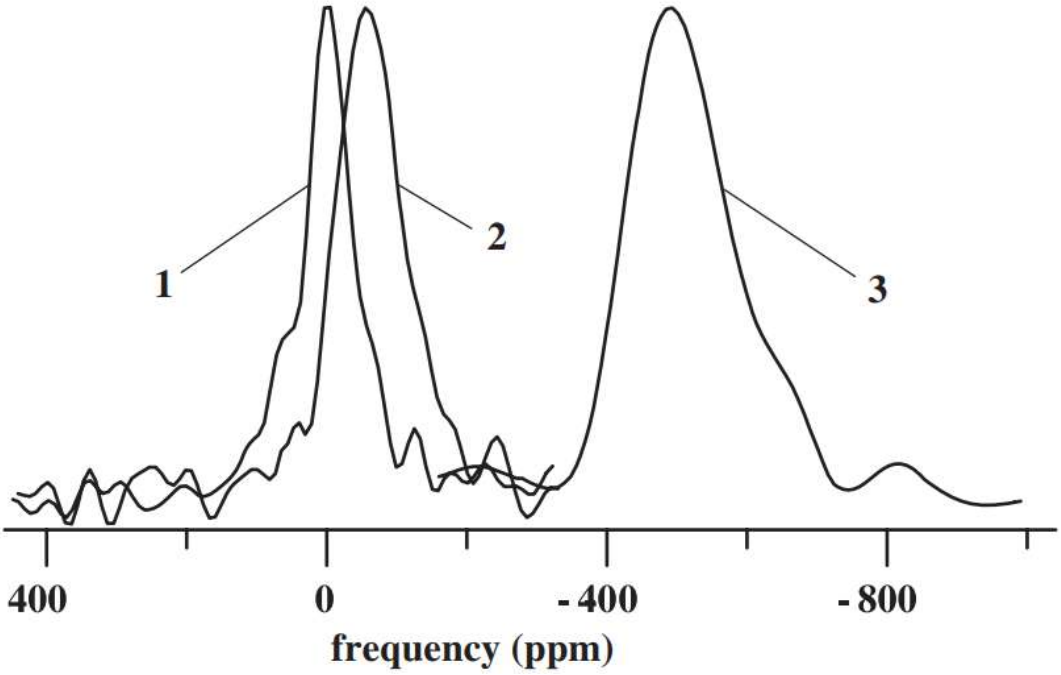

Figure 1.3 - NMR isotope lines ^{199}Hg in liquid mercury in a bulk sample (1) injected into the pores of artificial opal with an average diameter of silica spheres of 210 nm (2), injected into the pores of nanoporous glass with an average pore radius of 3 nm (3) [46].

In work [49] the results of the Knight shift study for isotopes are presented ^{71}Ga, ^{69}Ga and ^{115}In in a binary Ga-In melt in a bulk sample, thin film and pores of nanoporous glass with an average pore diameter of 5 nm. Figures 1.4 and 1.5 show the NMR lines for isotopes ^{71}Ga and ^{115}In respectively in the Ga-In melt in the samples described above.

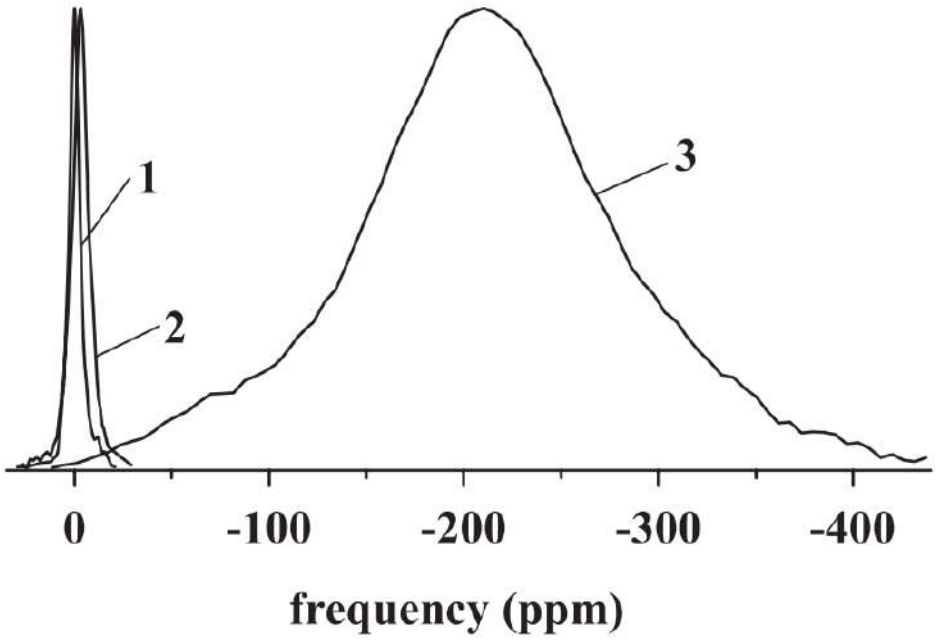

Figure 1.4 - NMR isotope line ^{71}Ga in a Ga-In melt in a bulk sample (1), a thin film (2) and a Ga-In melt injected into the pores of nanoporous glass with an average pore diameter of 5 nm (3) [49].

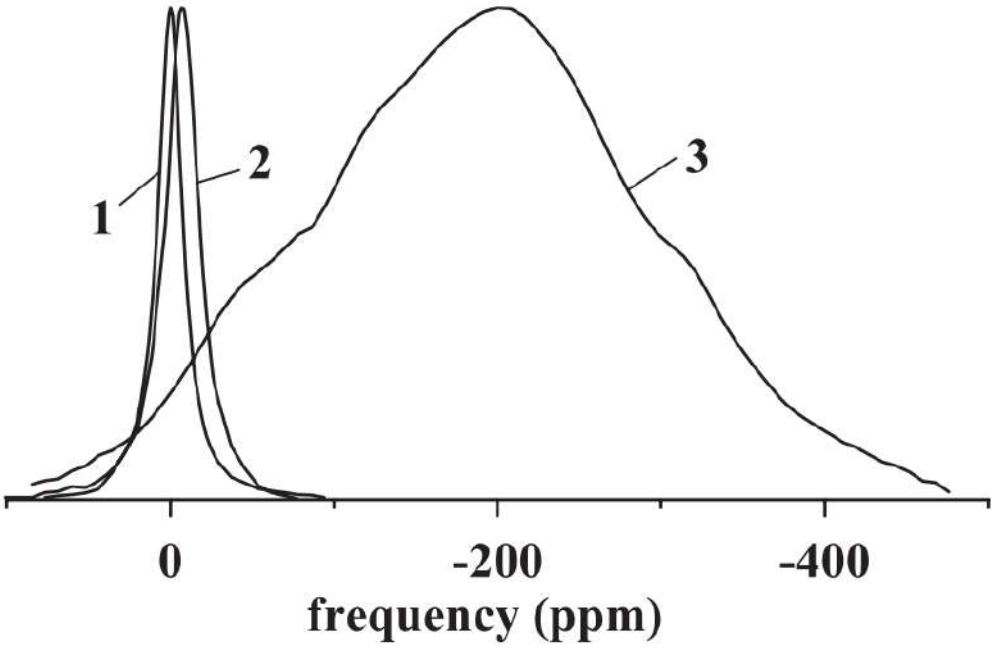

Figure 1.5 - NMR isotope lines ^{115}In in a Ga-In melt in a bulk sample (1), a thin film (2) and a Ga-In melt injected into the pores of nanoporous glass with an average pore diameter of 5 nm (3) [49].

Figure 1.6 shows the NMR lines for the isotope ^{71}Ga in the Ga-Sn binary melt in various samples that were studied in the work [48]. Bulk Ga-Sn alloy and an alloy injected into the pores of opal with a diameter of borosilicate spheres of about 210 nm and into the pores of nanoporous glasses with a pore diameter of 18 and 7 nm were used as samples.

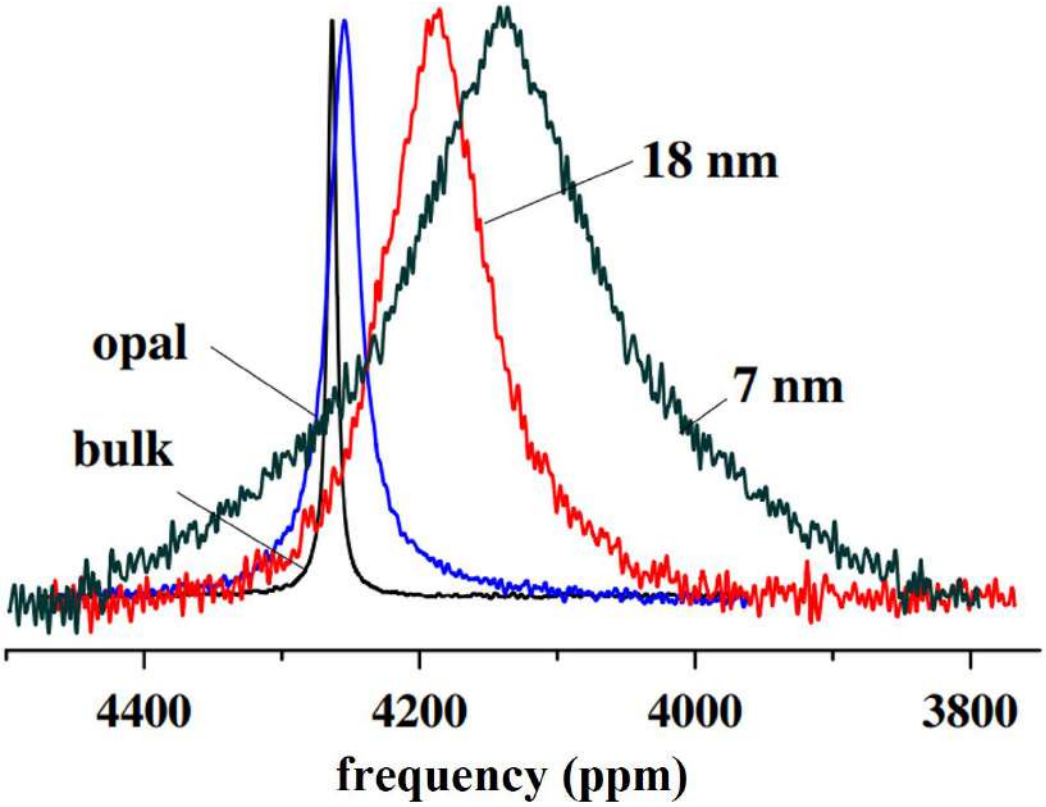

Figure 1.6 - NMR isotope lines ^{71}Ga in the Ga-Sn melt in various samples [48].

As can be seen from figures 1.4 – 1.6, the Knight shift shifts towards lower frequencies with a decrease in the characteristic sample size, and the NMR line itself is broadened, similar to what happens in the pure metals studied earlier.

1.2 NMR line shape function, Lorentz and Gaussian dependencies

From the description of the phenomenon of nuclear magnetic resonance [81] It is known that when a constant magnetic field B_0 is applied to a nuclear spin system, as a result of Zeeman splitting, 2I+1 energy levels are formed, determined by the value of the magnetic quantum number m. When an alternating magnetic field with an amplitude perpendicular to B_0 is applied to a nuclear spin system B_t^0, there are transitions of nuclei between Zeeman levels. In this case, only transitions between energy levels with magnetic quantum numbers that differ by 1 are possible.

The probability of the transition between the energy levels m' and m, where m' = m+1, is described by the following expression (1.1):

$$W_{m,m+1} = \frac{\pi}{2}\hbar\gamma^2(B_t^0)^2(I - m)(I + m + 1)\delta(\hbar\omega_0 - \hbar\omega) \qquad (1.1)$$

where the delta function denotes the resonant nature of the excitation when the induced transitions occur only when the frequency of the alternating magnetic field is equal to the frequency of Larmor precession: $\omega = \omega_0$. In view of the fact that as a result of the interaction of the nuclear spin with the magnetic fields created by the environment of the nucleus, the width of the energy levels is finite, the delta function is replaced by the function of the line shape $g(\omega)$: $\hbar\delta(\hbar\omega_0 - \hbar\omega) \Rightarrow g(\omega)$. The lineshape function is used to describe the resonant NMR curve, always having a non-zero width. There can be a large number of reasons for the broadening of the NMR resonance line, for example, the spread of local fields and frequencies of magnetic resonance, the inhomogeneity of chemical, Knight, and paramagnetic shifts for the corresponding types of substances, the scattering of local gradients of electric intracrystalline fields for nuclei with a quadrupole moment, a decrease in the lifetime of nuclear spin at the energy level as a result of flip-flop transitions, imperfect uniformity of constant magnetic induction field B_0 in the sample volume. There are two generally accepted functions for approximating experimentally observed line shapes: the Lorentz and Gaussian functions. The Lorentz function has the following expression:

$$g(\omega) = \frac{\delta}{\pi}\frac{1}{\delta^2 + (\omega - \omega_0)^2} \qquad (1.2)$$

where the parameter δ is equal to the half-width of the resonant line at half of its height. A Gaussian function is described by an expression

$$g(\omega) = \frac{1}{\Delta\sqrt{2\pi}}\exp\left[-\frac{(\omega - \omega_0)^2}{2\Delta^2}\right] \qquad (1.3)$$

where the parameter Δ is related to the half-width of the resonant line at half-height by the ratio $\delta = 1.18\Delta$. Figure 1.7 shows the Lorentz and Gaussian curves, the integral of which is normalized by one.

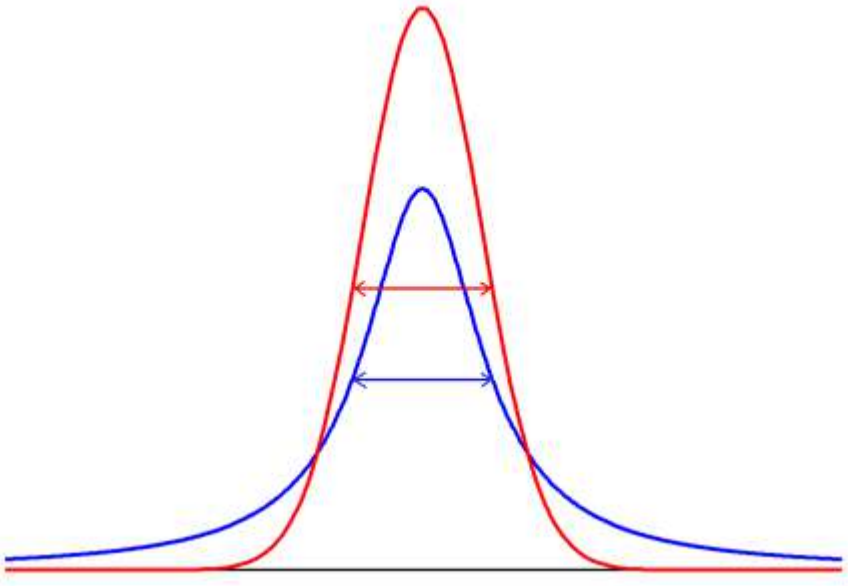

Figure 1.7 - Lorentz (blue line) and Gaussian (red line) curves.

The Gaussian curve decreases much faster with increasing value $|\omega - \omega_0|$ and has a wider upper part than the Lorentz curve. The Lorentz curve is often the most convenient way to approximate NMR signals from liquids, while the Gaussian line shape is typical for signals from some solids and powders. In this dissertation, the approximation of an experimental NMR signal of a complex shape was applied using the sum of two Lorentz functions with the use of baseline correction.

1.3 Nuclear spin-lattice relaxation, magnetic and quadrupole mechanisms of spin-lattice relaxation

The system of nuclear spins in a constant homogeneous magnetic field has an equilibrium population of Zeeman levels, which is distributed in such a way that the total magnetization of the nuclear spin system is not equal to zero and is directed along the constant magnetic field in the case of a positive gyromagnetic ratio of the nuclei and is opposite in the case of a negative one. When the equilibrium population of energy levels is disturbed by an electromagnetic pulse, the system returns to the equilibrium state after some time. The process of restoring the equilibrium state occurs due to the interaction of nuclear spins with oscillations of the crystal lattice for solids or molecular motion (translation, reorientation) for solids and liquids and is called spin-lattice relaxation. In most cases, the main characteristic of this process is the spin-lattice relaxation time T_1. Spin-lattice relaxation time

is the most important radiospectroscopic characteristic of materials. It contains valuable information about the magnitudes of intracrystalline fields, the nature of the chemical bond, the presence of structural defects, molecular motion, and much more. The term lattice in this case refers to a heat reservoir with a much larger heat capacity than that of the nuclear spin system, which includes thermal vibrations of atoms or molecules in solids, as well as molecular motion in both solids and liquids. Due to its significant superiority over the spin system in terms of heat capacity, the temperature of the grating remains constant throughout the relaxation process. The interaction of nuclear spins with crystal lattice vibrations or molecular motion refers to the interaction with alternating magnetic and electric fields resulting from oscillations of the crystal lattice and molecular motion, dipole magnetic and quadrupole moments of nuclei, resulting in induced transitions between energy spin levels.

In this dissertation, atomic mobility in metals and metal alloys was investigated by measuring the spin-lattice relaxation time. In addition to its informative value, this measurement method was the only available method for studying atomic mobility for our samples, since the gradient NMR method for diffusion measurement [96; 97] is not suitable for our studies because of the short relaxation times in the alloys we study, and also because it provides information on diffusion on the scale of several pores, rather than diffusion within a single pore. The impossibility of using the neutron scattering technique for nanostructured gallium was shown in the paper [98]. Spin-lattice relaxation in liquid metals occurs due to two main interaction mechanisms: magnetic dipole and electric quadrupole. The magnetic dipole mechanism consists in the interaction of the magnetic dipole moments of nuclei with the spin magnetic dipole moments of conduction electrons. The electric quadrupole mechanism consists in the interaction of the electric quadrupole moments of the nuclei with the gradients of electric fields created by charged neighboring atoms, which are changed as a result of the movement of atoms.

One of the most common methods for measuring the spin-lattice relaxation time T_1 is called saturation recovery and consists in observing the restoration of the complete magnetization of the nuclear spin system after full saturation, a state when the projection of total magnetization on the z-axis (the axis parallel to the homogeneous magnetic field) is zero. Ideally, this state of the nuclear spin system is reached by a single 90° pulse, but in a real experiment several 90° pulses have to be used. After resetting M_z after some time t, a 90° pulse is applied and a nuclear induction signal is registered, the amplitude of which is proportional to the instantaneous value of magnetization along the z-axis. Further, by changing t, the dependence of the precession amplitude A on the time passed since the saturation moment is plotted. Theoretical dependence A(t) according to [81] has the form

$$\frac{A(t)}{A_0} = \frac{M_z(t)}{M_z^0} = 1 - \exp\left(-\frac{t}{T_1}\right) \qquad (1.4)$$

where A_0 is the amplitude of the electromagnetic induction signal in the absence of saturation. It is convenient to calculate the time T_1 as the cotangent of the angle of slope of the line $-\ln(1 - A/A_0)$ to the t-axis.

The second common method of measuring T_1 is called inversion recovery, which differs from saturation recovery in that the projection of the total magnetization of the nuclear spin system on the z-axis is not made equal to zero by a series of 90° pulses, but inverted by a single 180° pulse. Theoretically, in the ideal case, a 180° pulse inverts the total magnetization, while the dependence of the amplitude of the precession signal after 90° pulse on the time between the inversion and the 90° pulse is described by the formula

$$\frac{A(t)}{A_0} = \frac{M_z(t)}{M_z^0} = 1 - 2\exp\left(-\frac{t}{T_1}\right) \tag{1.5}$$

In this method, it is also convenient to calculate the time T_1 from the angle of slope of the line $-\ln(1 - A/A_0)$ to the t-axis.

To measure the spin-lattice relaxation time T_1 in this dissertation, the inversion recovery method was used, and to interpret the experimental results, the calculations made by Paul Hubbard in his paper were used [99], which describes spin-lattice relaxation taking into account the quadrupole interaction. According to [99] for nuclei with spin I=3/2, the longitudinal quadrupole relaxation as a function of the time after influence of θ - degree pulse is the sum of two exponents

$$\langle M_z\rangle - \langle M_z\rangle^T = \langle M_z\rangle^T (\cos\theta - 1)\left[\frac{4}{5}\exp(-\alpha_1 t) + \frac{1}{5}\exp(-\alpha_2 t)\right] \tag{1.6}$$

where

$$\alpha_1 = 2(eQ/\hbar)^2 J_{-22}(2\omega_0)$$
$$\alpha_2 = -2(eQ/\hbar)^2 J_{-11}(\omega_0)$$

$\langle M_z\rangle^T$ is the thermally equilibrium value of magnetization $\langle M_z\rangle$, Q is the electric quadrupole moment of the nucleus, e is the charge of the electron, ω_0 is the frequency of Larmor precession in a constant homogeneous magnetic field B_0,
and $J_{lk}(\omega)$ is the spectral density

$$J_{lk}(\omega) = \frac{1}{2}\int_{-\infty}^{\infty} C_{lk}(t)\exp(i\omega t)\,dt \tag{1.7}$$

of correlation function of gradients of electric fields on the nucleus $C_{lk}(t)$. To simplify the expression describing the longitudinal quadrupole relaxation of time for nuclei with spin 3/2, a simplified form of the atomic motion correlation function $\exp(-t/\tau_c)$ is used [99], as a result of which the exponent indicators in the expres-

sion 1.6 take the form $-\frac{C\tau_c t}{(1+k^2\omega_0^2\tau_c^2)}$, where k = 1, 2, and τ_c - is the correlation time of atomic motion. For substances with high atomic mobility, for which the approximation of rapid motion is applicable $\omega_0\tau_c << 1$, the exponent indicators in expression 1.6 are reduced to - $C\tau_c t$ [100], where C is the quadrupole constant, which depends on the structure of the substance under study and is proportional to the square of the quadrupole moment of the nucleus. Under conditions where the approximation of fast motion is applicable, the recovery of the total magnetization of the spin system is described by a single exponent, and in this case $C\tau_c$ means a quadrupole contribution to spin-lattice relaxation rate R_{1q}:

$$C\tau_c = \frac{1}{T_{1q}} = R_{1q} \tag{1.8}$$

In addition to the quadrupole contribution for the gallium-containing alloys we study, it is necessary to take into account the magnetic contribution to spin-lattice relaxation. According to [101] magnetic relaxation is described by a single exponent, and the main parameter that characterizes it is the magnetic relaxation time T_{1m}. Taking into account the magnetic contribution, the equation describing spin-lattice relaxation is [47] takes the following form:

$$\frac{M(t)}{M_0} = 1 - b\left[\frac{4}{5}\exp\left(-\frac{C\tau_c t}{1+4\omega_0^2\tau_c^2}\right) + \frac{1}{5}\exp\left(-\frac{C\tau_c t}{1+\omega_0^2\tau_c^2}\right)\right]\exp\left(-\frac{t}{T_{1m}}\right) \tag{1.9}$$

where M(t) is the time-dependent magnetization, M_0 is the equilibrium magnetization, ω_0 is the Larmor precession frequency, C is the quadrupole constant, τ_c is the correlation time of atomic motion, and b is the adjustment coefficient that takes into account the incomplete inversion of the magnetization as a result of a 180-degree pulse. From this equation it can be seen that at the zero moment of time, the magnetization of the sample is completely inverted.

In this dissertation, equation 1.9 was used to process the experimentally obtained data for spin-lattice relaxation of gallium in Ga-In and Ga-In-Sn alloys.
Also, it should be noted that Paul Hubbard's description of spin-lattice relaxation when atomic motion is slowed down works approximately. More precisely, spin-lattice relaxation, which takes into account the dependence of the shift of the NMR resonant line on the magnetic field, is described by the theory of dynamic shift, discussed in Chapter 5.

Chapter 2. Liquid-liquid phase transition in a Ga-In alloy introduced into an opal matrix

2.1 Introduction

In recent decades, there has been considerable interest in the study of structural changes in fluids. In particular, the number of studies of structural transformations in liquid metals and alloys has increased significantly. It is known that some liquids, such as water [21; 22; 23; 24], phosphorus [25; 26], carbon [27; 28], SiO_2 [29; 30], Al_2O_3-Y_2O_3 [31; 32] have a phase transition between different fluid structures of the same composition (liquid-liquid phase transition). Experimental evidence for the presence of a liquid-liquid phase transition for most fluids, where it is expected, is associated with certain difficulties, due to the fact that such transitions often occur in a deeply supercooled regime and the phenomena of crystallization and glass transition make it difficult to directly observe this transition [38]. Gallium is capable of forming a large number of phases [33; 34; 35], has a low melting point and can remain in a supercooled liquid state for a long time [36; 37], all these properties could make it possible to observe a liquid-liquid phase transition in a given substance, but it has not been detected in bulk gallium. Figure 2.1 [102] the temperature dependence of the Knight shift for the isotope ^{69}Ga in a bulk sample is depicted. Reducing the derivative $\left(\frac{\partial K}{\partial T}\right)_p$ just below the melting point was considered by some researchers as a phase transition between two phases of liquid gallium, but in the end these assumptions were not confirmed.

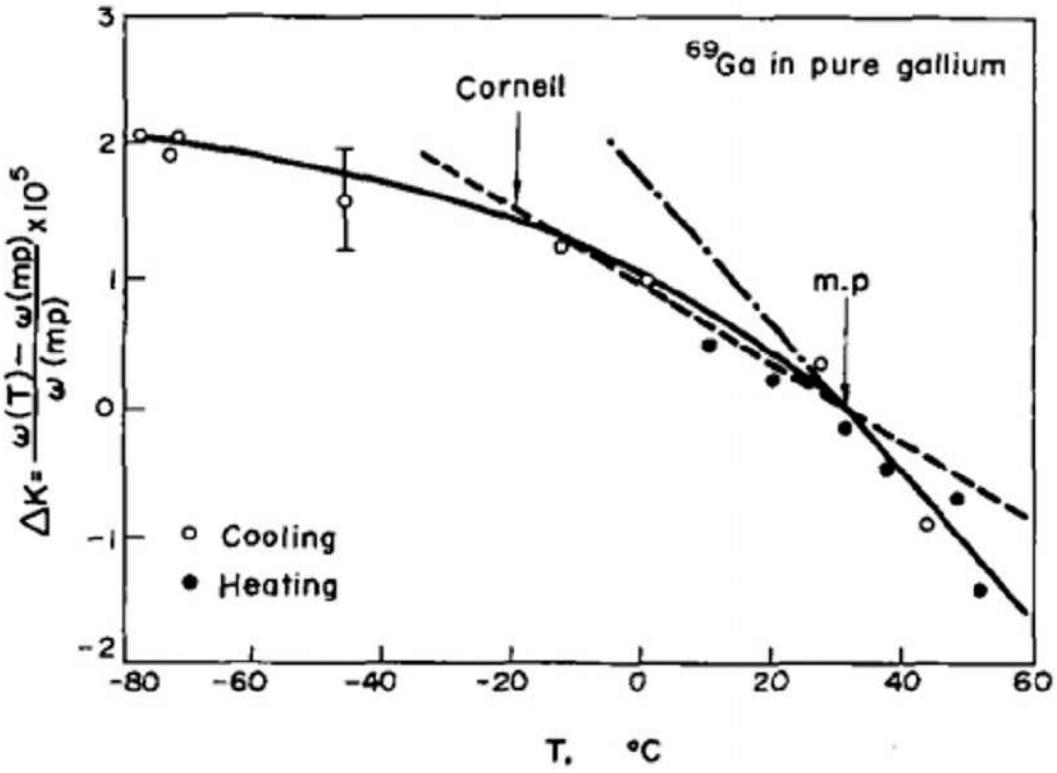

Figure 2.1 - Knight shift temperature dependence ^{69}Ga in liquid gallium [102]

On the other hand, under nanoconfinement conditions, a liquid-liquid phase transition is observed in pure gallium. In work [37] NMR measurements of supercooled liquid gallium in the opal matrix are represented and the simultaneous appearance of two peaks of the NMR line during cooling was explained as the presumed coexistence of two different liquid gallium structures in a temperature range of 220 to 260 K. Later, D.A.C. Jara et al. predicted the existence of a phase transition of the first kind from high-density liquid gallium to low-density liquid gallium, using the Molecular Dynamics Method [38]. It was found that the predicted liquid-liquid phase transition should occur at a temperature about 60 degrees below the melting point of gallium computed by the MEAM (Modified Embedded Atomic Model) method [103], and this is consistent with the degree of gallium supercooling observed in the experimental work of Tien et al. [37].

Recently, a large number of works have begun to appear on the liquid-liquid structural transition caused by temperature changes in various metal alloys [39]. In works devoted to the liquid-liquid phase transition in metals and alloys Ce [104], $Zr_{41.2}Ti_{13.8}Cu_{12.5}Ni_{10}Be_{22.5}$ [105], $Zr_{58.5}Cu_{15.6}Ni_{12.8}Al_{10.3}Nb_{2.8}$ [106] and $La_{50}Al_{35}Ni_{15}$ [107] it raises fundamental questions about metallic fluids, such as what atomic configurations they have and how those atomic configurations change with temperature changes. In work [40] reversible structural changes in the eutectic Ga-In alloy at temperatures from 400 to 550 K, manifested in changes in the X-ray scattering spectrum, were experimentally detected, as shown in figure 2.2.

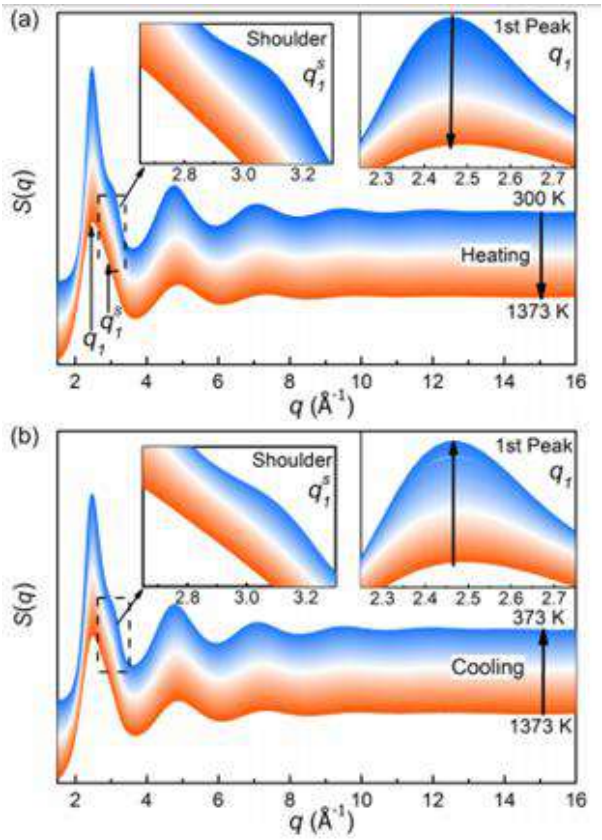

Figure 2.2 - Temperature evolution of a structural factor obtained by X-ray scattering. [40]

Also, these changes were modeled using the method of molecular dynamics and it was shown that the behavior of the temperature dependencies of heat capacity, free energy and atomic diffusion coefficient above and below the temperature range of the liquid-liquid structural transition is different. Experimental Results in [40] were confirmed by theoretical calculations using the AIMD (AB initio molecular dynamics) method.

In the present work, measurements of the Knight shift and spin-lattice relaxation time were made for two isotopes of gallium - ^{71}Ga and ^{69}Ga and Knight shift for ^{115}In in a liquid binary alloy $Ga_{94}In_6$ introduced into an opal matrix in different magnetic fields. As a result of the studies, the features of the phase diagram associated with structural changes in the melt (liquid-liquid phase transition), polymorphism and changes in melting points were observed [74].

2.2 Description of the sample and experiment

The sample for the study was a nanocomposite based on a gallium-indium alloy introduced into a nanoporous matrix. As a nanoporous matrix, artificial opal was used, obtained by sintering silicate spheres (spheres of the first order) into a dense face-centered cubic package. First-order spheres consist of second-order

spheres of smaller diameter, about 300-400 angstroms [108]. In this structure, we consider only first-order pores, because higher-order pores are very small and often closed as a result of sintering. In our case, the average diameter of the spheres of the first order was determined using an atomic force microscope (fig. 2.3) and is equal to 260 nm. According to Works [108; 109; 110]The porosity of the tight packing of ideal balls is ~26% and according to this packing method, there are octahedral and tetrahedral pores between the balls.

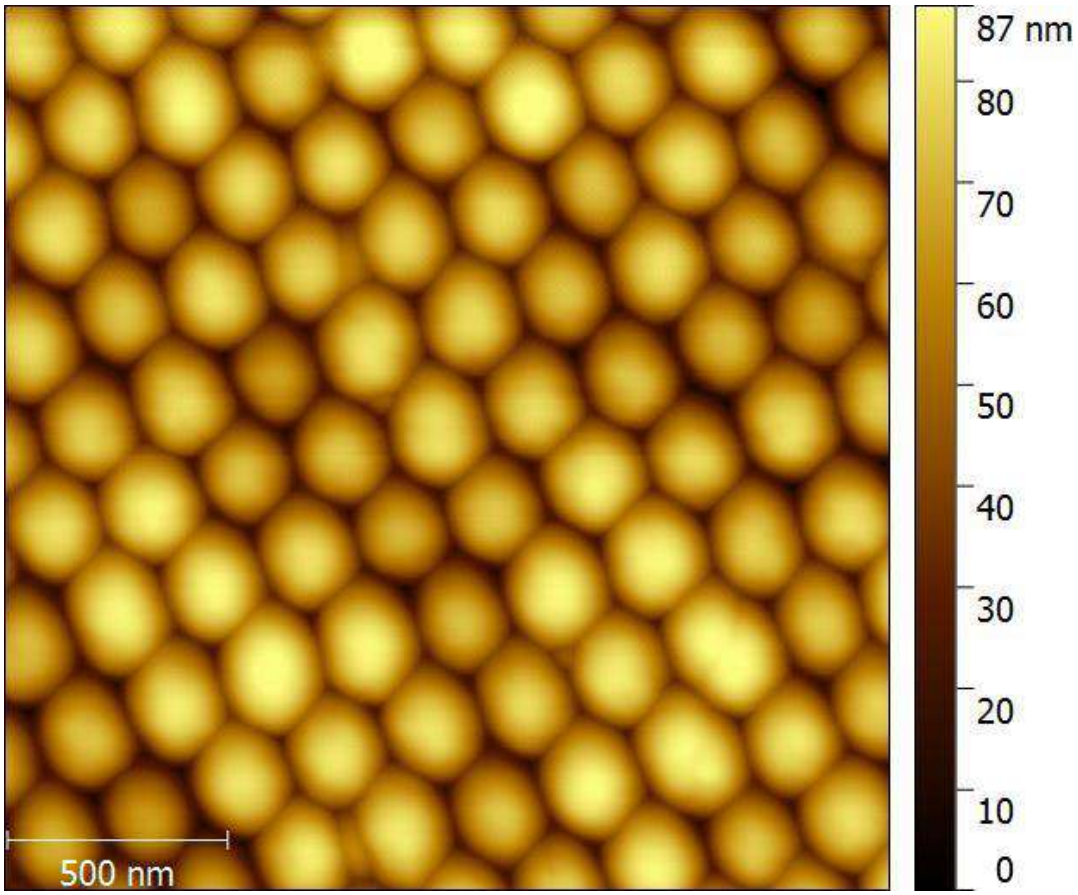

Figure 2.3 - Image of the surface of an opal matrix obtained with an atomic force microscope.

The dimensions of spheres, octahedral and tetrahedral voids in a dense pack are as follows: 1.000:0.441:0.225. As a result, according to theoretical estimates, the characteristic pore size (the diameter of the sphere inscribed in the pore) in an ideal opal with the size of the spheres of the opal we studied is 114.7 nm for octahedral pores and 58.5 nm for tetrahedral pores. But as a result of sintering, the pore size is slightly smaller than in the ideal case.

Liquid Ga-In alloy of the composition Ga - 94 at.%, In - 6 at.% was injected under pressure up to 10 kbar into the pores of the opal matrix. The pore filling factor was about 80% and was determined by weighing the empty and filled opal matrix. Crystallization of the bulk Ga-In alloy produces a stable modification α –Ga and the almost pure phase of indium, as shown in the phase diagram [111], shown in figure 2.4.

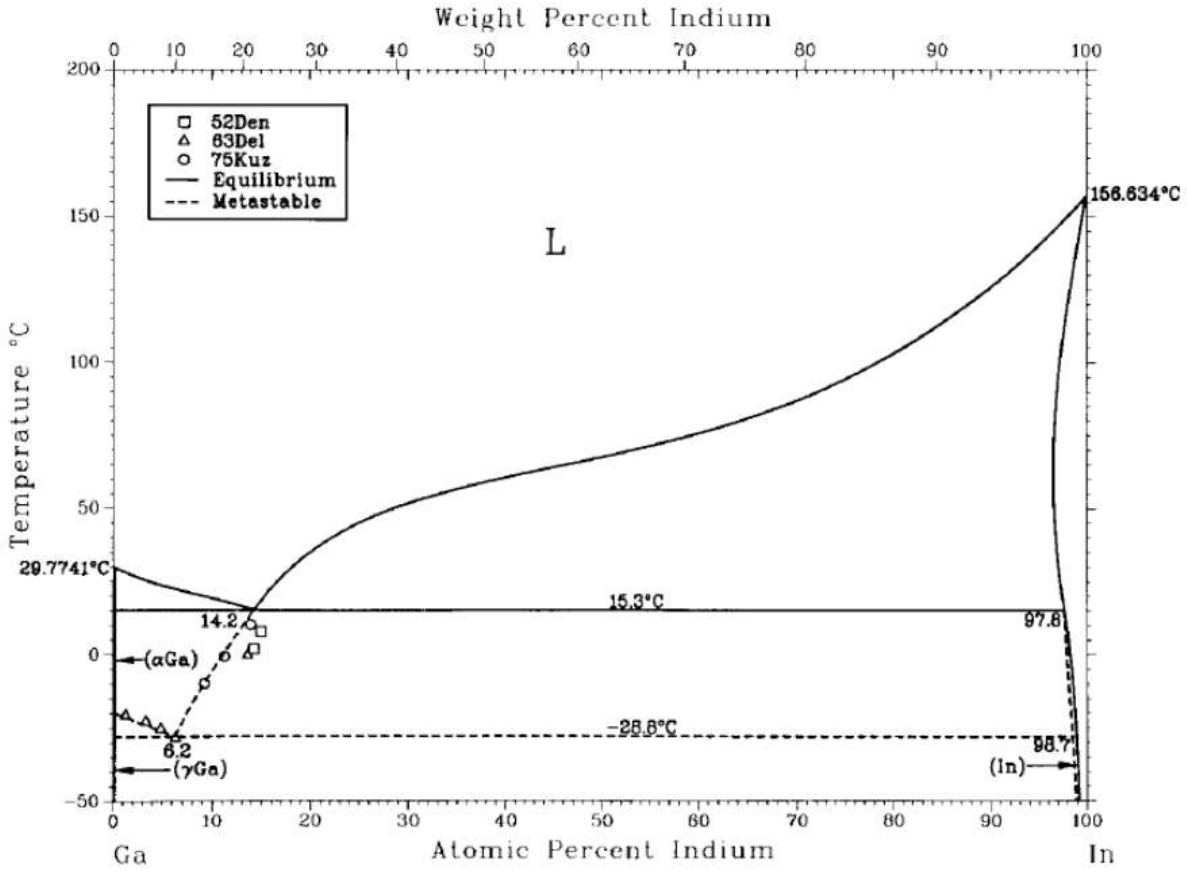

Figure 2.4 - Phase diagram of a Ga-In alloy [111]. Hereafter, we will refer to the β modification of gallium as the γ modification indicated in this phase diagram.

Also, under special cooling modes, a metastable β-phase, which is also shown in figure 2.4. Temperature of liquidus for gallium-indium alloy composition Ga - 94 at.%, In - 6 at.% when forming α – Ga is approximately 22.5 ˚C. Temperature of solidus is equal to 15.3 ˚C for α – Ga and -28.8 ˚C for β – Ga [111]. According to the NMR studies in this paper and the experimental data for melting and crystallization in the work [112] (and references in it), the Ga-In alloy in the pores is completely liquid even at a temperature significantly below room temperature. A decrease in the temperatures of the solidus and liquidus lines is observed for pure gallium and for other alloys and metals introduced into nanopores, and is presented in the results of acoustic and NMR studies carried out in the [82; 113; 114; 115]. Measurements were taken on Bruker Avance 400 spectrometers with a magnetic field of 9.4 T and resonant frequencies of 122.026 MHz for ^{71}Ga and 96.037 MHz for ^{69}Ga, a Bruker Avance 500 with a magnetic field of 11.7 T and resonant frequencies of 152.523 MHz for ^{71}Ga and 120.038 MHz for ^{69}Ga and a Bruker Avance 750 with a magnetic field of 17.6 T and resonant frequencies of 228.765 MHz and 180.041 MHz for ^{71}Ga and ^{69}Ga respectively. Line shapes for different temperatures were obtained using the Fourier transform of the free induction decay signal after a 90-degree pulse with phase cycling. The recovery of longitudinal magnetization after an inverting pulse

for different temperatures was also measured. To increase the signal-to-noise ratio, two thousand scans were used to obtain the shape of the line, and one thousand for the relaxation time. Measurements were carried out in the temperature range of 155 - 294 K using cryostats from Oxford and Janis. The rate of temperature change was less than 0.5 degrees per minute to prevent hypothermia or overheating. The position of the line was measured relative to the position of the signal from gallium in a $Ga(NO_3)_3$ salt solution and at room temperature for ^{71}Ga was 4454.2 ppm, and for ^{69}Ga - 4452.4 ppm and 4241.8 ppm for ^{71}Ga and 4239.7 ppm for ^{69}Ga relative to the signal from gallium in gallium arsenide GaAs. Subsequently, all provisions were recalculated for GaAs due to the fact that in all previous works in this direction GaAs was used as a reference.

2.3 Temperature dependence of Knight shift, intensity, and line shape

For both gallium isotopes at room temperature, a single line is observed in the NMR spectrum (line width 27.6 ppm for ^{71}Ga and 41.3 ppm for ^{69}Ga) corresponding to the melt. The Knight shift of the NMR line was indicated in the previous paragraph and is the same in the magnetic fields of 9.4, 11.7 and 17.4 T. The Knight shift was defined as the position of the maximum. As the temperature drops, the position of the line first changes towards high frequencies, and then it shifts towards the lower frequencies and a second component appears, which is at higher frequencies in relation to the first. As the temperature drops further, the original component disappears. Figure 2.5 illustrates the evolution of the ^{71}Ga signal as the temperature decreases.

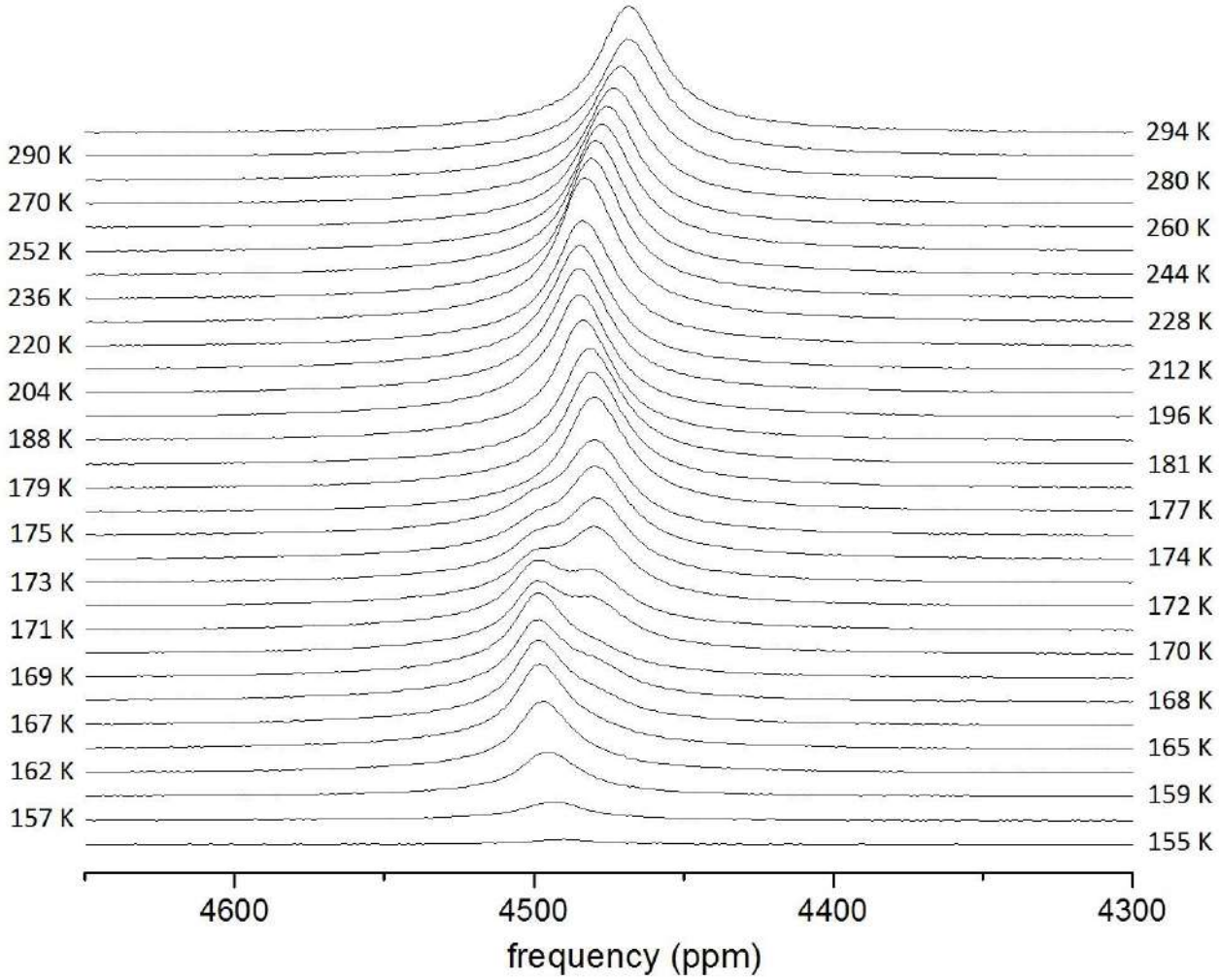

Figure 2.5 - Temperature evolution of the ^{71}Ga NMR signal for the Avance 500 spectrometer. Cooling.

In the temperature range from 165 to 177 K, where a complex line structure was observed, the signal was decomposed from ^{71}Ga into 2 components using baseline correction (fig. 2.6).

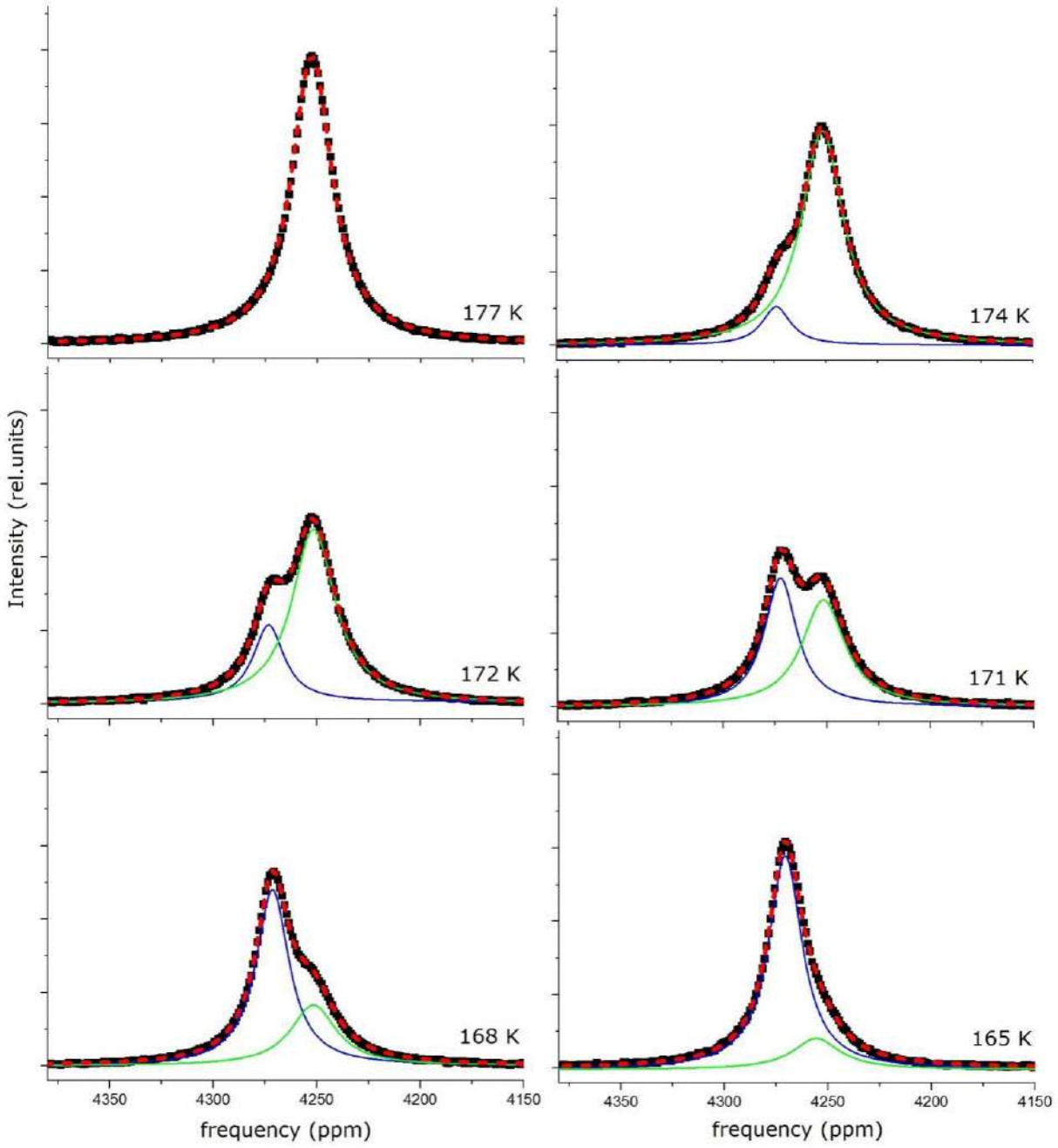

Figure 2.6 - Decomposition of a line into 2 components. The black dots are the experimental spectrum, the red dotted line is the adjustment curve, the green line is the low-frequency component, and the blue line is the high-frequency component.

In figure 2.6, the same scale is used for all plots to demonstrate the increase in the intensity of the high-frequency peak in the region of the NMR signal splitting temperatures. According to this observation, we can talk about the transfer of intensity from a low-frequency peak to a high-frequency peak. This conclusion is confirmed by the graph in figure 2.7, which shows the temperature dependence of the intensity of the NMR signal obtained on the Avance 500 spectrometer for ^{71}Ga and the temperature dependencies of the signal intensities on the components in the temperature range from 151 to 180 K obtained after the decomposition of the line.

The figure shows that in the temperature range of 165 - 175 K, the intensity of the high-frequency signal increases. Figure 2.7 also shows temperature dependency of the NMR signal intensity for ^{115}In.

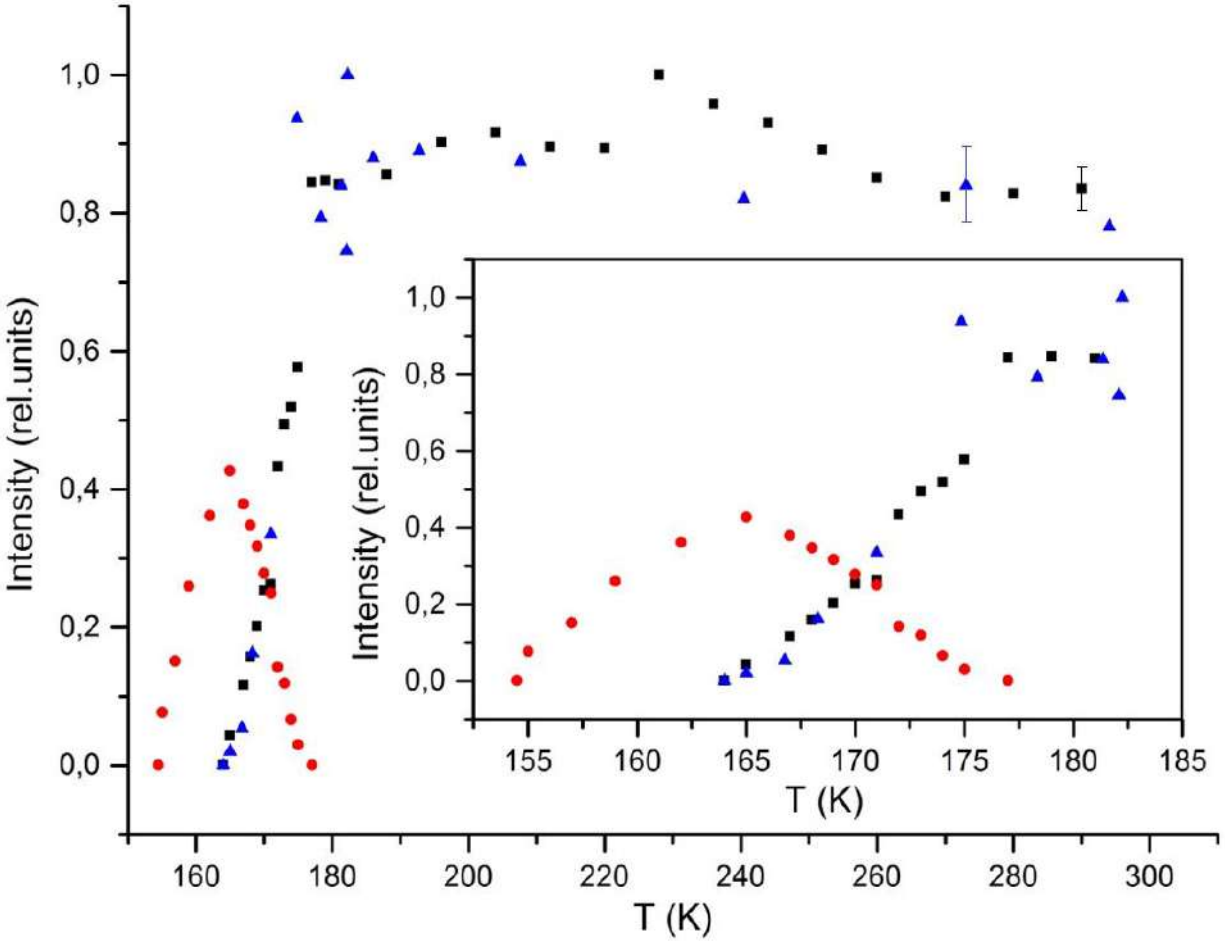

Figure 2.7 - The intensity of the NMR signal depends on the temperature. The black squares are the ^{71}Ga low-frequency component, the red circles are the ^{71}Ga high-frequency component. The blue triangles are ^{115}In. The insert shows the NMR intensity dependencies of ^{71}Ga and ^{115}In in the temperature range 151 - 185 K. Errors are indicated for the most indicative data.

Figure 2.8 shows the temperature dependence of the NMR line position for decomposed components.

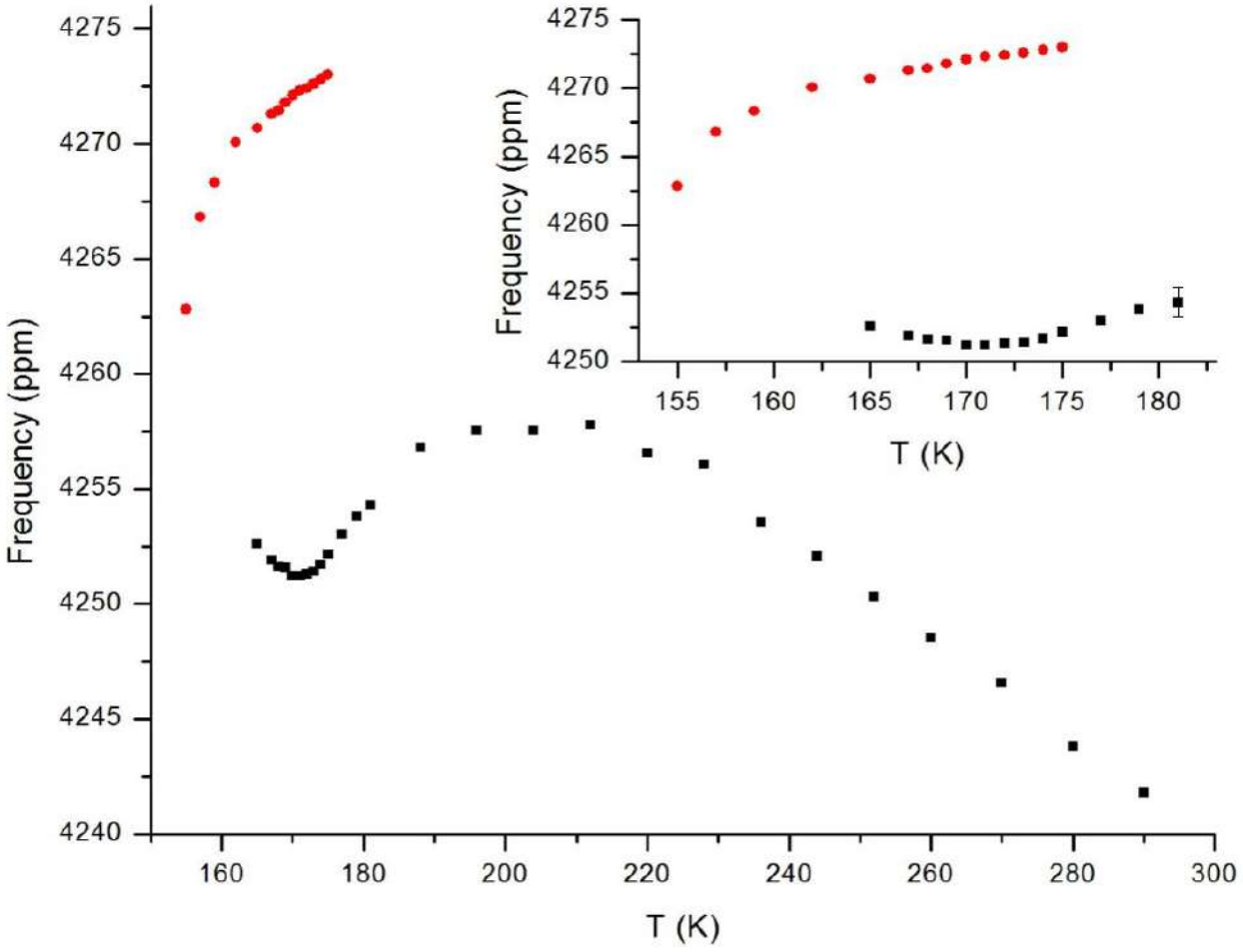

Figure 2.8 - Knight shift dependencies of the ^{71}Ga NMR line in the Ga-In alloy in opal as a function of temperature. The black squares are the low-frequency component, the red circles are the high-frequency component. The insert depicts the temperature dependencies of the Knight shift of the ^{71}Ga NMR signal for the low-frequency (black squares) and high-frequency (red circles) components in the temperature range of 151 - 185 K. Errors are indicated for the most indicative data.

2.4 Temperature dependence of spin-lattice relaxation time

For both gallium isotopes, a spin-lattice relaxation study was carried out and the temperature dependencies of the spin-lattice relaxation times were obtained. For the T_1 measurements, the signal was decomposed into 2 components in the temperature region of the signal splitting. Figure 2.9 shows the recovery of magnetization for the two components at a temperature of 171 K.

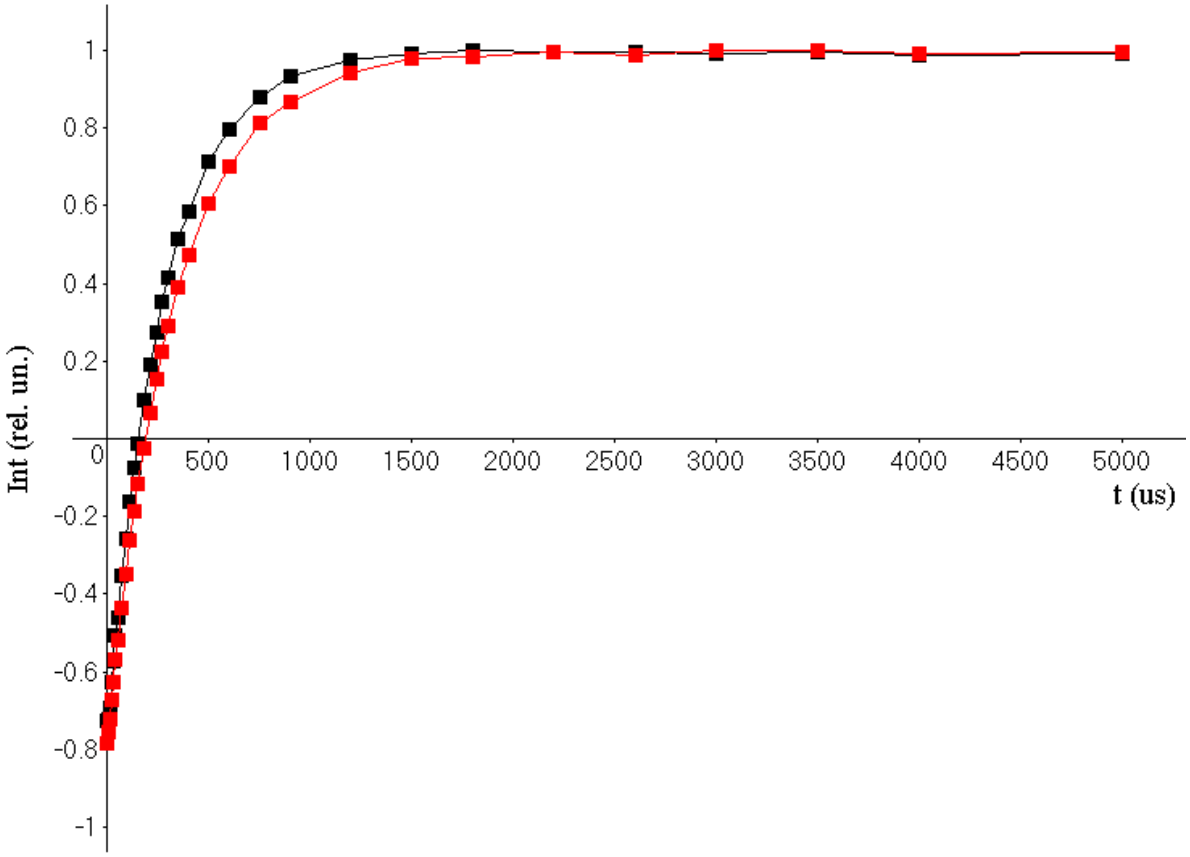

Figure 2.9 - Magnetization recovery for the high-frequency (153.198 MHz – red squares) and low-frequency (153.195 MHz – black squares) components of the ^{71}Ga signal in Ga-In alloy in opal at a temperature of 171 K.

As can be seen from the figure, the low-frequency component recovers faster at the same temperature than high-frequency. Figure 2.10 shows the temperature dependence of the spin-lattice relaxation time for the gallium isotope ^{71}Ga.

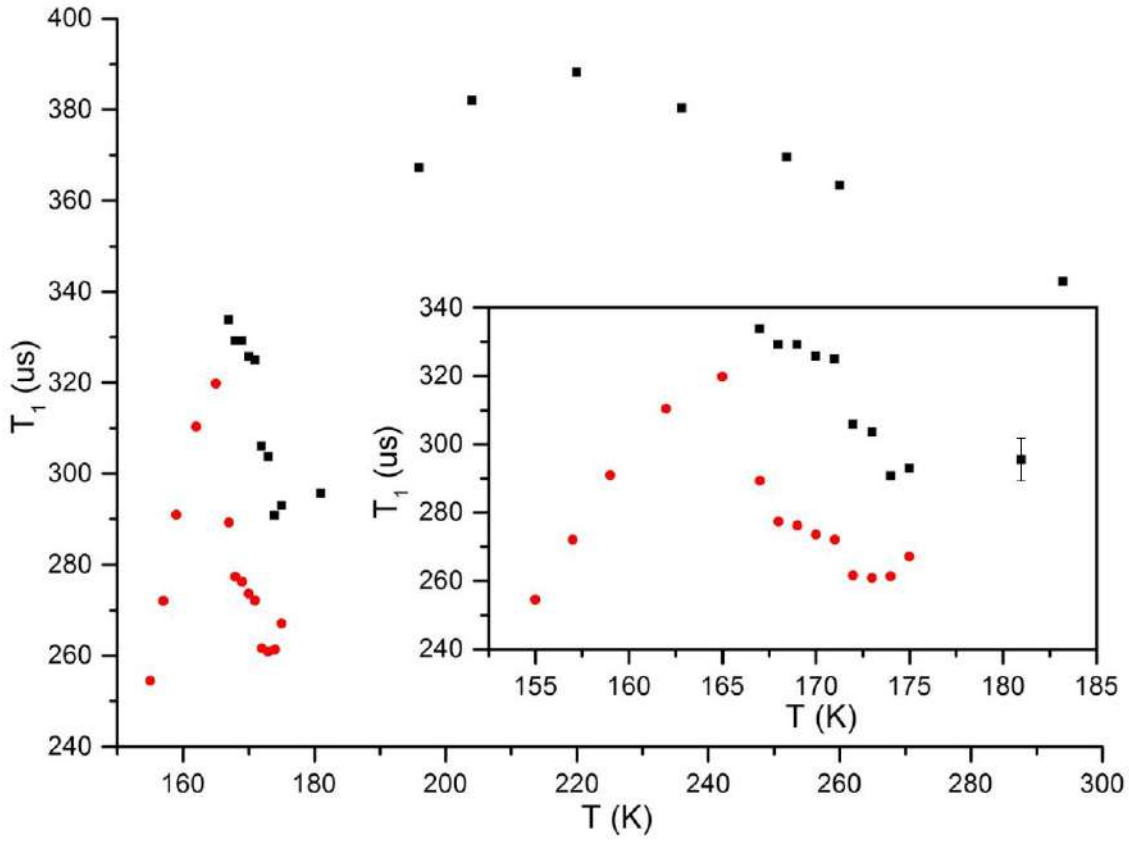

Figure 2.10 - Temperature dependence of time T_1 for ^{71}Ga in Ga-In alloy in opal. The black squares are the low-frequency component, the red circles are the high-frequency component. Errors are indicated for the most indicative data.

2.5 Discussion of results

As the $Ga_{94}In_6$ alloy introduced into the pores of artificial opal cools from room temperature, a single line corresponding to the liquid alloy is observed for the ^{71}Ga isotope in the NMR spectrum. Lower in temperature, at about 175 K, a second component of the NMR signal appears, also corresponding to the liquid alloy. In the temperature range of 165 -175 K, the two components of the NMR signal coexist, below 165 K the signal from the initial melt becomes indistinguishable due to low intensity. According to graphs 2.6 and 2.7, we can talk about the intensity pumping from low-frequency to high-frequency peak. This process takes place against the background of freezing of the eutectic alloy (the total integral intensity of both components falls). At the same time, an interesting fact is that the signal from ^{115} In significantly decreases in intensity in the upper part of the temperature splitting region and becomes indistinguishable at the moment of complete disappearance of the low-frequency component of the gallium signal, while the high-frequency component continues to exist when the temperature drops by about

10 degrees.

Thus, the formation of segregates with an indium structure takes place in the temperature range of about 175-165 K and ends at a temperature of 165 K, at which the intensity of the signal from gallium in the melt decreases only by half. Crystallization of gallium-rich segregates ends at about 155 K.

In order to interpret the peculiarities of the alloy crystallization process in the pores in the samples we examined, we assume that the observed behavior is due, firstly, to a significant shift of the eutectic point towards a lower concentration of indium and, secondly, to the blurring of the alloy crystallization process. The first assumption makes it possible to explain the fact that the signal from indium in the melt becomes indistinguishable at the noise level at a temperature significantly higher than the temperature at the end of crystallization of gallium-rich segregates (about 155 K). The second assumption explains the fact that the decrease in the intensity of the signal from gallium in the melt begins (as well as the crystallization of indium segregates) at about 175 K. Such blurring of phase transitions may be associated with the spread of pore sizes and nanoparticles in the pores, leading to different degrees of ultimate supercooling of the alloy in the pores. In a similar way, it is possible to explain the widening of the temperature area of the formation of gallium segregates below 165 K. In other words, in the process of freezing of the Ga-In alloy in the pores of opal in the temperature range of 175-165 K, a melt with a very low concentration of indium and a melt with a higher concentration of indium coexist. At temperatures below 165 K, the melt with a higher concentration of indium does not remain due to the crystallization of indium segregates, and a melt with a low concentration of indium completely freezes at a temperature well below about 155 K. When heated, judging by the signal intensity and the position of the resonant lines of indium and gallium, the properties of the melt completely coincide with the properties of the melt observed in the process of cooling from room temperature. Thus, due to the reproducibility of the results, we can speak of a reversible process of segregation formation.

It should be noted that the eutectic point shift for nanostructured alloys was previously observed for Ag-Pb and Au-Sb alloys in the works [116; 117]. These papers describe significant changes in the phase diagrams of eutectic binary alloys in the case of nanoscale particles. In particular, in these works, a decrease in the eutectic temperature and a shift in the eutectic point in concentration with a decrease in the diameter of the alloy particles were found.

As shown in Figure 2.7, there is a significant decrease in the crystallization temperatures of the Ga-In alloy in opal for both phases with different concentrations of indium compared to the bulk alloy. Also, in Figure 2.11 it is shown that the melting point of a nanostructured alloy is significantly lower than the melting point of a eutectic Ga-In alloy in the bulk case of α-gallium melting (phase diagram of Fig. 2.4).

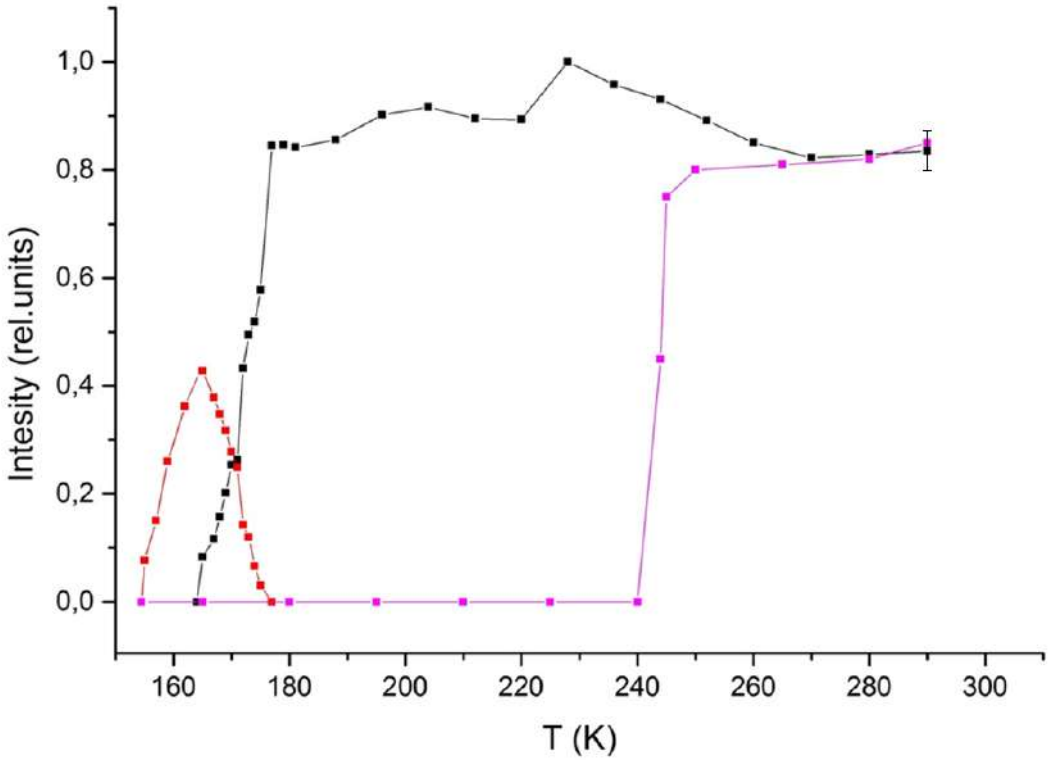

Figure 2.11 - Temperature dependence of the intensity of the ^{71}Ga NMR signal in the Ga-In alloy in opal. The black squares represent the low-frequency component (cooling), the red squares represent the high-frequency component (cooling), and the purple squares represent heating. Errors are indicated for the most indicative data.

Hereinafter, we will designate the phase of a solid alloy consisting of practically pure gallium by the structures of pure gallium in accordance with the phase diagram in Fig. 2.4. Judging by the melting point of the nanostructured Ga-In alloy, it should be assumed that the hysteresis loop "crystallization-melting" observed for the melt corresponds to the formation of β-modification of gallium in the pores.

In the bulk case, the eutectic point for β-gallium corresponds to a concentration of 6.2 at. % indium and the temperature of solidus is equal to 244.2 K. According to our estimates, under nanoconfinement conditions, the eutectic point for crystallization of gallium-rich segregates with a β-Ga structure has shifted to at least 1 at. % indium. At the same time, however, the melting of the alloy in the pores begins at temperatures close to the corresponding temperature of the solidus of the bulk alloy.

Thus, the results obtained indicate a significant change in the phase diagram of Ga-In in opal compared to the phase diagram for bulk alloy. Namely, the melt crystallizes with the formation of stable segregates with only the β-gallium structure. In this case, there is a significant shift in the eutectic point.

An important result obtained in the study of the Ga-In alloy in the pores of opal is the peculiarities of the temperature dependence of the Knight shift for gallium shown in Figure 2.8. There are two possible interpretations of the splitting of the NMR signal into two components under conditions of partial crystallization.

One interpretation is that when indium crystallizes in a Ga-In melt, the Knight shift for gallium should approach the position of the signal from pure gallium in opal. The fact that the Knight shift jump occurs in the crystallization region of almost the entire amount of indium supports this assumption.

The second interpretation is that during the crystallization of indium in the Ga-In alloy, a liquid-liquid phase transition occurs in uncrystallized, almost indium-free gallium. The basis for this assumption is the results obtained in the work [37], which describes a phase transition in supercooled pure gallium introduced into opal. In addition, the liquid-liquid phase transition in gallium has been predicted in theoretical work [38].

We have conducted additional experiments in favor of the liquid-liquid phase transition and against the assumption that the cleavage of the line is due exclusively to the different concentration of indium in the two stratified parts of the melt. The results of these experiments are shown in Fig. 2.12.

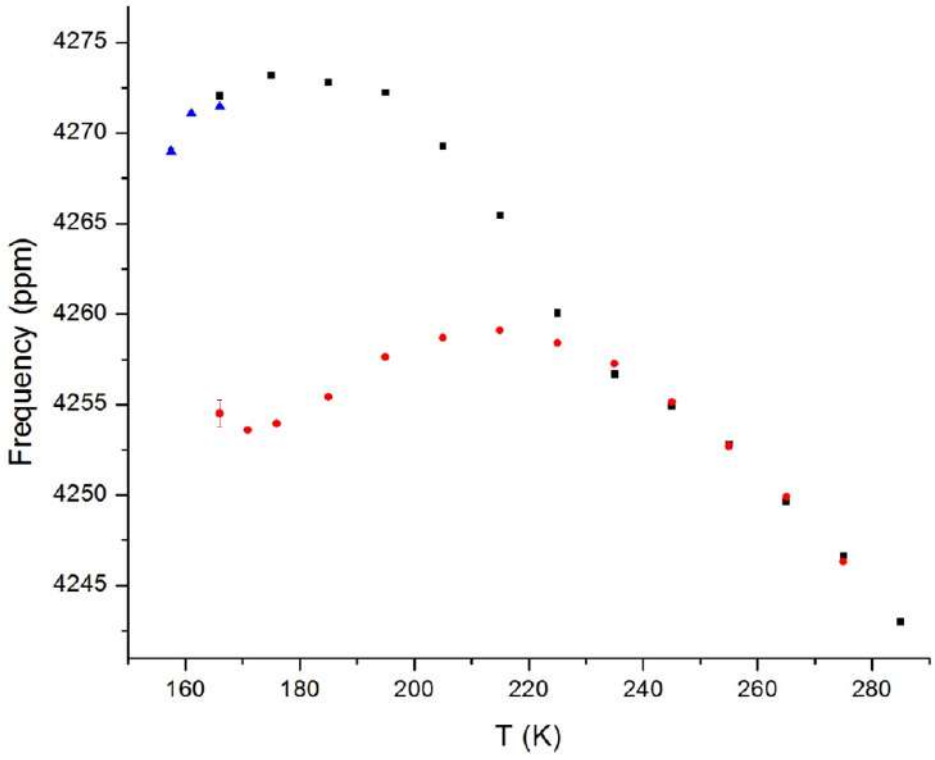

Figure 2.12 - Knight shift temperature dependence for ^{71}Ga in Ga-In alloy in opal. Red circles, blue triangles for cooling, black squares for heating. Errors are indicated for the most indicative data.

If the splitting of the NMR line for ^{71}Ga into two different Knight shift components were due to different concentrations of indium, then in the case of a measurement cycle where we freeze the low-frequency component and indium and, leaving the unfrozen high-frequency component, heat the sample, we would see a jump in the Knight shift towards the low-frequency one during the melting of indium and the frozen part of the gallium (it has been experimentally found that they melt at the same time) Components. But according to graph 2.12, we can see

that according to the Knight shift, the high-frequency component begins to coincide with the points of the low-frequency component, taken during cooling, almost 20 degrees earlier than the melting of indium and the frozen part of the gallium about 244 K. At the same time, no noticeable changes in the Knight shift of the signal from the gallium at the moment of melting of the indium and the crystallized part of the gallium were observed.

In addition, a low-temperature NMR experiment was carried out, in which the signals from Ga and In in the $Ga_{75}In_{17}Sn_8$ alloy injected into the pores of the opal were measured [75]. Similar to the fission in the liquid Ga-In alloy in the opal in the Ga-In-Sn melt, the signal from Ga was split against the background of the total freezing of indium in a temperature range of 225 to 248 K, while at the moment of freezing the indium low-frequency component of the gallium signal also disappeared. But the difference from the behavior of the Ga-In alloy was that Ga-In-Sn had a two-stage decrease in the intensity of the Ga signal and the In signal (Fig. 2.13), and if again the splitting of the gallium line would have been an artifact of the decrease in the concentration of indium, then along with the splitting of the signal from gallium in the temperature range from 225 to 248 K, the splitting would also have occurred at the first drop in the intensity of indium in the temperature range from 260 to 270 K.

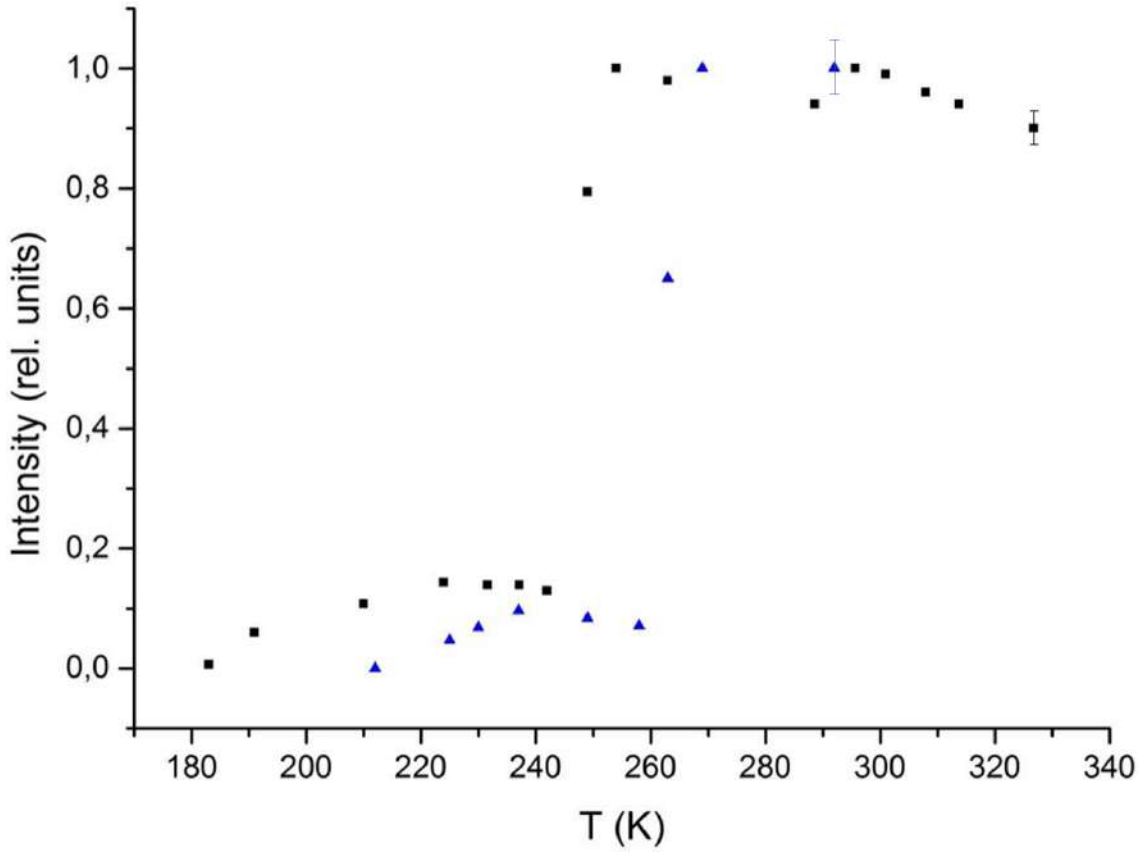

Figure 2.13 - Temperature dependence of NMR signal intensity for ^{71}Ga and ^{115}In in Ga-In-Sn alloy in opal (cooling). Black squares - ^{71}Ga (total line without decomposition into components), blue triangles – ^{115}In. [75]. Errors are indicated for the most indicative data.

Graphs 2.9 and 2.10 show that after an inverting pulse, the high-frequency component recovers more slowly than the low-frequency component. The relaxation rate of the high-frequency component can be slower compared to the low-frequency component, both by increasing the mobility in the melt and by decreasing the quadrupole constant C_q.

The restoration of longitudinal magnetization after an inverting pulse is described by formula 1.9 from Chapter 1:

$$\frac{M(t)}{M_0} = 1 - b \cdot \left(\frac{4}{5} e^{\frac{-C \cdot \tau \cdot t}{1+4 \cdot \omega^2 \cdot \tau^2}} + \frac{1}{5} e^{\frac{-C \cdot \tau \cdot t}{1+\omega^2 \cdot \tau^2}}\right) \cdot e^{\frac{-t}{T_{1m}}} \quad (2.1)$$

where $M(t)$ is the time-dependent magnetization, M_0 is the equilibrium magnetization, (1-b) is the relative magnetization immediately after the inverting pulse, ω is the frequency of Larmor precession, C is the constant, which depends on the structure of the substance under study and is proportional to the square of the quadrupole moment of the nucleus
$C = 2\pi^2 C_q^2 (1 + \eta^2/3)/5$, C_q - quadrupole constant, η - anisotropy, τ is the correlation time of atomic motion.

Using the extreme atomic constriction condition ωτ<<1, the formula for magnetization recovery is simplified:

$$\frac{M(t)}{M_0} = 1 - b \cdot e^{-C \cdot \tau \cdot t} \cdot e^{\frac{-t}{T_{1m}}} \quad (2.2)$$

where the product Cτ has the meaning of the velocity of quadrupole spin-lattice relaxation:

$$R_{1q} = C\tau \quad (2.3)$$

For room temperature, the spin-lattice relaxation rates for both gallium isotopes at different temperatures were decomposed into quadrupole and magnetic components. For this purpose, the system of equations 2.4 was solved:

$$\begin{cases} \frac{R_{1q}^{69}}{R_{1q}^{71}} = \left(\frac{Q^{69}}{Q^{71}}\right)^2 \approx 2{,}51 \\ \frac{R_{1m}^{69}}{R_{1m}^{71}} = \left(\frac{\gamma^{69}}{\gamma^{71}}\right)^2 \approx 0{,}62 \\ R_1^{69} = R_{1q}^{69} + R_{1m}^{69} \\ R_1^{69} = R_{1q}^{71} + R_{1m}^{71} \end{cases} \quad (2.4)$$

Where R_1^{69} is the spin-lattice relaxation rate of ^{69}Ga,
R_1^{71} – spin-lattice relaxation rate of ^{71}Ga,

R_{1q}^{69} – quadrupole contribution to spin-lattice relaxation rate of ^{69}Ga,
R_{1q}^{71} – quadrupole contribution to the spin-lattice relaxation rate of ^{71}Ga,
R_{1m}^{69} – magnetic contribution to spin lattice relaxation rate of ^{69}Ga,
R_{1m}^{71} – magnetic contribution to the spin-lattice relaxation rate of ^{71}Ga.
Further, taking into account that the rate of magnetic relaxation should be linearly dependent on temperature, a line was constructed through the point (0,0) and the value R_{1m}^{71} for the room temperature on the graph R_{1m}^{71} (T), from the slope of which the values R_{1m}^{71} for the remaining temperatures were calculated.

On the basis of the obtained magnetization recovery curves for different temperatures, using the values R_{1m}^{71} calculated for each temperature, the product of the quadrupole interaction constant and the time of correlation of atomic motion were adjusted and estimated, using the formula 2.2. Figure 2.14 shows the temperature dependence of the fitted values of the product Cτ.

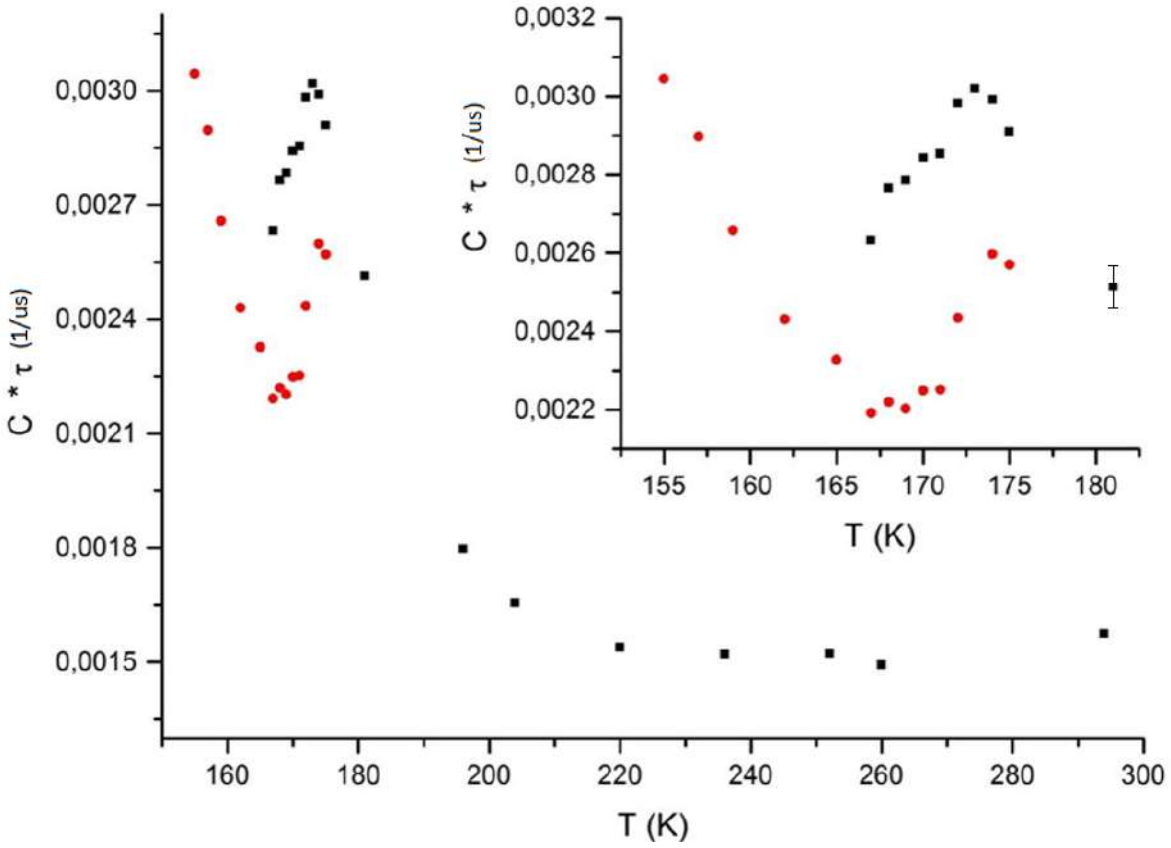

Figure 2.14 - Temperature dependence of the product of the constant C and the time of correlation of atomic motion τ for ^{71}Ga in a Ga-In alloy in opal. The black squares are the low-frequency component, the red circles are the high-frequency component. Errors are indicated for the most indicative data.

The above values of the product Cτ, taking into account the formula 2.2, satisfy the expression 2.5 for each temperature.

$$R_1 = R_{1q} + R_{1m} \quad (2.5)$$

The difference in the values of $C\tau$ for the low-frequency and high-frequency components at the same temperatures can indicate both different mobility in the components of the stratified alloy Ga-In (difference in the correlation times of atomic motion) and the difference in their structures (difference in the constants of the quadrupole interaction).

2.6 Conclusion

Thus, low-temperature NMR studies of the isotopes ^{71}Ga and ^{69}Ga in a liquid gallium-indium alloy introduced into the pores of artificial opal revealed significant differences in the phase diagram of a binary alloy in nanoconfinement from the bulk case. In particular, a shift in the temperature of the eutectic point towards a lower concentration of indium was detected. The results obtained for the melting process of the melt in the pores showed that the segregates, enriched with gallium, they have the structure of β-gallium. In a part of the supercooled melt with a low concentration of indium, a structural liquid-liquid phase transition was detected, similar to the transition in pure supercooled gallium in the pores of opal.

Chapter 3. NMR studies of a phase with the β-gallium structure in the Ga-In alloy within opal matrix

3.1 Introduction

Recently, there has been a renewed interest in the study of the Ga-In eutectic alloy due to the possibilities of its potential application in modern microelectronics, medical diagnostics and soft robotics [9; 10; 11; 118]. Many of the advanced technologies developed in recent decades are based on the application of ultra-thin flexible electronics. Alloy Ga−In, along with gallinstan, is widely used in the creation of elastic electronic elements due to their stable electrical properties (high electrical conductivity and low viscosity) under conditions of mechanical deformations. Also, these alloys are low-toxic and at room temperature they are in a liquid state of aggregation. New ways of using gallium-containing alloys include, among other things, the creation of electronic elements based on thin films and nanowires, as well as on the basis of dendritic nanostructures. The constant desire to reduce the size of electronic elements contributes to the development of the study of the effect of downsizing on the physical properties of gallium-containing alloys. Among the effects observed at the nanoscale for metals and alloys is the reduction of atomic mobility in metal melts [45; 48; 49; 60], liquid-liquid structural phase transition in liquid metals and alloys [37; 74; 75], changes in the position of the solidus and liquidus lines [75; 119], changes in the ultrafine electron-nuclear interaction [46; 78].

For pure gallium, which is predisposed to polymorphism in volume, under conditions of limited geometry, the formation of additional structural modifications that do not form in the bulk case, and stabilization of crystalline phases unstable in volume is observed [44; 120; 121]. Also, for the Ga-In alloy under nanoconfinement conditions, a complex pattern of melting and crystallization was observed with the formation of several segregated phases with a structure different from that of α-Ga [49; 75; 112].

In this work, temperature NMR studies of isotopes ^{71}Ga and ^{69}Ga in the nanostructured alloy eutectic alloy Ga-In injected into the pores of artificial opal, the appearance of a gallium-rich crystalline phase with a β-Ga structure stable in the pores of opal and metastable in the bulk alloy was shown. A simple hysteresis loop of melting-crystallization along with a melting point well below 303 K (melting point of α-Ga) suggested that the Ga-In alloy under nanoconfinement conditions lacks a phase with a structure α-Ga and only the phase with the β-Ga structure occurs (the melting point of β-Ga is approximately 256.5 K in volume [121]). Temperature dependencies of the isotropic shift of the NMR line and quadrupole constants for both gallium isotopes were obtained. It was found that the Ga-In alloy in the pores melted close to the solidus temperature in the bulk alloy

for segregated β-Ga [77]. The temperature dependence of the nuclear spin-lattice relaxation rate for the isotope was also obtained ^{71}Ga, which showed that in the temperature range from 215 to 240 K, relaxation is due to two main mechanisms: quadrupole and magnetic. The temperature dependence of the correlation time of atomic motion was obtained, as well as the activation energy [76].

3.2 Description of the sample and experiment

The investigated sample is described in Chapter 2. Temperature measurements of NMR lines and spin-lattice relaxation times of gallium isotopes ^{71}Ga and ^{69}Ga in the eutectic alloy Ga-In introduced into the pores of artificial opal in the temperature range from 11 K to 293 K were carried out. The studies were carried out on Bruker pulsed NMR spectrometers Avance 400 and Avance 500 with magnetic fields of 9.4 T and 11.7 T, respectively. For measurements on both spectrometers, a low-temperature HPBBLT sensor with Janis cryostat. The Bruker Avance 400 spectrometer also used the HPBBHT wide-line sensor. To avoid temperature overlaps, the rate of temperature change did not exceed 0.5 K/min. Once the temperature had been reached, the specimen was additionally held at this temperature for 20 min before the measurement began. A GaAs crystal was used as a reference sample. To obtain NMR signals from the liquid alloy, a single-pulse sequence with a 90-degree pulse was used. A solid-echo sequence consisting of two 90-degree pulses was used to observe the signals from the solid phase. To measure the spin-lattice relaxation time, a magnetization recovery curve after a 180-degree inverting pulse (inversion recovery method) was obtained.

3.3 Temperature dependencies of isotropic shift and quadrupole constant

In contrast to the crystallization of a gallium-rich phase with a α-Ga structure in a bulk Ga-In alloy with 6 at.% In, for which the liquidus temperature is clearly different from the solidus temperature and is approximately equal to 295.5 K, the liquidus and solidus temperatures in the formation of a gallium-rich phase with a β-Ga structure are approximately the same [111]. Under conditions of limited geometry, the solidus and liquidus temperature lines for the Ga-In alloy are reduced [75; 112], which implies that at room temperature in the test sample, the Ga-In alloy is completely melted. This assumption is supported by the absence of a change in the intensity of the NMR signal of gallium isotopes from the liquid phase when heated from room temperature to 330 K.

For data accuracy, the crystallization of the alloy in pores was studied on the basis of measurements of the intensity of the NMR line of the isotope ^{71}Ga in a liquid alloy, due to the fact that this isotope has a smaller nuclear quadrupole moment and a greater gyromagnetic ratio compared to the isotope ^{69}Ga and whose signal has the best signal-to-noise ratio. The study of the change in the intensity of the NMR line from the liquid Ga-In alloy at a decrease in temperature demonstrated the beginning of the crystallization process at about 175 K and its completion at a temperature of 155 K [75], as evidenced by a drop in the integral intensity of the NMR signal for the isotope ^{71}Ga in a liquid Ga-In alloy to zero. In the cooling process, when about 50% of the melt crystallized, at a temperature of about 160 K, wide NMR lines corresponding to the solid alloy were recorded, having the form of powder spectra for the central transition. The appearance of the lines from the solid phase is consistent with the multidirectionality of the crystallographic axes in the nanocrystals in the pores. The integral intensity of the NMR signal from the solid phase increased rapidly when cooled to 155 K and then gradually increased with further cooling according to Curie law. Upon heating, the NMR signal from the solid phase was observed up to 240 K. This temperature corresponds to the beginning of the rapid stepwise melting of the nanostructured alloy. Figure 3.1 shows an example of an NMR powder line for an isotope ^{71}Ga at a temperature of 180 K.

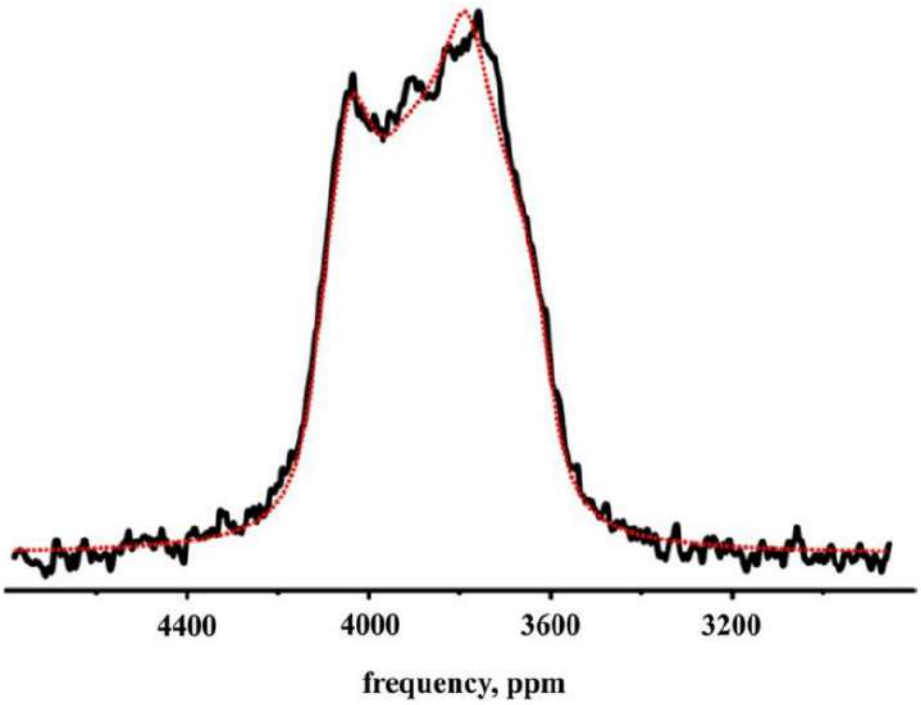

Figure 3.1 - ^{71}Ga NMR line in Ga–In solid alloy at 180 K (solid line) and fitting (dashed line).

The resulting lines were fitted using Avance spectrometers quadrupole

broadening software, since both gallium isotopes, ^{71}Ga and ^{69}Ga, have spin 3/2 and fairly large quadrupole moments of 0.107 and 0.171 b, respectively. An example of fitting is shown in Figure 3.1 as a red dashed line. By means of fitting, the values of the isotropic shift of the NMR line δ_{iso} and the quadrupole constant C_q were obtained. The main contributor to the isotropic shift δ_{iso} is the Knight shift, which is caused by the interaction of the quadrupole moment of the nuclei with conduction electrons. The quadrupole constant is obtained by the formula $C_q = eQV_{ZZ}/h$, where e is the charge of the electron, Q is the quadrupole moment, V_{ZZ} - is ZZ component of the gradient tensor of electric fields in its system of principal axes, and h is Planck constant. Isotropic shift temperature dependencies δ_{iso} and quadrupole constants C_q for the isotopes ^{71}Ga and ^{69}Ga are shown in figures 3.2 and 3.3.

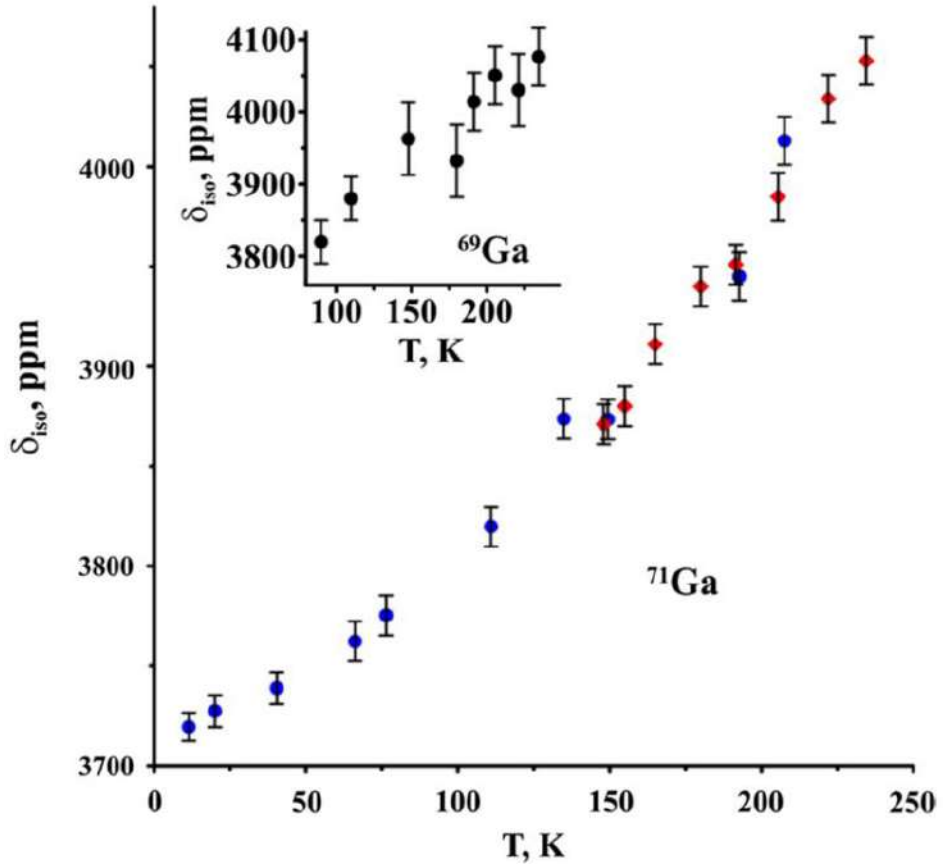

Figure 3.2 - Temperature dependence of the isotropic shift δ_{iso} of the NMR line of the ^{71}Ga isotope in the Ga–In solid alloy. Circles and rhombuses are measurements on the Avance 500 and Avance 400 spectrometers, respectively. The insert is the temperature dependence of the isotropic shift of the NMR line of the ^{69}Ga isotope.

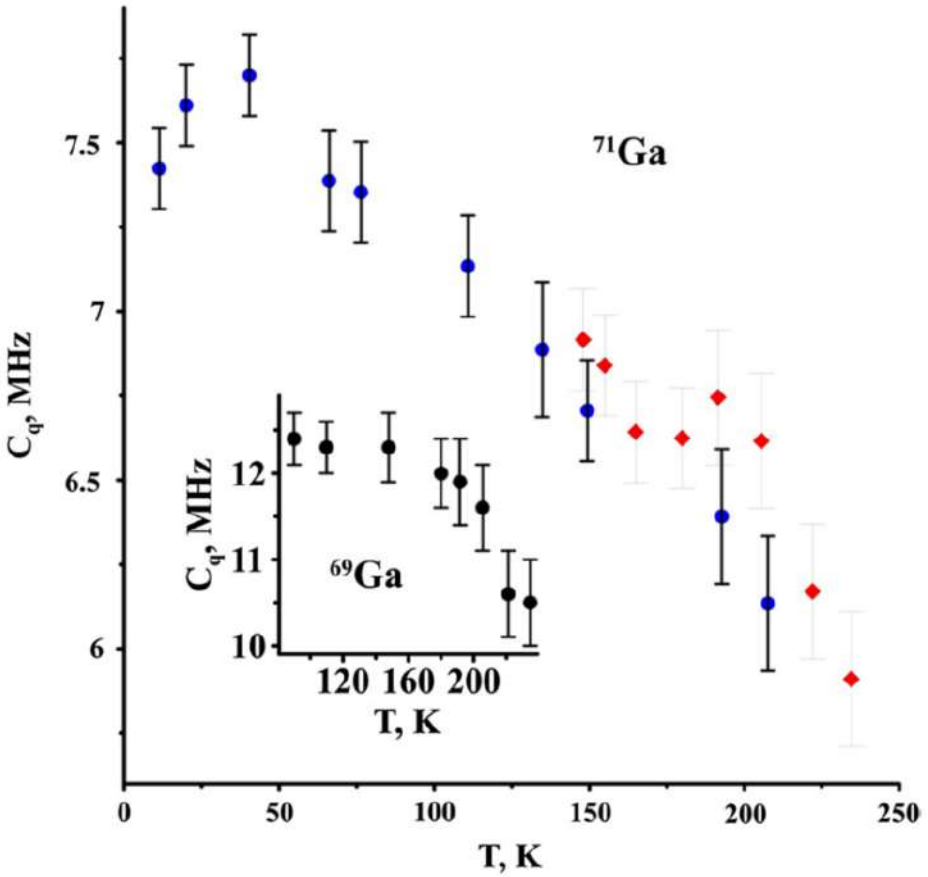

Figure 3.3 - Temperature dependence of the quadrupole constant C_q of the isotope ^{71}Ga in the solid Ga–In alloy. Circles and rhombuses are measurements on the Avance 500 and Avance 400 spectrometers, respectively. The insert is the temperature dependence of the quadrupole constant of the isotope ^{69}Ga.

The isotropic shifts for both isotopes coincided within the error range. The isotropic shift found at the melting point is close to the Knight shift for a liquid Ga-In alloy at a temperature just above the melting point (≈ 4250 ppm) [75]. Though δ_{iso} has never been obtained experimentally for a bulk hard Ga–In alloy, it is known that the structure of an ordinary stable orthorhombic α-Ga differs significantly from the short-range structure of liquid gallium, which in particular explains the decrease in the volume of gallium during melting [122; 123]. This results in a huge difference between the Knight shift for liquid gallium and the isotropic shift for α-Ga [124]. On the other hand, the β-Ga unit cell is monoclinic (space group C2/c) and the near-order β-Ga and liquid gallium are similar [122; 123]. Therefore, the isotropic shift for β-Ga should be close to the Knight shift in a liquid alloy. It can be concluded that the NMR lines from the solid Ga–In alloy correspond to the crystalline phase with the β-Ga structure. In turn, quadrupole frequencies ν_q directly related to the quadrupole constants C_q have been found for β-Ga in ordinary gallium by nuclear quadrupole resonance (NQR) in operation [125].

For cores with spin 3/2 $C_q = 2\nu_q$. Quadrupole constant for isotope ^{71}Ga at a temperature of 77 K, computed from the corresponding quadrupole frequency

found in the paper [125], was equal 7.82 MHz. The data around this temperature in the current paper (figure 3.3) correlate well with the data computed from the [125], although the C_q values we obtained slightly different to the lesser side. In work [125] the temperature dependence of the quadrupole frequency for the isotope ^{69}Ga was obtained over a temperature range of 77 K to a melting point of β-Ga (256.8 K). As the temperature increased, the quadrupole frequency decreased and corresponded to the quadrupole constant C_q around 235 K approximately equal to 10.8 MHz, which is very close to the value in the current work. Comparison of our data for quadrupole constants with those computed from the work [125] confirm the assumption that the NMR line from the Ga-In solid alloy under nanoconfinement conditions belongs to the segregated phase with the β-Ga structure. It should be noted that the quadrupole frequencies in β-Ga turned out to be significantly lower than in the stable α-Ga [126]. According to our measurements, the alloy in the nanopores completely melted at a temperature of 245 K, which is consistent with [75]. This temperature is close to the solidus temperature (244.4 K) in the bulk Ga-In alloy, which corresponds to the emergence of the β-Ga structure [111]. This fact demonstrates that the dimensional effects of alloy melting are small against the background of experimental error. NMR signals from other solid gallium structures were not observed, due to the fact that for α-Ga quadrupole coupling is much stronger and NMR lines are significantly wider. Also, the melting in the Ga-In alloy injected into the pores of the opal is quite abrupt and occurs in a single step, which is also reported in the paper [75], suggesting that a single gallium-rich crystalline modification is present in the opal matrix. Therefore, it can be concluded that there is no segregated phase with a α-Ga structure in the pores of artificial opal. The formation in small droplets and nanoparticles of various crystalline modifications other than bulk has been repeatedly reported ([120; 127] and links therein). In [112] acoustic and NMR measurements of Ga-In alloys of various concentrations were carried out, where complex melting-crystallization hysteresis loops were also demonstrated, indicating the formation of several gallium-rich crystalline modifications. In the current study, the formation of only the β-Ga structure in the Ga–In alloy under opal nanoconfinement conditions is presented for the first time. The results shown in figures 3.1-3.3 were fully reproduced in different cooling-heating temperature cycles and did not change over time over a period of two years. This confirms that opal nanoconfinement stabilizes the gallium-rich phase with a β-Ga structure in the Ga–In alloy. The effect of size reduction on crystalline phases has been observed for various substances such as water, sodium, silver, and some oxides [128; 129; 130; 131; 132]. However, there is little evidence of size-induced polymorphism. The present studies provided new information regarding the appearance of stable polymorphic phases for the Ga-In alloy under nanoconfinement conditions.

3.4 Temperature dependence of spin-lattice relaxation rate, correlation time and activation energy of atomic motion

Similar to the isotope ^{71}Ga -based alloy crystallization study, due to the higher signal-to-noise ratio compared to the ^{69}Ga isotope, spin relaxation was also investigated for the ^{71}Ga isotope. In the temperature range of 125-240 K, the magnetization recovery curves within the error range are described by a single exponent. Figure 3.4 shows examples of magnetization recovery curves for temperatures of 150 and 235 K.

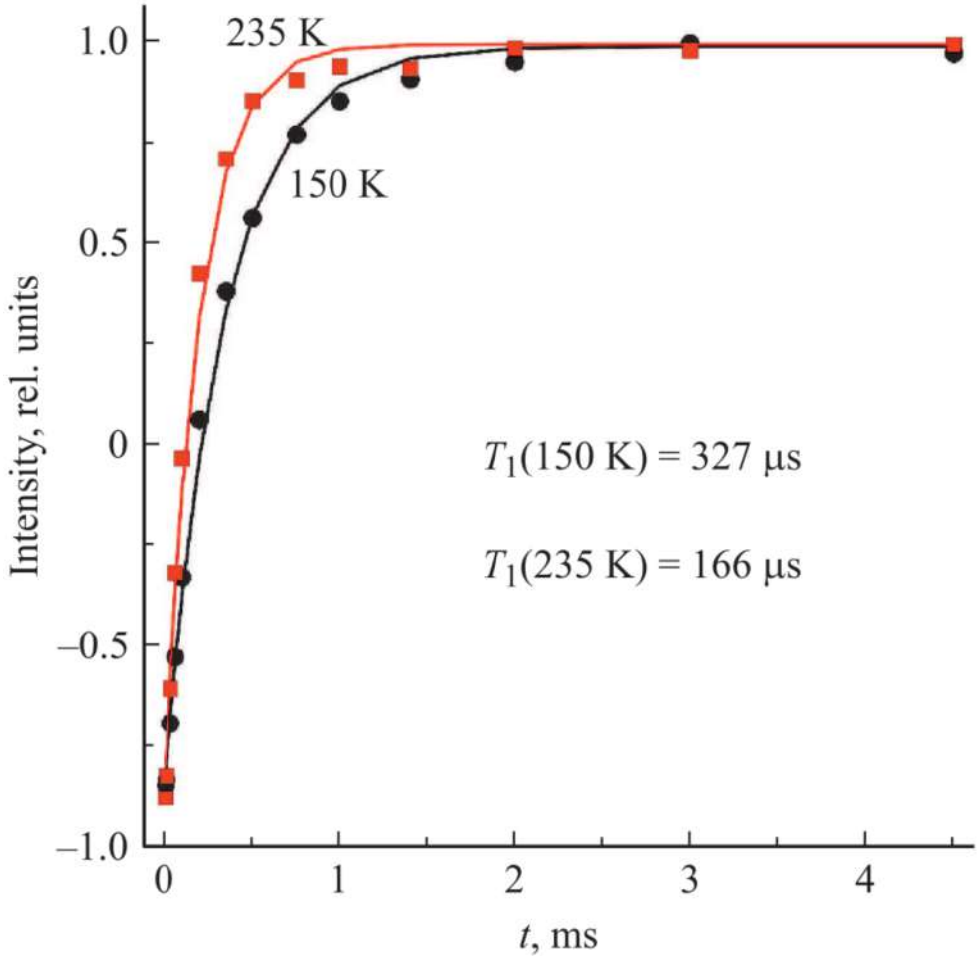

Figure 3.4 - Recovery of the ^{71}Ga NMR line after exposure to an inverting pulse at temperatures of 150 K (circles) and 235 K (squares). Solid lines are exponential fits.

Figure 3.5 shows the temperature dependence of the calculated values of the spin-lattice relaxation rate $1/T_1$.

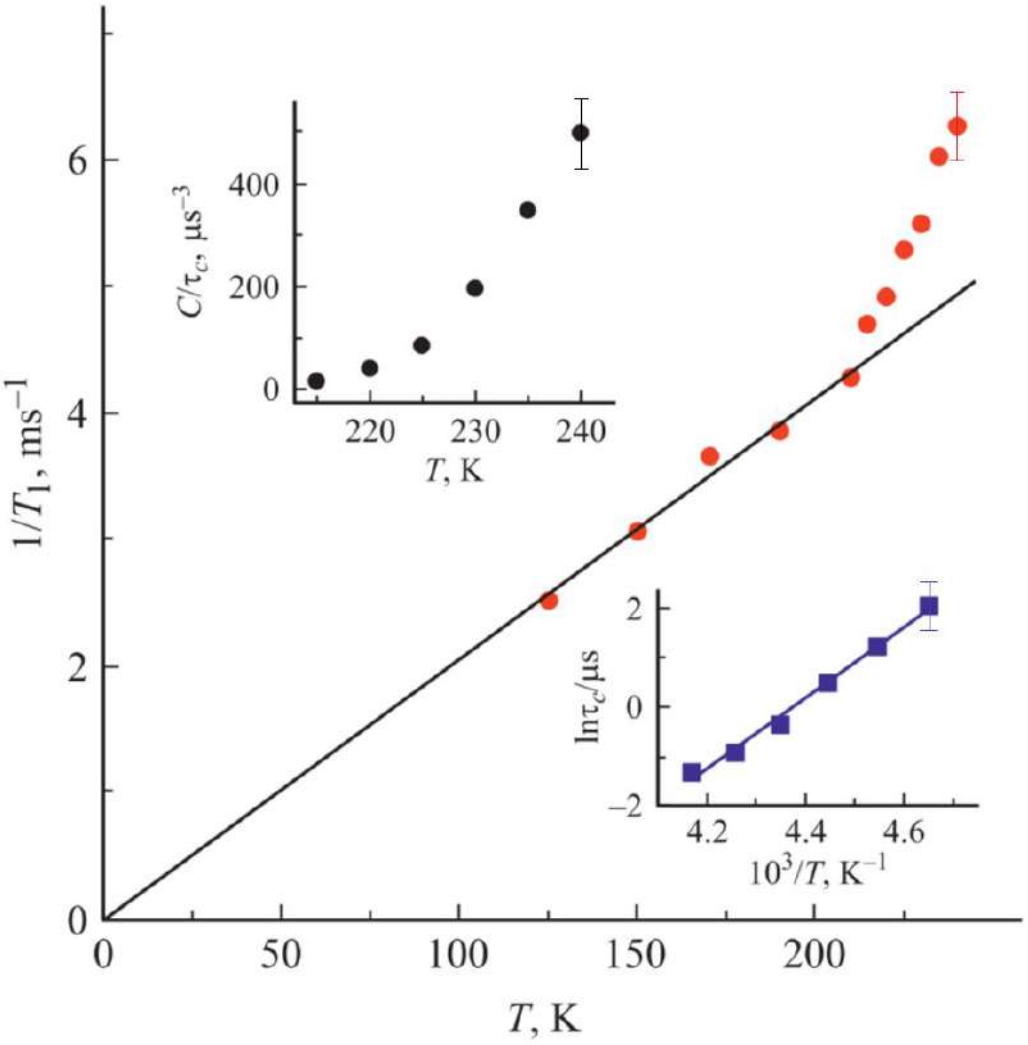

Figure 3.5 - Inverse time of spin-lattice relaxation $1/T_1$ of the gallium isotope ^{71}Ga as a function of temperature. The top insert is the temperature dependence of the C/τ_c ratio. The bottom insert is the Arrhenius graph for τ_c. Errors are indicated for the most indicative data.

At temperatures below 215 K, the spin-lattice relaxation rate demonstrates a linear dependence on temperature. Above 215 K, there is a significant deviation from the linear dependence in the direction of increasing values. For nuclei with a non-zero electric quadrupole moment in conductors, nuclear spin-lattice relaxation occurs due to two main mechanisms: the interaction of nuclear magnetic moments with conduction electrons and the interaction of quadrupole moments of nuclei with dynamic gradients of electric fields resulting from the motion of atoms [60; 133]. At low temperatures, as a result of the slowing down of the motion of atoms, the quadrupole contribution to spin-lattice relaxation becomes negligible. The rate of magnetic dipole relaxation is directly proportional to temperature [133].

Figure 3.5 shows the dominance of the magnetic dipole mechanism of spin-lattice relaxation for a phase with a β-Ga structure below 215K. The dependence of spin-lattice relaxation time on temperature is described by the equation

$$\frac{1}{T_{1m}(T)} = AT \qquad (3.1)$$

where A = 21 $s^{-1}K^{-1}$. Above a temperature of 215 K, the quadrupole contribution to spin-lattice relaxation increases significantly. The use of the concept of relaxation time to present experimental data over the entire temperature range of the study is due to the proximity of the NMR line restoration to the exponential dependence in this work, as well as in the [134], despite the fact that, in general, quadrupole relaxation for spin 3/2 is not exponential [99].

The magnetization recovery curve with time t due to the mechanisms of magnetic dipole and electric quadrupole relaxation is described by the expression (1.9) from Chapter 1 [60]

$$I(t) = 1 - b\exp\left(-\frac{t}{T_{1m}}\right)\left[0.8\exp\left(-\frac{C\tau_c t}{1+4\omega_0^2\tau_c^2}\right) + 0.2\exp\left(-\frac{C\tau_c t}{1+\omega_0^2\tau_c^2}\right)\right] \qquad (3.2)$$

where I(t) is the intensity, C is a constant proportional to the square of the quadrupole moment and is equal to $C = 2\pi^2 C_q^2(1+n^2/3)/5$, τ_c is the correlation time of atomic motion, ω_0 is the Larmor frequency, b is the numerical coefficient that takes into account the partial inversion of magnetization. For the solid alloy, it is assumed that the condition $\omega_0\tau_c \gg 1$ is satisfied. Given the approximation of slow atomic motion, expression (3.2) is converted to the form

$$I(t) = 1 - b\exp\left(-\frac{t}{T_{1m}}\right)\left[0.8\exp\left(-\frac{C}{\tau_c}\frac{t}{4\omega_0^2}\right) + 0.2\exp\left(-\frac{C}{\tau_c}\frac{t}{\omega_0^2}\right)\right] \qquad (3.3)$$

Approximation by means of expression (3.3) of the experimental curves of magnetization recovery after inversion in the temperature range of 215-240 K was obtained the temperature dependence of the ratio C/τ_c. It was taken into account that $\omega_0/2\pi$ = 122MHz, and the magnetic relaxation time T_{1m} was obtained from equation (3.1). Temperature dependence of the C/τ_c ratio is shown in the top insert in figure 3.5. To obtain the temperature dependence of the correlation time of atomic motion τ_c, the values of C were used, which in turn were calculated from the values of C_q obtained in Section 3.3. The temperature dependence $\tau_c(T)$ is shown in the lower insert of figure 3.5. The value of the quadrupole constant is weakly dependent on the temperature in the temperature range of 215-240 K. However, this de-

pendence was taken into account when obtaining the values τ_c. Atomic motion has a thermoactivation character, and the correlation time of atomic motion is described by the expression

$$\tau_c = \tau_0 \exp\left(\frac{E_a}{k_B T}\right) \quad (3.4)$$

where E_a is the activation energy, k_B is the Boltzmann constant, and τ_0 is the correlation time of atomic motion in the high-temperature limit. Dependency ln τ_c from the reverse temperature of 1/T according to expression (4) linear (lower insert in Figure 3.5). Slope coefficient of the graph ln τ_c(1/T) gives the activation energy value E_a = 7200 K = 0.62 eV. Due to the fact that data on diffusion in solid bulk gallium or a Ga-In alloy with a β-Ga structure have not been previously obtained, the results in the current work can only be compared with data for other hard metals. Obtained value of atomic motion correlation time τ_c = 0.27 μs at 240K belongs to the range of values observed for bulk metals and alloys below melting point [135]. Correlation Time Derived from Diffusion Coefficient [136], at a temperature close to the melting point, differs upwards from τ_c at a temperature of 240 K in the present work by more than two orders of magnitude. On the other hand, for a single sodium crystal near the melting point, the correlation time of atomic motion is two orders of magnitude shorter than the τ_c value obtained in the current work for the phase with the β-Ga structure under nanoconfinement conditions at a temperature of 240 K. Hence, it can be assumed that the introduction of the alloy into the pores does not lead to significant anomalies of atomic mobility in the solid phase of segregates with the β-Ga structure.

3.5 Conclusion

NMR studies of the isotopes ^{71}Ga and ^{69}Ga in the nanostructured eutectic alloy Ga–In injected into the pores of the opal matrix demonstrated the emergence of a gallium-rich crystalline phase with a β-Ga structure. This phase was found to be stable under nanoconfinement conditions, while it is metastable in volume. It should be noted that the NMR line from the aggregate of particles with the α-Ga structure cannot be observed due to the large the value of the quadrupole constant and, accordingly, a strong broadening of the resonance line, even if such a structure is formed in the pores. However, the single-step view of the crystallization-melting hysteresis loop suggests that only the phase with the β-Ga structure is present in the Ga-In solid alloy in the opal nanoconfinement. The temperature de-

pendencies of the isotropic shift of the NMR line δ_{iso} and the quadrupole constants C_q for both isotopes of gallium in solid alloy were obtained. It was found that the nanostructured alloy completely melted at a temperature of 245 K, close to the solidus of the bulk Ga–In alloy for β-Ga segregation.

NMR measurements of the nuclear spin-lattice relaxation rate in the solid segregated phase of a nanostructured Ga−In alloy with a β-Ga structure have shown that in the temperature range of 215-240 K, relaxation is due to two main mechanisms: the interaction of nuclear quadrupole moments with dynamic gradients of electric fields arising during the movement of atoms and the interaction of magnetic moments of nuclei with conduction electrons. In a given temperature range, the correlation time decreased from 7.9 to 0.27 μs. The activation energy of atomic motion E_a = 7200 K = 0.62 eV was calculated.

Chapter 4. Atomic mobility in a Ga-In-Sn ternary eutectic alloy

4.1 Introduction

In recent years, there has been a significant increase in the number of studies on gallium-containing binary alloys and a triple alloy based on gallium, indium and tin (Ga-In-Sn). This is due to the active implementation of these alloys in various practical areas of application. Much less work is devoted to the study of the Ga-In-Sn triple alloy, as well as to other triple alloys, than to the study of binary alloys. According to the phase diagram of the Ga-In-Sn alloy (figure 4.1) [137], which is a phase diagram of the eutectic type, the concentration of the alloy corresponding to the eutectic point is 75 at.% Ga, 17 at.% In and 8 at.% Sn.

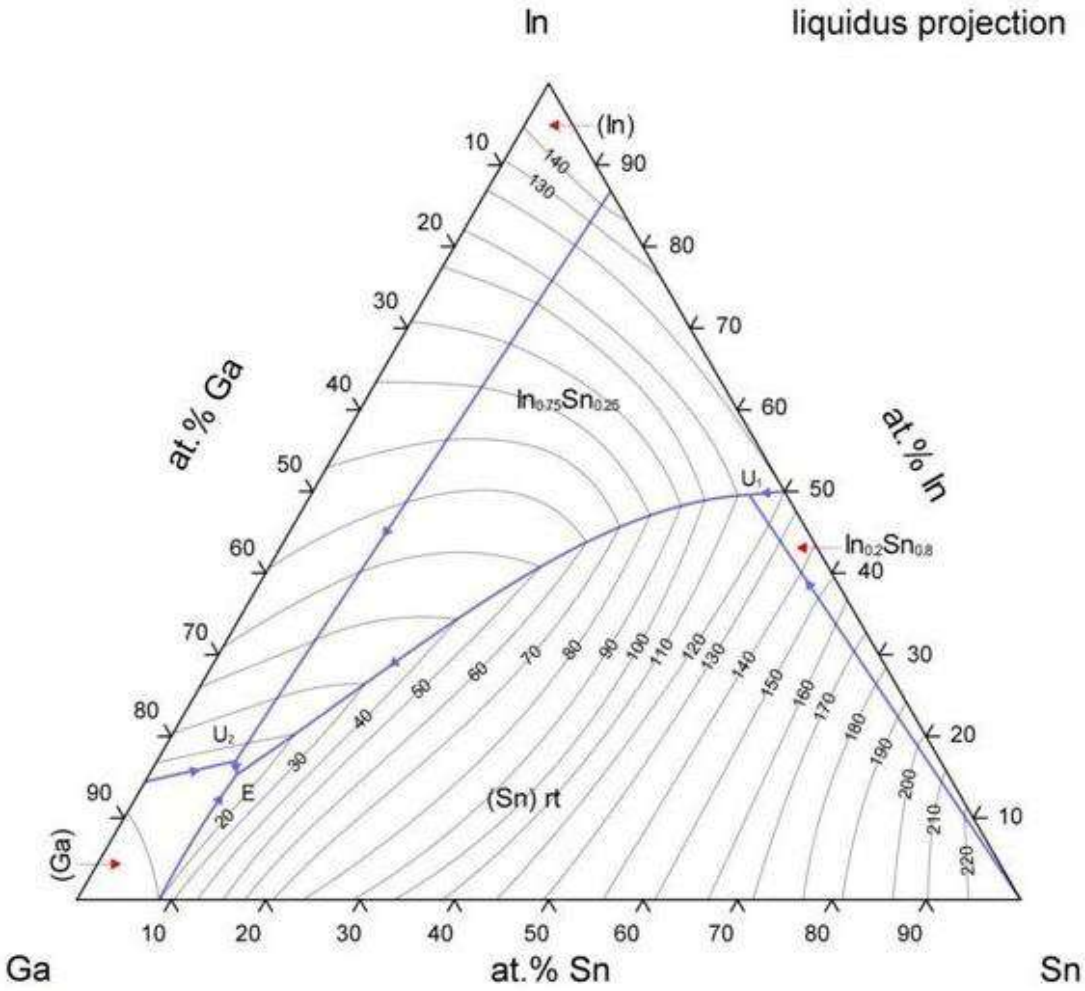

Figure 4.1 - Phase diagram of a ternary Ga-In-Sn alloy. [137]

The melting point of the alloy at the eutectic point is about 285 K [137]. In industry, Ga-In-Sn alloy is usually used, with an unknown exact concentration of components and the name "Galinstan" (The trademark belongs to a German com-

pany Geratherm Medical AG.[50]). An interesting fact is that the declared melting point of galinstane is much lower than the melting point of an alloy of eutectic composition and is equal to 254.15 K. It is assumed that such an effect of a significant reduction of the melting point can be achieved by adding a small amount of such metals as Bi to increase flow and Sb to improve oxidation stability [138]. It has also become customary to call any eutectic alloy of similar composition galinstan. Galinstan, due to its non-toxicity and very low vapour pressure (10^{-6} at 773.15 K) has a great advantage over mercury in the application in the various applications where it is used, and is gradually beginning to replace it primarily in household thermometers [51]. Galinstan is also a substitute for mercury in many applications where liquid metals are used, such as biotechnology [51], in electromechanical relays [52], as a coolant [53] and in ionic sources [54]. In addition, galinstan is beginning to be used in micromechanical systems [55; 56; 57; 58], but due to rapid oxidation, the introduction of galinstan into this application is slow [139]. In connection with the prospects for the use of Ga-In-Sn alloy in nanocomposites, the study of the effect of nanoconfinement on such alloy properties as atomic diffusion and viscosity is becoming more and more relevant. In works [48; 49; 60] studies of liquid Ga and binary liquid alloys Ga–Sn and Ga–In, introduced into nanoporous matrices, were carried out by the method of nuclear magnetic resonance, and a significant increase in the correlation time of atomic motion compared to the bulk case was found. The effect of size constraints on the Ga-In-Sn triple alloy has not been investigated until now.

In the present study, the effect of nanoconfinement on the atomic mobility of a Ga-In-Sn melt introduced into three nanoporous matrices with different pore shapes and sizes was studied using the NMR method [61].

4.2 Samples and experiment

The samples for this study were nanocomposites based on a triple Ga-In-Sn alloy of eutectic composition introduced into an opal matrix with an average diameter of amorphous silica balls of 210 nm and into porous glasses of two types: with an average pore diameter of 7 and 18 nm. Artificial opal is described in Chapter 2. It is worth noting that for the opal used in this study, with a ball diameter of 210 nm, the octahedral and tetrahedral cavities should be about 87 and 47 nm respectively, according to the mathematical model, but as mentioned in Chapter 2, the pores become slightly smaller when sintered. As with the opal matrix described in Chapter 2, the sizes of the opal balls in this study were obtained using atomic force microscopy.

The porous glasses used as nanoporous matrices in this study were a scaffold of amorphous silica with a connected network of cylindrical-like pores. The process of creating nanoporous glasses consists in the preparation of a sodium-

borosilicate mixture at high temperatures, liquation and further leaching of sodium and boron from the cooled workpiece.

After leaching, the pore diameter was measured and then a liquid Ga-In-Sn alloy was injected into the pores at a pressure of approximately 10 kbar. For the accuracy of the measurement, the pore size was determined using two types of porometry: nitrogen and mercury. Pieces of approximately 0.2 cm^3 were cut from the filled porous glasses. The surface of the cut pieces was carefully cleaned of alloy droplets to exclude the signal from the bulky substance. The pore fill factor for all samples was approximately 80% and was measured by weighing nanoporous matrices before and after the alloy was injected into the pores. Also, for comparison, a bulk Ga-In-Sn alloy of the same composition that was introduced into nanoporous matrices was measured. Nuclear magnetic resonance was used to measure spin-lattice relaxation and Knight shift times for gallium isotopes ^{71}Ga and ^{69}Ga, as well as the indium isotope ^{115}In. The studies were carried out at room temperature in three different magnetic fields of 9.4, 11.75 and 17.6 T to construct dependencies on the quantizing magnetic field. The NMR spectrum was obtained by means of the Fourier transform of the free induction decay signal after 90° pulse. To measure the spin-lattice relaxation time, a pulse sequence called "inversion recovery" was used, in which a 180° pulse inverts the nuclear magnetization and becomes counterdirected to a constant magnetic field. Then, at certain intervals specified in a special list in the pulse sequence program, a 90° pulse is applied to remove the free induction decay and a Fourier transform is applied to the received signals. Based on the obtained spectra, the NMR signal intensity is plotted from the time between the applied 180° and 90° pulses, and the spin-lattice relaxation time T_1 is calculated from the adjustment of the resulting longitudinal magnetization recovery curve. To improve the signal-to-noise ratio, from 2,000 to 16,000 scans were used in one experiment. A single GaAs crystal was used as a reference for gallium isotopes, and an $In(NO_3)_3$ molar salt solution was used for indium. Also, based on the data obtained, the correlation time of atomic motion τ_c was calculated.

As mentioned in the review, the gradient technique of NMR, which is widely used for the analysis of diffusion processes in non-metallic liquids, is widely used [96] It is not applicable to molten metals due to the short times of nuclear spin relaxation, and due to the decrease in the diffusion rate as a result of nanostructuring, the neutron scattering method also becomes uninformative [98]. It should also be emphasized that the method we use provides information about the change in mobility within individual pores, whereas the gradient NMR technique provides information about the movement of atoms between pores.

4.3 Results of the study of atomic mobility in the Ga-In-Sn eutectic alloy

For all the studied alloy nuclei, a broadening of the NMR line with a decrease in pore size was observed. For example, in a magnetic field of 9.4 T, the indium resonant line was widened from 23 ppm for a bulk sample to 280 ppm for an alloy in porous glass with a pore diameter of 18 nm.

Another effect that occurs with an increase in the degree of nanoconfinement is a downward displacement of the NMR lines for all isotopes. As an example, figure 4.2 shows the NMR lines of the ^{71}Ga isotope in the 9.4 T field for all samples examined.

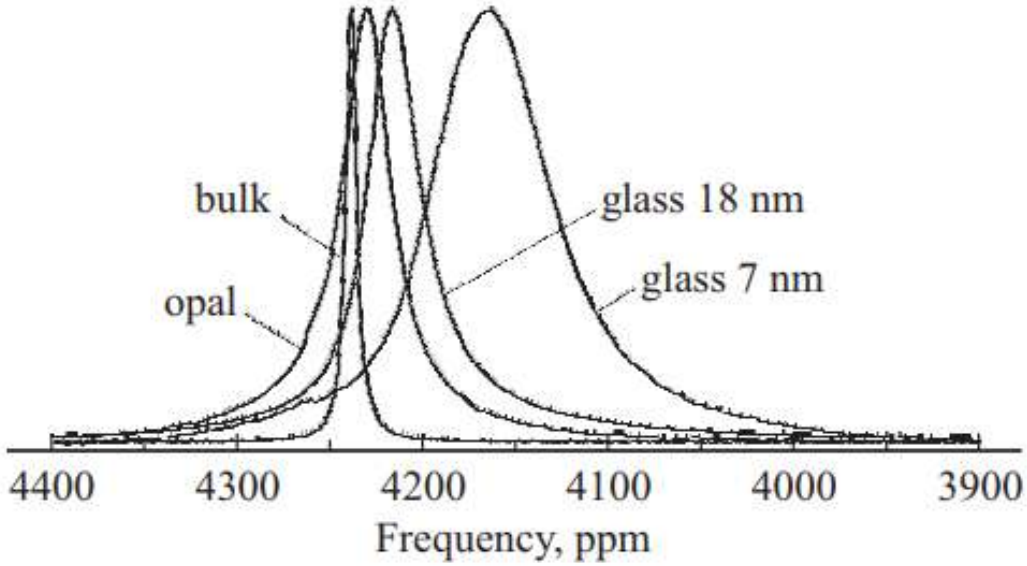

Figure 4.2 - NMR spectra of the isotope ^{71}Ga in bulk alloy Ga-In-Sn and alloy introduced in opal and porous glasses with pore sizes of 7 and 18 nm measured in a field of 9.4 T.

According to the figure, the smallest Knight shift has an alloy line in porous glass of 7 nm, which is equal to 4163 ± 5 ppm, which is about 80 ppm less, than the largest Knight shift for the available specimens corresponding to the bulk alloy. Tables 4.1 to 4.3 show all Knight shift measurements. Due to the significant broadening of the signal, indium measurements were made only for samples in porous glass with a pore diameter of 18 nm and in opal in magnetic fields of 9.4 and 11.75 T.

Table 4.1 - Knight shift K, longitudinal relaxation time T_1 and quadrupole relaxation time T_{1Q} for the isotope ^{71}Ga in Ga-In-Sn alloy in bulk sample, opal, nanoporous glasses with pore diameters of 18 and 7 nm in various magnetic fields with induction B.

Sample	Bulk	Opal			Glass 18 nm			Glass 7 nm		
B, T	9.4	17.6	11.75	9.4	17.6	11.75	9.4	17.6	11.75	9.4
K, ppm	4238 ± 1	4235 ± 1	286 ± 10	290 ± 20	4231 ± 3	265 ± 10	266 ± 10	4163 ± 5	120 ± 20	110 ± 20
T_1, μs	437 ± 5	290 ± 20	560 ± 40	570 ± 80	259 ± 10	480 ± 40	490 ± 40	130 ± 20	150 ± 30	140 ± 30
T_{1Q}, μs	2500 ± 300	570 ± 80			470 ± 30			170 ± 30		

Table 4.2 - Knight shift K, longitudinal relaxation time T_1 and quadrupole relaxation time T_{1Q} for the isotope ^{69}Ga in Ga-In-Sn alloy in bulk sample, opal, nanoporous glasses with pore diameter of 18 and 7 nm in different magnetic fields with induction B.

Sample	Bulk	Opal			Glass 18 nm			Glass 7 nm		
B, T	9.4	17.6	11.75	9.4	17.6	11.75	9.4	17.6	11.75	9.4
K, ppm	4239 ± 1	4233 ± 1	174 ± 15	164 ± 15	4229 ± 5	180 ± 20	170 ± 20	4159 ± 8	50 ± 20	50 ± 20
T_1, μs	483 ± 5	180 ± 20	210 ± 20	220 ± 20	180 ± 20	220 ± 20	210 ± 30	70 ± 20	60 ± 20	50 ± 20
T_{1Q}, μs	1000 ± 100	220 ± 30			220 ± 30			80 ± 20		

Table 4.3 - Knight shift K, longitudinal relaxation time T_1 and quadrupole relaxation time T_{1Q} for isotope ^{115}In in Ga-In-Sn alloy in bulk sample, opal, nanoporous glass with pore diameter of 18nm in different magnetic fields with induction B.

Sample	Bulk	Opal		Glass 18 nm	
B, T	9.4	11.75	9.4	11.75	9.4
K, ppm	8431 ± 1	8409 ± 10		8401 ± 10	
T_1, μs	170 ± 5	62 ± 7	61 ± 7	57 ± 7	53 ± 7
T_{1Q}, μs	370	78		70	

Like most bulk liquid metals and alloys [83], the recovery of longitudinal magnetization for the nuclei studied in the bulk melt studied in the current work was uniexponential and could be described by the spin-lattice relaxation time T_1. For each sample, the spin-lattice relaxation times were the same in different mag-

netic fields within the error range. The fact that the restoration of longitudinal magnetization after an inverting pulse can be described by a single exponent, and that the value of the spinlattice relaxation time is the same in different magnetic fields, suggests that an approximation of extreme constriction is being performed, which is also evidenced by narrow NMR lines. As described in the works [48; 49; 60], for some liquid metals and binary alloys under nanoconfinement conditions, there is a significant increase in the correlation time of atomic motion τ_c and at the same time, the approach of extreme narrowing begins to be disrupted. According to the estimate τ_c as shown in the section below, for specimens in opal and glass with a pore diameter of 18 nm, the approximation of extreme constriction is still performed. Similar to the bulk case, spin-lattice relaxation in alloys introduced into these matrices can be described by the relaxation time T_1. Tables 4.1 to 4.3 show the average T_1 values calculated from several measurements.

Despite the fact that for the melt in opal and in porous glass with a pore diameter of 18 nm, the spin-lattice relaxation times are significantly shorter than for the bulk case, for each of these samples the dependence of T_1 on the magnetic field is not observed, which indicates that the approximate extreme constriction has been performed.

Figures 4.3 and 4.4 show the longitudinal magnetization vs. time dependencies for ^{69}Ga obtained on the 500 MHz NMR spectrometer and for ^{115}In on the 400 and 500 MHz NMR spectrometers.

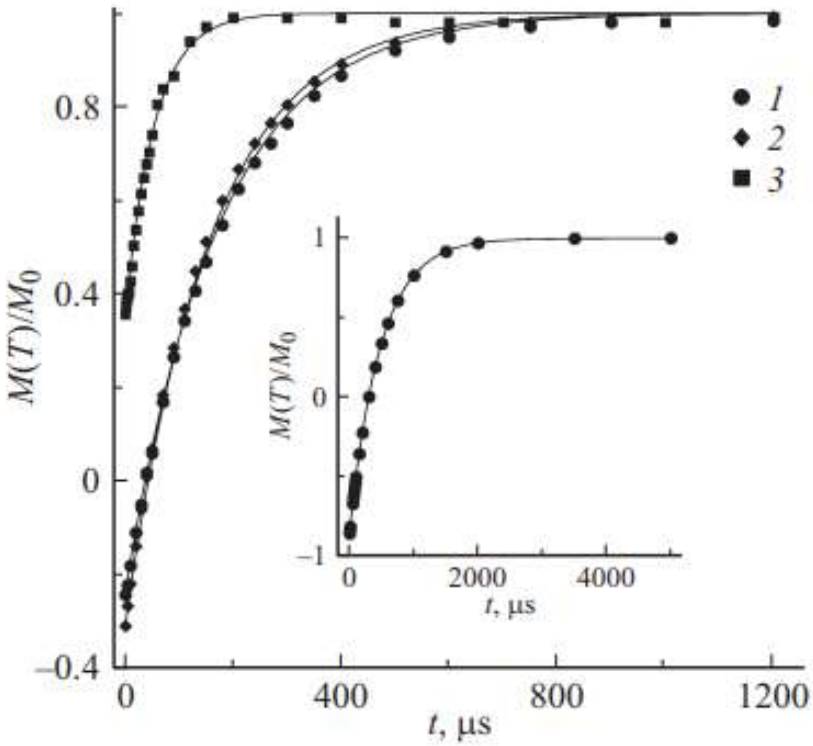

Figure 4.3 - Recovery of relative longitudinal magnetization from time after 180° momentum for the isotope ^{69}Ga in a magnetic field of 11.75 T. (1) – opal, (2) – porous glass 18 nm, (3) porous glass 7 nm. Solid lines are theoretical curves. The insert shows the recovery of the relative longitudinal magnetization for the isotope ^{69}Ga in a bulk liquid alloy.

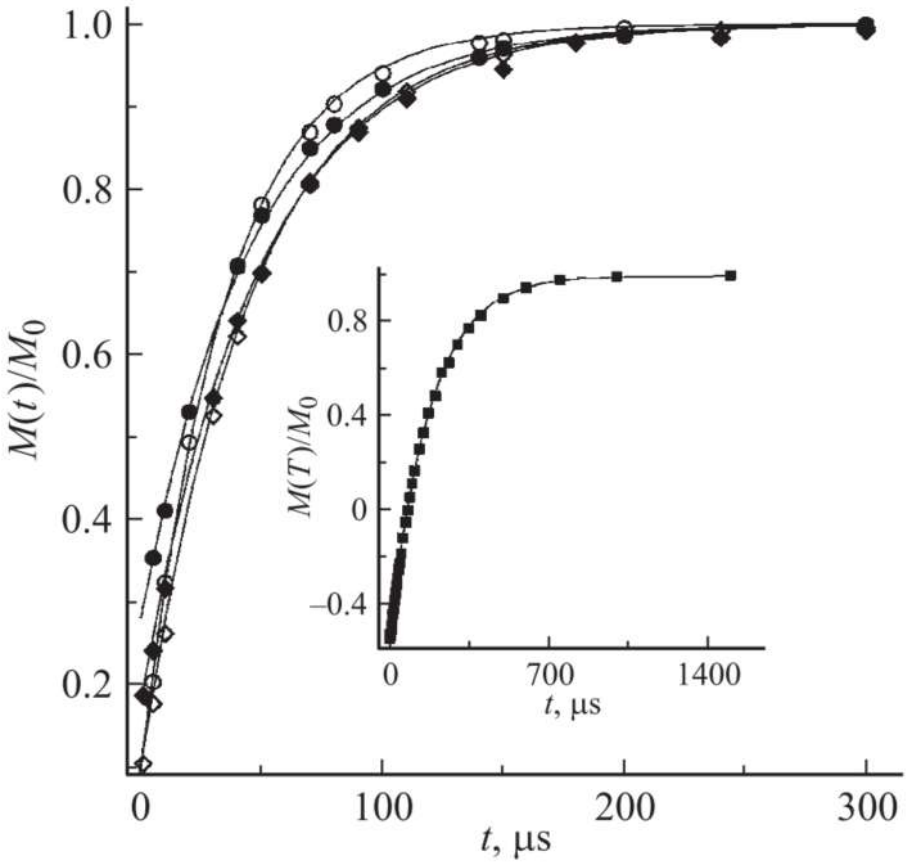

Figure 4.4 - Recovery of the relative longitudinal magnetization as a function of time after 180° pulse for the isotope ^{115}In in a magnetic field of 11.75 T - rhombuses and in a field of 9.4 T - circles for a liquid alloy in opal. The filled symbols are in opal, the hollow symbols are in 18 nm porous glass. Solid lines are theoretical curves. The insert shows the recovery of the relative longitudinal magnetization for the isotope ^{115}In in a bulk liquid alloy in a magnetic field of 9.4T.

As can be seen from these figures, for an alloy in porous glass with a pore diameter of 7 nm, spin-lattice relaxation occurs much faster than in the bulk case. Also, for this sample, the dependence of the longitudinal magnetization recovery rate on the value of the magnetic field strength is observed, which indicates the inapplicability of the approach of extreme constriction.

Figure 4.5 shows the longitudinal magnetization recovery curves for ^{71}Ga in porous glass with a pore diameter of 7 nm in magnetic fields of 9.4, 11.75 and 17.6 T.

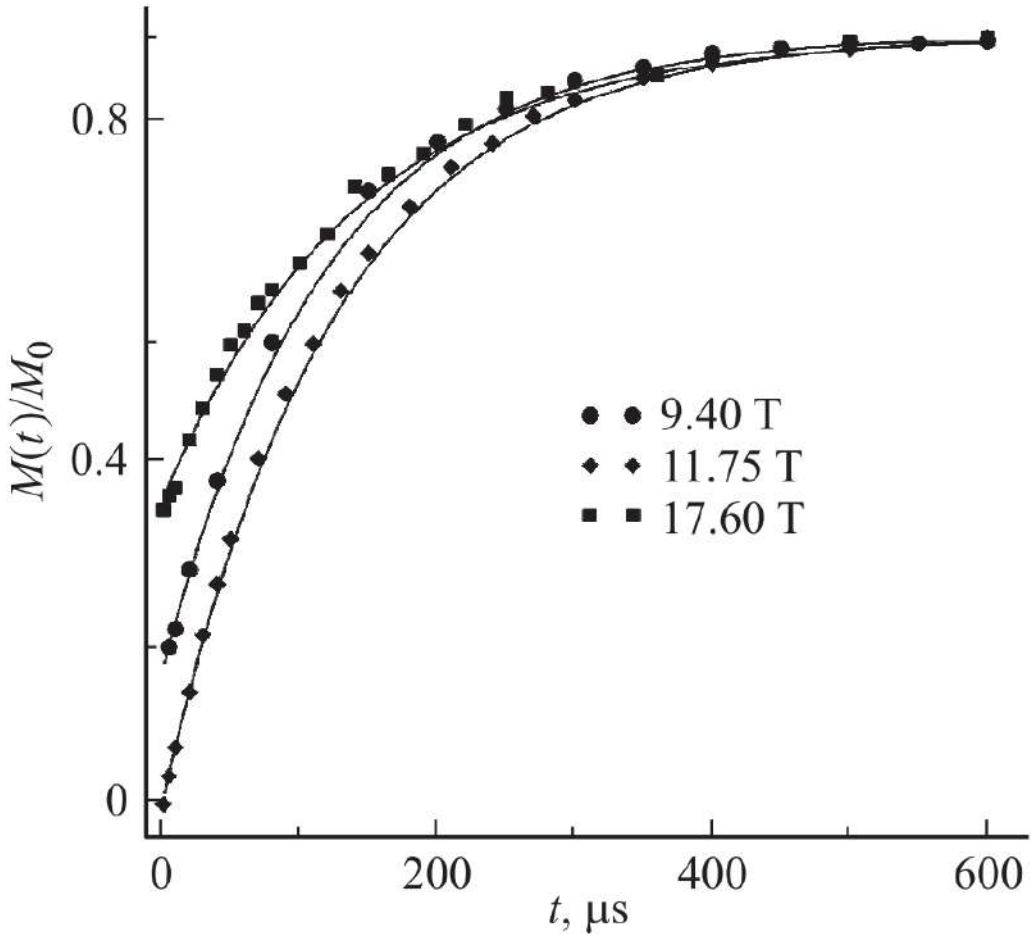

Figure 4.5 - Recovery of the relative longitudinal magnetization from time after 180° pulse for the isotope ^{71}Ga in different magnetic fields for a liquid alloy in porous glass of 7 nm. Solid lines are theoretical curves.

The figure clearly shows the difference in the rate of longitudinal magnetization recovery for different magnetic fields. If the approximation of the extreme constriction is violated, then the recovery of longitudinal magnetization cannot be described by a single exponent and therefore by time T_1 [99]. Although for isotopes ^{69}Ga and ^{71}Ga the process of spin-lattice relaxation is described by two exponentials, it was concluded in the paper [134] that the recovery of magnetization in this case remains approximately single exponential and can be characterized by time T_1 in the first approximation. This fact greatly facilitates the possibility of comparison with the process of spin-lattice relaxation in the bulk case.

4.4 Discussion and interpretation of results

The main mechanisms that provide relaxation in bulk melts and liquid metals are the interaction of nuclear magnetic dipoles with conduction electrons and the interaction of electric quadrupole moments with dynamic gradients of electric fields arising from the movement of atoms in a liquid [133].
In the bulk case, the magnetic relaxation mechanism is the main one. In this case, the approximation of the extreme contraction is performed for both relaxation mechanisms, and the relaxation curve is described by a single exponent. The corresponding relaxation time satisfies the following expression

$$(T_1)^{-1} = (T_{1m})^{-1} + (T_{1q})^{-1} \quad (4.1)$$

where T_{1Q} and T_{1m} are the times corresponding to the quadrupole and magnetic relaxation mechanisms. The relationship between the times T_{1Q} and T_{1m} for gallium isotopes is described by expressions (4.2) and (4.3)

$$T_{1Q}^{69} = \frac{T_{1Q}^{71} Q_{71}^2}{Q_{69}^2} \quad (4.2)$$

$$T_{1Q}^{69} = \frac{T_{1Q}^{71} \gamma_{71}^2}{\gamma_{69}^2} \quad (4.3)$$

where γ and Q are the gyromagnetic ratio and the quadrupole moment. Solving the system of equations (4.1)-(4.3), it is possible to calculate the contributions of magnetic and quadrupole relaxation of the isotopes ^{69}Ga and ^{71}Ga in the bulk alloy Ga-In-Sn.
The calculated magnetic relaxation times were T_{1m}^{71} = 580 ± 10 μs and T_{1m}^{69} = 937 ± 17 μs, and the corresponding values of the quadrupole relaxation times are presented in Tables 4.1 and 4.2. The following values of gyromagnetic ratios and quadrupole moments were used for calculations: γ_{71} = 8.18·107 rad·T $^{-1}$·s^{-1}, γ_{69} = 6.44·107 rad· T^{-1}·s^{-1}, Q_{71} = 0.107b and Q_{69} = 0.171 b.

Knight shift values K obtained for Ga-In-Sn melt in pores of opal and porous glass with pore size of 18 nm and magnetic relaxation time T_{1m} calculated for bulk alloy with good accuracy satisfy the Korringa relation $T_{1m}TK^2$ = const/γα [140] (T is the temperature, α is a coefficient of the order of one, which takes into account the effects of electron exchange and correlation), therefore, it can be argued that the magnetic relaxation time T_{1m} for these three samples is almost the same. In view of the fact that the Knight shift for nanoporous samples in opal matrix and porous glass with a pore size of 18 nm changed insignificantly, taking into account the Korringa relation, it can be stated that the effect of alloy nanostructuring on the magnetic relaxation time T_{1m} is small. Computed using the expression (4.1), taking

into account the above fact, the quadrupole relaxation times T_{1Q} are presented in Tables 4.1 and 4.2. According to the tables, during the transition from bulk to nanostructured samples, the quadrupole relaxation time T_{1Q} decreases several times. The same situation with a little-changing Knight shift occurs for a binary liquid alloy Ga-In [95]. As was done for the bulk case, for nanostructured samples in porous glass with a pore diameter of 18 nm and opal, the magnetic and quadrupole relaxation times can be computed using the system of equations (4.1)-(4.3). At the same time, the obtained times T_{1m} and T_{1Q}, within the margin of error, coincide with the results obtained using the Korringa relation and expression (4.1) and presented in Tables 4.1 and 4.2. As mentioned above in the section describing the results of the study, for a melt in porous glass with a pore diameter of 7nm, a field dependence of spin-lattice relaxation is observed, and this fact indicates that the approximation of extreme constriction for this size of melt particles is no longer performed. Since the Korringa relation for a 7 nm sample is valid and, consequently, the magnetic relaxation time T_{1m} also changes only slightly compared to the bulk case, the non-fulfillment of the extreme contraction approximation is due to the quadrupole contribution to spin-lattice relaxation. Similar conclusions have been made in previous studies of metals and binary alloys under nanoconfinement conditions [48; 49; 60]. The general formula for restoring magnetization parallel to a constant magnetic field is represented by expression (1.9) from Chapter 1:

$$\frac{\mathrm{M(t)}}{\mathrm{M_0}} = 1 - b\left[\frac{4}{5}\exp\left(-\frac{\mathrm{C\tau_c t}}{1+4\omega_0^2\tau_c^2}\right)\right] + \frac{1}{5}\exp\left(-\frac{\mathrm{C\tau_c t}}{1+\omega_0^2\tau_c^2}\right)exp\left(-\frac{\mathrm{t}}{\mathrm{T_{1m}}}\right) \quad (4.4)$$

where M(t) is the time-dependent magnetization t, M_0 is the equilibrium magnetization, 1−b is the relative magnetization immediately after the inverting pulse, is the Larmor precession frequency, C is the quadrupole constant, which depends on the structure of the substance under study and is proportional to the square of the quadrupole moment of the nucleus, τ_c is the correlation time of atomic motion. Since quadrupole constants are proportional to the square of the quadrupole moment, C_{69} and C_{71} for isotopes ^{69}Ga and ^{71}Ga are related by the following ratio:

$$C_{69}/C_{71} = Q_{69}^2/Q_{71}^2 \quad (4.5)$$

The expressions (4.4) describing the relaxation process for gallium isotopes contain only two fitting parameters, C_{71} and τ_c, and C_{69} is computed from equation (4.5). Table 4.4 shows the calculated fitting parameters C_{71} and for a sample in porous glass with a pore diameter of 7nm.

Table 4.4. - Quadrupole constant C_{71}, atomic motion correlation time τ_c and ratio of atomic motion correlation time in a nanostructured alloy to atomic motion correlation time in the bulk case τ_c/τ_c^{bulk}

Sample	Bulk	Opal	Glass 18 nm	Glass 7 nm
C_{71}, μs^{-2}	28 ± 3	28 ± 3	28 ± 3	53 ± 5
τ_c, 10^{-6} μs	14 ± 2	67 ± 5	75 ± 5	230 ± 20
τ_c/τ_c^{bulk}	1	4.8	5.4	16

In the case of the bulk alloy Ga-In-Sn and the samples in opal and porous glass with a pore diameter of 18nm, an approximation of the extreme constriction $\omega_0\tau_c \ll 1$ is performed, and the expression (4.4) takes the form as follows:

$$\frac{M(t)}{M_0} = 1 - b * \exp(-C\tau_c t)\, exp\left(-\frac{t}{T_{1m}}\right) \qquad (4.6)$$

whence it follows that the inverse time of quadrupole relaxation is equal to the product of the quadrupole constant and the time of correlation of atomic motion: $T_{1Q}^{-1} = C\tau_c$.

The value for pure bulk gallium was taken as the atomic motion correlation time τ_c of the bulk melt [60]. Based on known values of T_{1m}, T_{1Q}, and τ_c for the studied samples, the quadrupole constants C_{71} were estimated using equation (4.6). In view of the fact that the structure of the melt introduced into the pores of a relatively large size should not differ much from the structure of the bulk melt, it can be assumed that the quadrupole constant C_{71} for the melt in the pores of opal and nanoporous glass with a pore diameter of 18 nm does not differ from the quadrupole constant for the bulk melt Ga-In-Sn. Guided by this assumption, the correlation time of atomic motion τ_c was calculated for specimens in opal and porous glass with a pore size of 18 nm. Computed values τ_c and C_{71}, as well as the value of τ_c for bulk melt are presented in Table 4.4. According to the data in Table 4.4, compared to the bulk case, the correlation time of atomic motion τ_c in Ga-In-Sn melt in opal and porous glass with a pore diameter of 18 nm increased by about 5 times. The effect of nanoconfinement on the correlation time of atomic motion, which also manifested itself in the form of a violation of the approach of extreme constriction, was much more significant for the melt in porous glass with a pore diameter of 7nm.

Isolation of magnetic and quadrupole spin-lattice relaxation times for an isotope ^{115}In looks a bit more complicated. Despite the fact that, similarly to gallium, indium has two stable isotopes ^{115}In and ^{113}In, the method used for gallium to separate relaxation into quadrupole and magnetic components cannot be applied, due to the fact that the quadrupole moments and gyromagnetic ratios of indium isotopes are very close [133]. In addition, the isotope ^{113}In It has a very low natural propagation and, as a result, the signal-to-noise ratio for this isotope is very small, which is further complicated by the relatively large line width, which is difficult to distin-

guish against the background of ringing that usually arises from a coil at low frequencies. In the current study, the method proposed in the paper was used to distinguish quadrupole and magnetic relaxation times [49].

Taking into account the approximation of extreme constriction, the spin-lattice relaxation time for a bulk melt, a sample in opal and porous glass with a pore diameter of 18nm can be represented by the following ratios:

$$\begin{aligned} (T_1^{bulk})^{-1} &= C_{115}\tau_c^{bulk} + \left(T_{1m}^{bulk}\right)^{-1} \\ \left(T_1^{opal}\right)^{-1} &= C_{115}\tau_c^{opal} + \left(T_{1m}^{bulk}\right)^{-1} \\ (T_1^{18nm})^{-1} &= C_{115}\tau_c^{18nm} + \left(T_{1m}^{bulk}\right)^{-1} \end{aligned} \qquad (4.7)$$

where τ_c^{bulk}, τ_c^{opal} and τ_c^{18nm} are the atomic motion correlation times for bulk melt, opal melt, and porous glass with a pore size of 18 nm, which were computed from the spin relaxation times T_1. As described above, the melt structure should not change much when injected into nanopores of relatively large diameter, so it is assumed that the quadrupole constant C_{115} is considered to be the same for all samples in which an extreme constriction approximation is performed. Also, in view of the slight difference between the Knight shift and the Korringa relation, it is assumed that the magnetic relaxation time T_{1m} for the melt in these matrices remains unchanged with respect to the bulk case. The system of equations (4.7) has two unknowns, C_{115} and T_{1m}^{bulk}. Having solved this system, we obtained the following values: $C_{115} \cong 190$ μs^{-2} and $T_{1m}^{bulk} \cong 310$ μs. From the data presented in Table 4.3, it can be seen that the quadrupole relaxation time T_{1Q} for ^{115}In is significantly reduced for the melt under nanoconfinement conditions due to the increase in the atomic motion correlation time and the quadrupole relaxation mechanism begins to dominate compared to the bulk case, in which the magnetic relaxation mechanism dominates.

The correlation time of atomic motion τ_c in a fluid is inversely proportional to the diffusion coefficient D and is described by the expression:

$$\tau_c = d^2/6D \qquad (4.8)$$

where d is the average magnitude of the atom's jump. Thus, the data obtained on the increase in the correlation time of atomic motion in a triple melt Ga-In-Sn introduced into nanoporous arrays indicates a slowdown in diffusion processes within pores. Moreover, as the diameter of the pores decreased, the diffusion slowed down.

4.5. Conclusion

As a result of the study of nuclear spin-lattice relaxation and Knight shift of gallium and ^{115}In isotopes in a liquid triple alloy Ga-In-Sn of eutectic composition, in the pores of artificial opal and porous glasses with a pore size of 18 and 7 nm, an increase in the rate of spin-lattice relaxation and a decrease in the Knight shift with a decrease in pore size were found. The correlation time of atomic motion for melt under nanoconfinement conditions is calculated. that the correlation time increases and, accordingly, the atomic mobility in the melt decreases with the decrease in pore size. At the same time, the correlation time of atomic motion for a sample with a pore size of 7 nm is 16 times longer than for a bulk melt.

Chapter 5. Dynamic shift of the NMR line in Ga-In-Sn alloy in porous glasses with pore diameters of 7 and 25 nm

5.1 Introduction

As mentioned above in the introduction to the dissertation, much attention has recently been paid to the study of various substances, including various metals and alloys introduced into nanoporous matrices, and the NMR method is widely used as a method sensitive to local changes in matter. The size of the pores into which the metal or alloy is introduced has a significant impact on various properties of the substance under study, including electronic susceptibility, melting-crystallization phase transition temperatures, and atomic mobility [45; 47; 141]. Atomic mobility is particularly interesting to study because it is directly related to the diffusion coefficient and viscosity and is responsible for the rate at which a fluid flows through porous media. To study atomic mobility in a liquid under conditions of nanoconfinement between pores, a technique is used to measure the attenuation of a spin echo with an applied magnetic field gradient [59]. However, this method cannot be applied to liquid alloys due to the short spin-lattice relaxation time. As an alternative, a technique was proposed in which the spin-lattice relaxation time of spin nuclei with spin is measured $I > {}^{1}/_{2}$[60; 61]. This technique provides information about the change in atomic mobility within individual pores, as well as neutron scattering. In this method, the contribution of the quadrupole relaxation mechanism is singled out from the general relaxation process, which is due to the interaction of the nuclear quadrupole moment with the dynamic gradients of electric fields that arise during the movement of the liquid. In electron paramagnetic resonance, the change in the position of resonance lines due to internal motion in the system is called dynamic displacement [62; 63; 64; 65; 66; 67]. Dynamic shifts can be observed when the condition is met $\omega_0\tau \geq 1$[65], where ω_0 is the resonant frequency, and τ is the correlation time of atomic motion. Initially, dynamic shifts were observed only in EPR spectra, but later, with the appearance of strong quantizing fields in NMR spectrometers, it became possible on NMR spectra of viscous liquids with a long atomic motion correlation time [68; 69; 70; 71; 72] and solids with high atomic mobility [73]. Combination of static measurements (NMR line position and shape) and spin-lattice relaxation measurements [60] It can improve the quality of determination of atomic mobility in melts under nanoconfinement conditions.

In the present work, NMR measurements of the line shape and time of spin-lattice relaxation T_1 were carried out for two isotopes of gallium ^{71}Ga and ^{69}Ga in a liquid alloy Ga-In-Sn introduced into nanoporous glasses with different pore diameters in different magnetic fields.

To interpret the results, the model of the dynamic shift of the NMR line was applied and it was found that the result of determining the correlation time of atomic motion using the dynamic shift model of the NMR line is consistent with the result of determining the correlation time of atomic motion based on measurements of nuclear spin-lattice relaxation [78].

5.2 Samples and experiment

Porous glasses filled with Ga-In-Sn alloy were used as samples in this chapter. The average pore diameter of porous glasses was 7 and 25 nanometers. Also, for comparison, a bulk sample of the Ga-In-Sn alloy was examined.

The preparation of borosilicate porous glasses and nanocomposite samples based on them was described in the previous chapter. The only thing is that for this study, samples with ribs of about 4 mm were cut out of the filled porous glass, which only affected the coil fill factor and the intensity of the NMR signal compared to the study in Chapter 4. Melt droplets of about 0.5 mm in diameter, placed in glass capsules, were used as a bulk sample.

NMR studies were carried out on Bruker pulsed NMR spectrometers Avance 400, Avance 500 and Avance 750 with magnetic fields of 9.4, 11.6 and 17.6 T, respectively. Measurements were made at room temperature for both gallium isotopes ^{71}Ga and ^{69}Ga. The spin of both isotopes is 3/2, and the gyromagnetic ratios γ and quadrupole moments Q are equal to $\gamma_{69} = 6.44 \cdot 10^7$ rad s^{-1} T^{-1}, Q_{69} = 17.1 fm^2 and $\gamma_{71} = 8.18 \cdot 10^7$ rad s^{-1} T^{-1}, Q_{71} = 10.7 fm^2. ^{71}Ga and ^{69}Ga have similar natural abundances of 39.892% and 60.108% respectively.

To obtain the shape of the line, a signal of free precession of the magnetization of the sample after a 90-degree pulse was recorded, followed by the application of the Fourier transform. The position of the line was determined by the position of the maximum intensity relative to the position of the maximum intensity of the signal from the GaAs single crystal. Spin-lattice relaxation time was measured using a sequence of inverting 180° and 90° pulses. Up to 16,000 scans were used to increase the signal-to-noise ratio, which is proportional to $\sqrt{n}$, where n is the number of scans.

5.3 Results of the NMR study of the Ga-In-Sn alloy

In the case of a bulk sample, the position of the NMR lines for the isotopes ^{71}Ga and ^{69}Ga was the same for all spectrometers. This is consistent with earlier data for liquid metals [61; 141]. The position of the line relative to the reference

(Knight shift) was 4247.3 ppm. For the alloy in porous glass with a pore diameter of 25 nm, the difference in Knight shifts of gallium isotopes in different fields was also less than the error, but the Knight shift was reduced compared to the shift in the bulk alloy by 20 ppm. The shape of the line in the case of bulk alloy and porous glass with a pore diameter of 25 nm was approximated by lorencean. In the 25-nanometer pores, the lines were slightly wider than in the bulk case. For an alloy in porous glass with a pore diameter of 7 nm, the dependence of the position of the line on the isotope number and the magnetic field strength was traced. At the same time, the shape of the line differed significantly from Lorenz line shape. The shape of the lines was asymmetrical and significantly widened, with broadening for the isotope ^{69}Ga there was much more. As an example, figure 5.1 shows the NMR lines for ^{71}Ga in a bulk alloy and an alloy introduced into porous glass with a pore diameter of 7 nm, in magnetic fields of 9.4 and 17.6 T.

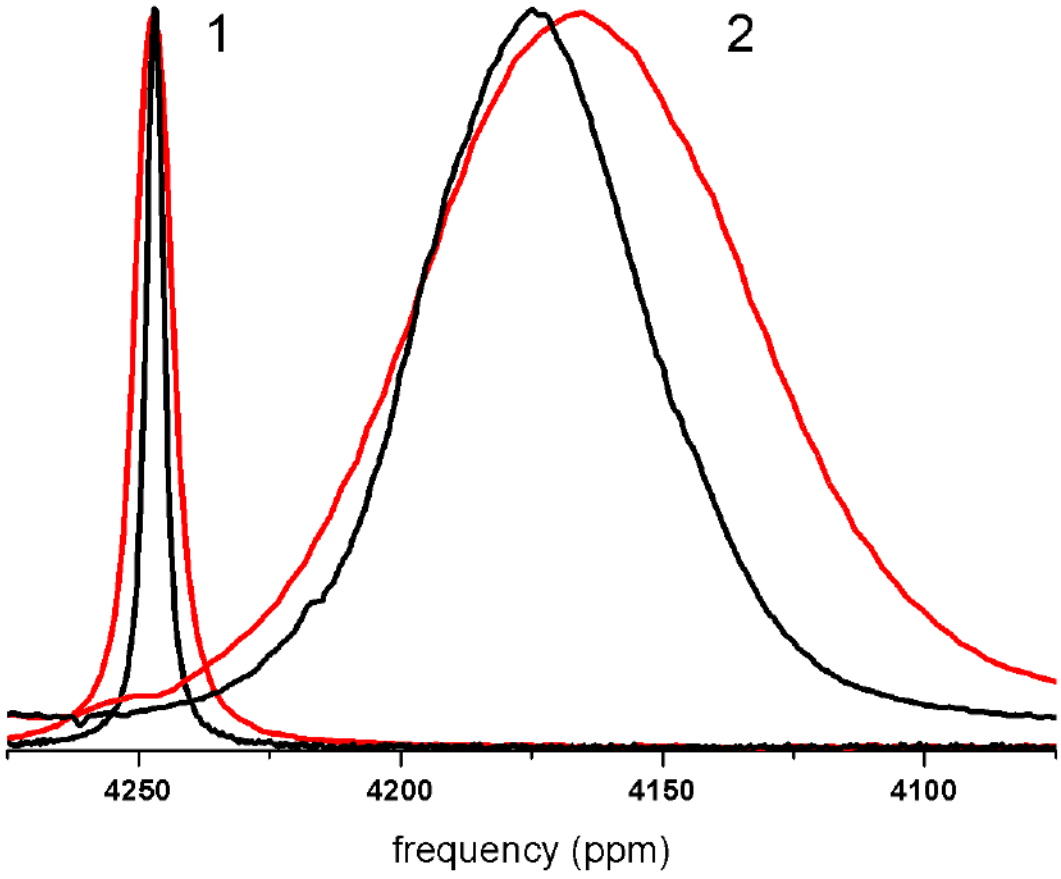

Figure 5.1 - NMR line shapes for ^{71}Ga for bulk eutectic alloy Ga-In-Sn (1) and Ga-In-Sn alloy in porous glass with pore size of 7 nm (2) in fields of 9.4 T (red lines) and 17.6 T (black lines).

Graph 5.2 shows the dependencies of the NMR line position for ^{71}Ga as can be seen from the figure, the Knight shift decreases almost linearly with increasing inverse pore size.

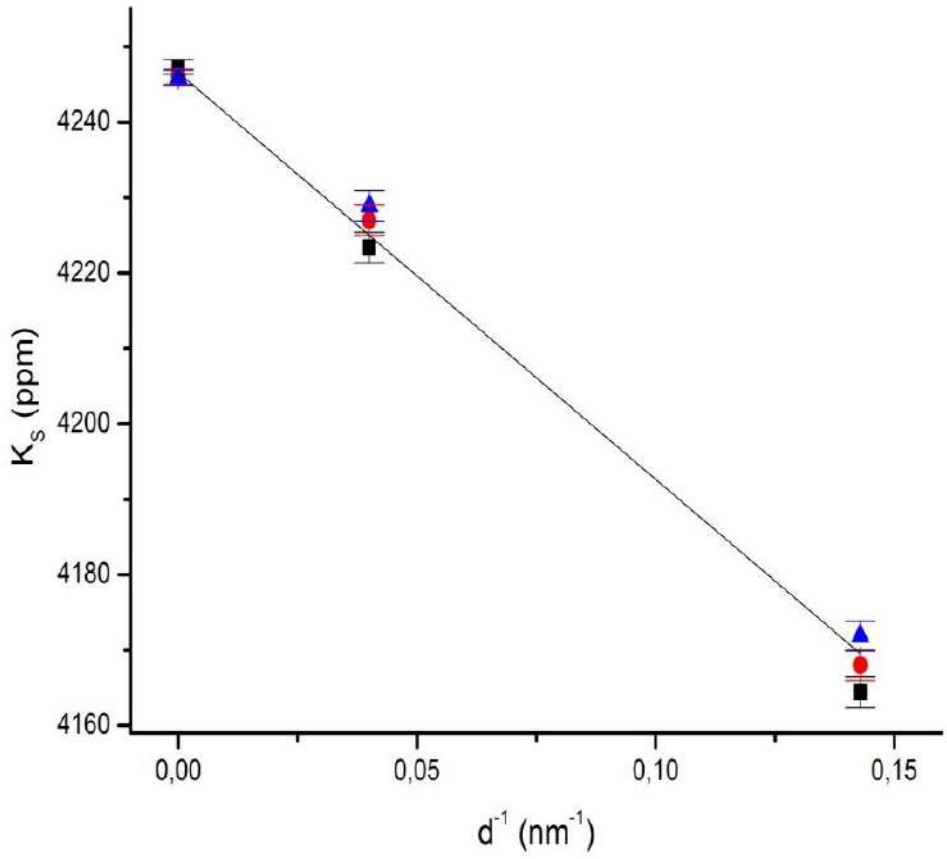

Figure 5.2 - Dependence of the position of the NMR line of the ^{71}Ga isotope on the inverse pore size for the fields 9.4 T (black squares), 11.7 T (red circles) and 17.6 T (blue triangles). The straight line shows the linear relationship obtained by the least squares method.

Figure 5.3 shows the positions of the NMR isotope lines ^{71}Ga and ^{69}Ga in the case of porous glass with a pore size of 7 nm in different magnetic fields.

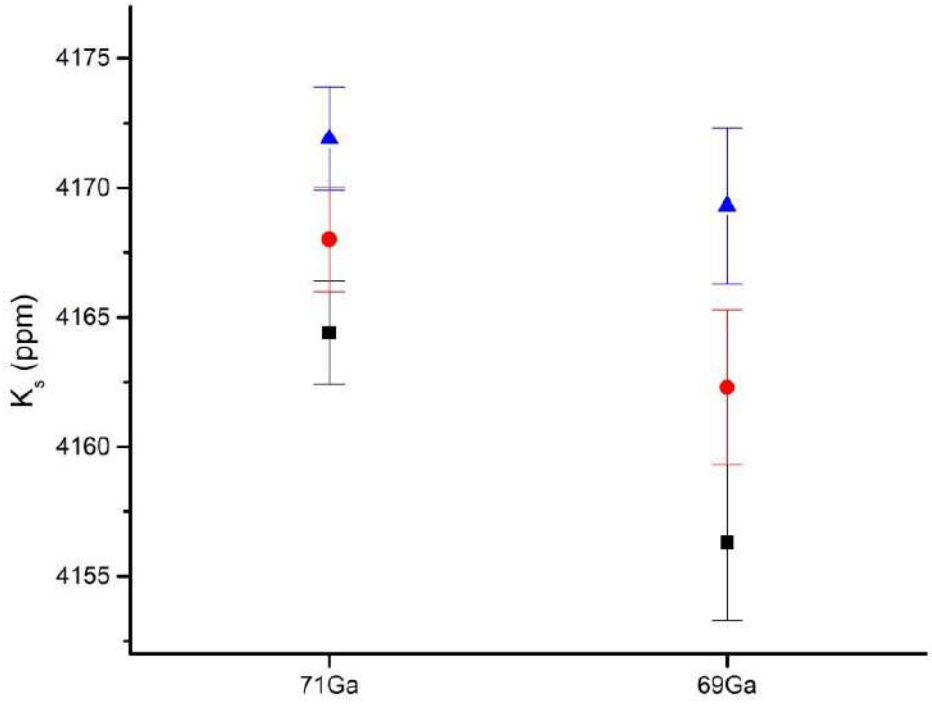

Figure 5.3 - Positions of the maximum of the NMR line of the isotopes ^{71}Ga and ^{69}Ga in the case of glass with a pore diameter of 7 nm for fields of 9.4 T (black squares), 11.7 T (red circles) and 17.6 T (blue triangles).

In the bulk melt for both gallium isotopes, the recovery of longitudinal magnetization after a 180-degree momentum occurred according to an exponential law, and the spin-lattice relaxation time was equal to $T_{1,bulk}^{69}$ = 483 ± 10 μs and $T_{1,bulk}^{71}$ = 437 ± 10 μs. The obtained relaxation times did not depend on the magnetic field strength and corresponded to the data from the work [61]. It was also independent of the magnetic field and was exponential spin-lattice relaxation for a melt in porous glass with a pore size of 25 nm. At the same time, the spin-lattice relaxation time compared to the bulk case was shorter and equal to T_1^{69} = 143 ± 10 μs and T_1^{71} = 257 ± 10 μs. In turn, in the case of the liquid alloy Ga-In-Sn introduced into porous glass with a pore diameter of 7 nm, the recovery of longitudinal magnetization could not be described by a single exponent and it occurred much faster than in the bulk case and porous glass with a pore diameter of 25 nm. Also, for an alloy in porous glass with a pore diameter of 7 nm, the spin-lattice relaxation time depended on the magnetic field strength. Figure 5.4 shows the longitudinal magnetization recovery curves for both gallium isotopes in different melt fields in glass with a pore diameter of 7 nm. The insert to figure 5.4 compares the magnetization recovery curves for a 7 nm melt and for a bulk melt measured with a Bruker Avance 400 spectrometer.

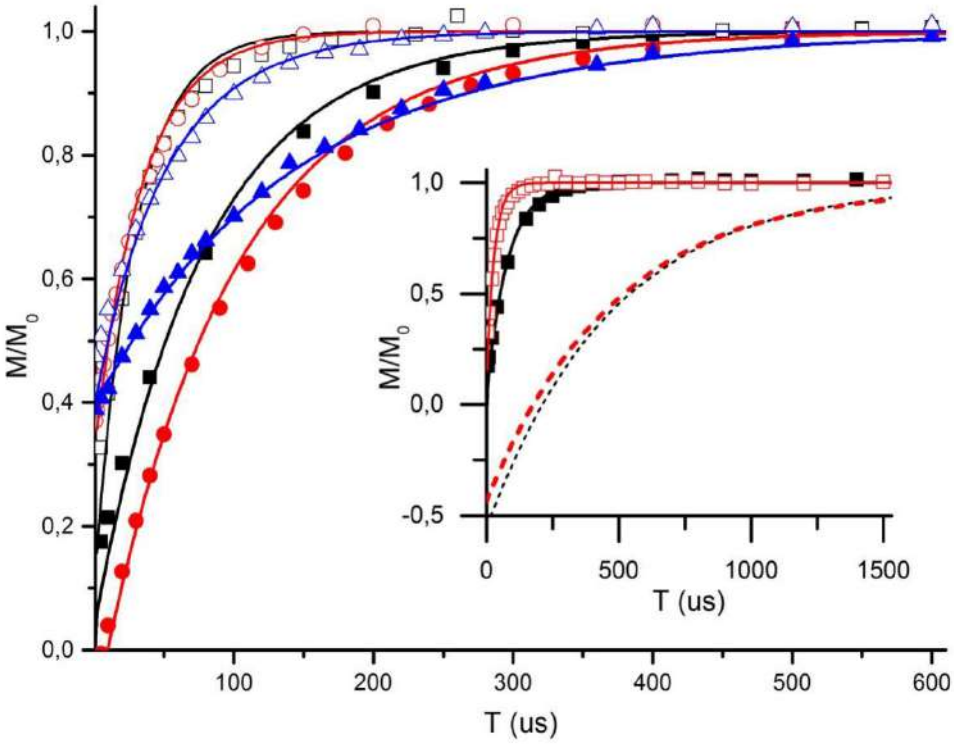

Figure 5.4 - Magnetization recovery for isotopes ^{71}Ga (filled symbols) and ^{69}Ga (blank symbols) in Ga-In-Sn alloy in porous glass with pore diameter 7 nm in magnetic fields of 9.4 T (black squares), 11.7 T (red circles) and 17.6 T (blue triangles). Solid lines depict theoretical dependencies. The inset presents experimental curves of magnetization recovery in a melt introduced into porous glass with pore diameter 7 nm, for the isotope ^{71}Ga (filled black squares) and the isotope ^{69}Ga. (empty red squares) and theoretical curves (solid lines) compared to bulk alloy magnetization recovery curves for the isotope ^{71}Ga (black dashed line) and the isotope ^{69}Ga. (red dashed line) in a magnetic field of 9.4 T.

5.4 Discussion and interpretation of the results, comparison of the characteristics of atomic motion calculated on the basis of the dynamic quadrupole shift model and on the basis of spin relaxation measurements

For the first time, a decrease in the spin-lattice relaxation time for the Ga-In-Sn melt under conditions of limited geometry compared to the bulk case was observed in the work [61]. This was interpreted as a consequence of the slowing down of atomic motion, which leads to an increase in the role of the quadrupole relaxation mechanism in a similar way to the results for other metals and alloys in

nanoporous matrices [60]. The inability to describe the recovery of magnetization in an alloy introduced into porous glass with a pore diameter of 7 nm by a single exponent indicates that the approximate extreme constriction is not performed in this sample [140]. Therefore, the obtained dependence of the position of the NMR line on the magnetic field strength for the Ga-In-Sn alloy introduced into porous glass with a pore diameter of 7 nm, and the different position of the resonance lines of gallium isotopes can be explained on the basis of a theoretical model of dynamic shift. The quadrupole interaction of nuclei with gradients of changing electric fields caused by atomic motion is responsible for the dynamic shift. It should be noted that the dependence of the position of the lines on the magnetic field strength was experimentally discovered earlier for gallium isotopes in the Ga-In melt introduced into porous glass with a pore size of 5 nm [141]. In order to interpret the shapes and positions of NMR lines for gallium isotopes in different magnetic fields, it is necessary to take into account that, in general, the resonant line of the nucleus with spin I = 3/2 is the sum of two components having a Lorentz form [99],

$$g(\omega) = \frac{2T_{21}}{1 + (\omega - \omega_0 - \delta_1)^2 T_{21}^2} + \frac{3T_{22}}{1 + (\omega - \omega_0 - \delta_{12})^2 T_{22}^2} \tag{5.1}$$

where T_{21} and T_{22} are the spin-spin relaxation times for each of the components, characterizing the line width, and δ_1 and δ_2 are the shifts of the maxima of the components from the resonant frequency. It should be noted that in (5.1) the Knight shift is included in the resonant frequency. The times ω_0 of T_{2i} and the shifts of the δ_i components are defined by the expressions

$$T_{21} = \frac{2}{C\tau\left(\frac{1}{1 + (\omega_0\tau)^2} + \frac{1}{1 + (2\omega_0\tau)^2}\right)},$$

$$T_{22} = \frac{2}{C\tau\left(\frac{1}{1 + (\omega_0\tau)^2} + 1\right)}, \tag{5.2}$$

$$\delta_1 = \frac{C\omega_0\tau^2}{2}\left(\frac{2}{1 + (2\omega_0\tau)^2} - \frac{1}{1 + (\omega_0\tau)^2}\right),$$

$$\delta_2 = \frac{C\omega_0\tau^2}{2(1 + (2\omega_0\tau)^2)} \tag{5.3}$$

where C is the quadrupole constant proportional to the square of the nuclear quadrupole moment Q, which is entered in the same way [61]. Given the approach of extreme constriction ($\omega_0\tau \ll 1$) expressions (5.2) and (5.3) are simplified. At the same time, dynamic shifts δ_i tend to zero, the widths of the components become close to each other, and the broadening of the lines is small. That is, there is one narrow resonant line at the frequency ω_0. In the case of slow atomic motion, i.e., a

long correlation time ($\omega_0\tau \gg 1$) expressions (5.2) and (5.3) are also simplified and written as follows

$$T_{21} = \frac{8\omega_0^2\tau}{5C}, T_{22} = \frac{2}{C\tau} \quad (5.4)$$

$$\delta_1 = -\frac{C}{4\omega_0}, \delta_2 = \frac{C}{2\omega_0} \quad (5.5)$$

According to (5.4), the second component is much wider and cannot be observed experimentally. Only one component with shift δ_1 remains. In the intermediate case, both components are observed shifted relative to each other, which leads to an asymmetry of the total NMR line.

In addition to dynamic broadening, other broadening mechanisms that are always present in the spin system must be taken into account to describe the experimental NMR line. In the present study, quadrupole broadening caused by spatial inhomogeneity of electric field gradients on nuclei, magnetic dipole broadening, and broadening due to different pore sizes were taken into account. Related to the latter is the dependence of the Knight shift on the size of the pores, shown in Fig. 5.2. Dipole and quadrupole broadening were taken into account by introducing a Gaussian line shape with fitting parameters. The pore size distribution was obtained by adsorption nitrogen porometry. Based on this distribution, the resonant frequency distribution function was recalculated, taking into account the assumed linear dependence of the Knight shift on the inverse pore size. The total shape of the line, taking into account dynamic broadening, was in the form of a convolution

$$G(\omega) = n \iiint g(\omega - \omega_2) e^{\frac{-(\omega_2-\omega_1)^2}{2D^2}} e^{\frac{-(\omega_3-\omega_2)^2}{2(PQ)^2}} \times f(\omega_1) d\omega_1 d\omega_2 d\omega_3 \quad (5.6)$$

where is $f(\omega_1)$ the function of the distribution of resonant frequencies due to the inhomogeneity of the Knight shift, obtained from the size distribution of pores, D and P are the fitting parameters characterizing the inhomogeneous dipole and quadrupole broadening, respectively, n is the normalization coefficient. Fitting parameters can be obtained by fitting experimentally measured forms of the NMR line for gallium isotopes in different fields. Recall that the Larmor frequencies and quadrupole parameters of gallium isotopes are different, and the quadrupole constants are related by the following ratio, $C_{69} = C_{71}Q_{69}^2/Q_{71}^2$[61]. Figs. 5.5 and 5.6 show a comparison of the obtained fitting curves of the NMR lines for two gallium isotopes in different fields with the experimental lines. For the convenience of visualization, vertical lines are drawn through the positions of the maxima of the experimental NMR lines.

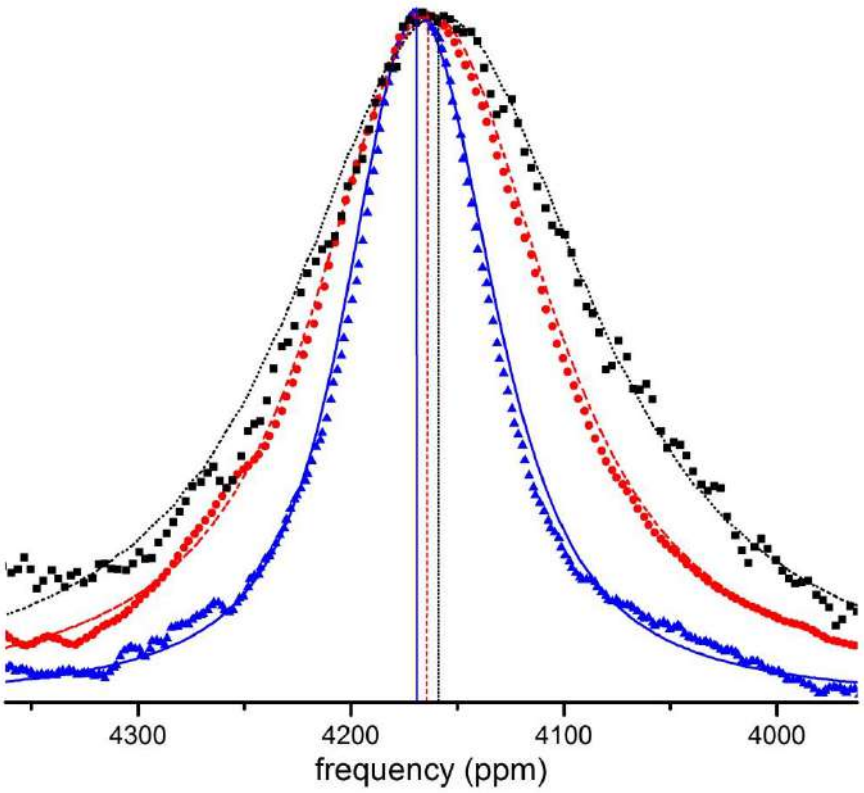

Figure 5.5 - Shapes of ^{69}Ga NMR lines (point-experiment, line-theoretical fitting) in Ga −In−Sn alloy introduced into porous glass with pore diameter 7 nm, in fields 9.4 T (squares and dotted line), 11.7 T (circles and dashed line), 17.6 T (triangles and solid line). The vertical lines correspond to the positions of the maximums of the NMR signals.

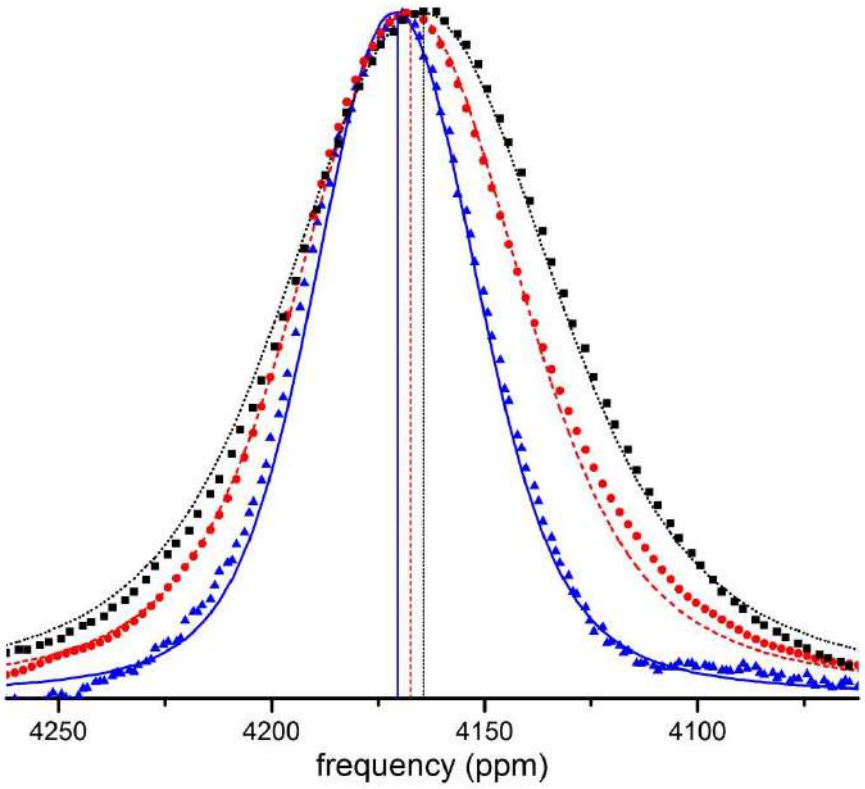

Figure 5.6 - Shapes of ^{71}Ga NMR lines (dots-experiment, lines-theoretical fitting) in Ga−In−Sn alloy introduced into porous glass with a pore diameter of 7 nm, in fields 9.4 T (squares and dotted line), 11.7 T (circles and dashed line), 17.6 T (triangles and solid line). The vertical lines correspond to the positions of the NMR signal maxima.

The fitting parameters were equal D = 0.8 rad/μs, P = 0.007 rad/μs·fm^2, K_s = 4385 ppm, C_{69} = 78 ± 2 μs^{-2}, τ = 6.6·10^{-10} s. Also, the fitting parameters C_{69} and τ, according to [61] should be consistent with the spin-lattice relaxation measurements. As is known, in conductor melts, the relaxation of quadrupole nuclei occurs due to the dipole contribution due to the interaction of the nuclear magnetic dipole moment with conduction electrons, and the quadrupole contribution due to the interaction of the nuclear quadrupole moment with dynamic gradients of electric fields resulting from motion in the liquid.

The dependence of the longitudinal magnetization recovery for cores with spin 3/2 on the time t is described by the expression (1.9) from Chapter 1:

$$\frac{M(t)}{M_0} = 1 - b \cdot \left(\frac{4}{5} e^{\frac{-C \cdot \tau \cdot t}{1+4 \cdot \omega_0^2 \cdot \tau^2}} + \frac{1}{5} e^{\frac{-C \cdot \tau \cdot t}{1+\omega_0^2 \cdot \tau^2}} \right) \cdot e^{\frac{-t}{T_{1m}}} \qquad (5.7)$$

where is b is a coefficient that takes into account the incomplete impulse inversion of the specimen's magnetization, T_{1m} – relaxation time due to the contribution of

the magnetic mechanism to relaxation, M and M_0 is the time-dependent and equilibrium magnetization. Following the description in [61] method for dividing the spin-lattice relaxation time into magnetic and quadrupole components in a bulk alloy obtained T_{1m}^{71} = (580 ± 10) μs and T_{1m}^{69} = (937 ± 17) μs. Next, six experimental dependencies of longitudinal magnetization recovery, shown in Fig. 5.4 were fitted using formula (5.7). The adjustment curves are also shown in Fig. 5.4. By means of fitting, the correlation time of atomic motion was obtained τ and an independent quadrupole constant C_{69}. Within the margin of error, the τ and C_{69} coincided with the results of the fitting of the shape and position of the NMR lines. The results obtained from relaxation measurements and measurements of the shape and position of NMR lines are consistent with each other, which indicates the validity of the application of these approaches.

5.5. Conclusion

In this work, for the first time, we discovered the difference in the frequency shift of the NMR resonant line for gallium isotopes ^{71}Ga and ^{69}Ga in the Ga-In-Sn ternary alloy introduced into porous glass with a pore size of 7 nm, at the same temperatures and in the same magnetic fields, as well as the dependence of the shift of the NMR resonant line on the strength of the constant magnetic field. For a bulk melt and for a nanocomposite with a pore size of 25 nm, no such effects were observed. The detected phenomena were interpreted using the dynamic quadrupole shift model of the NMR line. In addition, this model was used to determine the parameters of atomic motion in nanostructured melts of conductors, for which, due to a strong deceleration of atomic motion, the rapid motion approximation ceases to be performed. It was shown that the results of determining the correlation time of atomic motion, obtained on the basis of measurements of nuclear spin-lattice relaxation and on the basis of the dynamic shift model, are consistent.

Conclusion

The main results obtained in the dissertation:

1) Temperature measurements of the shape of the NMR line and spin-lattice relaxation were carried out for the isotopes of gallium ^{69}Ga and ^{71}Ga and indium ^{115}In in the liquid binary eutectic alloy $Ga_{94}In_6$ injected into the pores of artificial opal. Significant differences between the phase diagram of the Ga-In binary alloy under conditions of limited geometry and the phase diagram of the bulk Ga-In alloy have been revealed. It was found that the crystallization of the alloy in pores occurs with the formation of gallium-rich segregates with a β-Ga structure. A shift of the eutectic point towards a lower concentration of indium was revealed.

2) It was revealed that in a part of the binary melt $Ga_{94}In_6$ there is a liquid-liquid phase transition similar to the phase transition in supercooled pure gallium under nanoconfinement conditions. It was found that when cooled in the temperature range of 165-175 K, the difference in Knight shift for the two phases of the $Ga_{94}In_6$ alloy reached 20 ppm, and the difference in spin-lattice relaxation times was in the range of 25-54 us.

3) For the eutectic alloy Ga_{94In6} introduced into the pores of artificial opal, it was shown that in the segregated phase with the β-Ga structure in the temperature range of 215-240 K, spin-lattice relaxation is due to two main mechanisms: the interaction of nuclear quadrupole moments with dynamic gradients of electric fields arising during the motion of atoms, and the interaction of magnetic moments of nuclei with conduction electrons. Based on the relaxation rate measurement, the The activation energy of atomic motion E_a = 7200 K = 0.62 eV was calculated.

4) A decrease in the Knight shift for the isotopes of gallium ^{69}Ga and ^{71}Ga and indium ^{115}In in the Ga-In-Sn melt introduced into various nanoporous matrices at room temperature in different magnetic fields (9.4, 11.7 and 17.6 T) compared to the bulk melt was revealed. It is shown that the decrease in Knight shift increases with a decrease in the characteristic pore size.

5) Based on measurements of the rate of recovery of nuclear magnetization of gallium and indium isotopes, the correlation times of atomic motion were calculated and a slowdown in atomic diffusion in a triple Ga-In-Sn melt introduced into nanoporous matrices compared to a bulk melt was revealed. At the same time, the slowing of diffusion correlates with the characteristic pore size.

6) The difference in the resonance shift of the NMR line for the gallium isotopes ^{69}Ga and ^{71}Ga, as well as the dependence of the shift of the NMR resonant line of gallium isotopes on the strength of the constant magnetic field for a triple Ga-In-Sn melt introduced into the pores of nanoporous glass with a characteristic pore size of 7nm, was revealed. This phenomenon was interpreted using a dynamic quadrupole shift model. The correlation time of atomic motion within the model was calculated dynamic quadrupole shift. It is shown that the obtained result is consistent with the data obtained by measuring spin-lattice relaxation.

NMR research was carried out using the equipment of the «Center for Diagnostics of Functional Materials for Medicine, Pharmacology and Nanoelectronics» of Research park of St.Petersburg State University.

References

[1] Okpala, C.C. The benefits and applications of nanocomposites // Int. J. Adv. Eng. Tech. - 2014. - 4. - 12-18.
[2] Singh, R.P., Choi, J.-W., Tiwari, A., Pandey, A.C. Utility and Potential Application of Nanomaterials in Medicine, Biomedical Materials and Diagnostic Devices, - 2012, pp. 215-262.
[3] Christenson, H.K. Confinement effects on freezing and melting // Journal of Physics: Condensed Matter. - 2001. - 13(11). - R95.
[4] Xu, Q., Sharp, I., Yuan, C., Yi, D., Liao, C., Glaeser, A., Minor, A., Beeman, J., Ridgway, M., Kluth, P., Ager, J., Chrzan, D., Haller, E. Large melting-point hysteresis of Ge nanocrystals embedded in SiO2 (vol 97, art no 155701, 2006) // Physical Review Letters. - 2006. - 97(20). -.
[5] Petrov, O.V., Furó, I. NMR cryoporometry: Principles, applications and potential // Progress in Nuclear Magnetic Resonance Spectroscopy. - 2009. - 54(2). - 97-122.
[6] Charnaya, E., Tien, C., Lee, M., Kumzerov, Y. NMR studies of metallic tin confined within porous matrices // Physical Review B. - 2007. - 75(14). -.
[7] Tien, C., Charnaya, E.V., Lee, M.K., Baryshnikov, S.V., Sun, S.Y., Michel, D., Böhlmann, W. Coexistence of melted and ferroelectric states in sodium nitrite within mesoporous sieves // Physical Review B. - 2005. - 72(10). - 104105.
[8] Lefebvre, L.P., Banhart, J., Dunand, D.C. Porous Metals and Metallic Foams: Current Status and Recent Developments // Adv. Eng. Mater. - 2008. - 10(9). - 775-787.
[9] Tavakoli, M., Malakooti, M.H., Paisana, H., Ohm, Y., Green Marques, D., Alhais Lopes, P., Piedade, A.P., de Almeida, A.T., Majidi, C. EGaIn-Assisted Room-Temperature Sintering of Silver Nanoparticles for Stretchable, Inkjet-Printed, Thin-Film Electronics // Adv. Mater. - 2018. - 30(29). - 1801852.
[10] Dickey, M.D. Stretchable and Soft Electronics using Liquid Metals // Adv. Mater. - 2017. - 29(27). - 1606425.
[11] Zhou, L.-Y., Gao, Q., Zhan, J.-F., Xie, C.-Q., Fu, J.-Z., He, Y. Three-Dimensional Printed Wearable Sensors with Liquid Metals for Detecting the Pose of Snakelike Soft Robots // ACS Applied Materials & Interfaces. - 2018. - 10(27). - 23208-23217.
[12] Yang, Y., Sun, N., Wen, Z., Cheng, P., Zheng, H., Shao, H., Xia, Y., Chen, C., Lan, H., Xie, X., Zhou, C., Zhong, J., Sun, X., Lee, S.-T. Liquid-Metal-Based Super-Stretchable and Structure-Designable Triboelectric Nanogenerator for Wearable Electronics // ACS Nano. - 2018. - 12(2). - 2027-2034.
[13] Aimi, J., Wang, P.-H., Shih, C.-C., Huang, C.-F., Nakanishi, T., Takeuchi, M., Hsueh, H.-Y., Chen, W.-C. A star polymer with a metallo-phthalocyanine core as a tunable charge storage material for nonvolatile transistor memory devices // Journal of Materials Chemistry C. - 2018. - 6(11). - 2724-2732.
[14] Yadav, M., Velampati, R.S.R., Sharma, R. Colloidal Synthesized Cobalt Nanoparticles for Nonvolatile Memory Device Application // IEEE Transactions on Semiconductor Manufacturing. - 2018. - 31(3). - 356-362.
[15] Wadayama, H., Okabe, T., Taniguchi, J. Fabrication of multilayered structure of silver nanorod arrays for plasmon memory // Microelectronic Engineering. - 2018. - 193. - 47-53.
[16] Liu, Y., Shang, T., Liu, Y., Liu, X., Xue, Z., Liu, X. Highly sensitive platinum nanoparticles-embedded porous graphene sensor for monitoring ROS from living cells upon oxidative stress // Sensors and Actuators B: Chemical. - 2018. - 263. - 543-549.
[17] Gentile, A., Ruffino, F., Grimaldi, M.G. Complex-Morphology Metal-Based Nanostructures: Fabrication, Characterization, and Applications // Nanomaterials. - 2016. - 6(6). - 110.
[18] Song, G., Yu, L., Duan, G., Wang, L. Strong Coupling in the Structure of Single Metallic Nanoparticle Partially Buried in Molecular J-Aggregates // Plasmonics. - 2018. - 13(3). - 743-747.
[19] Xiong, Y., Lu, X. Metallic nanostructures // Springer International Publishing. DOI. - 2015. - 10. - 978-3.
[20] Vogel, M. NMR studies on simple liquids in confinement // The European Physical Journal Special Topics. - 2010. - 189(1). - 47-64.
[21] Ito, K., Moynihan, C.T., Angell, C.A. Thermodynamic determination of fragility in liquids and a fragile-to-strong liquid transition in water // Nature. - 1999. - 398. - 492-495.

[22] Mallamace, F., Broccio, M., Corsaro, C., Faraone, A., Majolino, D., Venuti, V., Liu, L., Mou, C.-Y., Chen, S.-H. Evidence of the existence of the low-density liquid phase in supercooled, confined water // Proceedings of the National Academy of Sciences. - 2007. - 104(2). - 424.
[23] Mishima, O., Stanley, H.E. The relationship between liquid, supercooled and glassy water // Nature. - 1998. - 396. - 329-335.
[24] Poole, P.H., Sciortino, F., Essmann, U., Stanley, H.E. Phase behaviour of metastable water // Nature. - 1992. - 360. - 324-328.
[25] Monaco, G., Falconi, S., Crichton, W.A., Mezouar, M. Nature of the First-Order Phase Transition in Fluid Phosphorus at High Temperature and Pressure // Physical Review Letters. - 2003. - 90(25). - 255701.
[26] Katayama, Y., Inamura, Y., Mizutani, T., Yamakata, M., Utsumi, W., Shimomura, O. Macroscopic Separation of Dense Fluid Phase and Liquid Phase of Phosphorus // Science. - 2004. - 306. - 848-851.
[27] Glosli, J.N., Ree, F.H. Liquid-Liquid Phase Transformation in Carbon // Physical Review Letters. - 1999. - 82(23). - 4659-4662.
[28] Togaya, M. Pressure Dependences of the Melting Temperature of Graphite and the Electrical Resistivity of Liquid Carbon // Physical Review Letters. - 1997. - 79(13). - 2474-2477.
[29] Ivan, S.-V., Peter, H.P., Francesco, S. Fragile-to-strong transition and polyamorphism in the energy landscape of liquid silica // Nature. - 2001. - 412. - 514-517.
[30] Poole, P.H., Hemmati, M., Angell, C.A. Comparison of Thermodynamic Properties of Simulated Liquid Silica and Water // Physical Review Letters. - 1997. - 79(12). - 2281-2284.
[31] Aasland, S., McMillan, P.F. Density-Driven Liquid-Liquid Phase-Separation in the System Al2O3-Y2O3 // Nature. - 1994. - 369. - 633-636.
[32] Greaves, G., Fearn, S., Langstaff, D., Kargl, F., Cox, S., Vu Van, Q., Majérus, O., Benmore, C., Weber, J.K.R., Wilding, M., Hennet, L. Detection of First-Order Liquid/Liquid Phase Transitions in Yttrium Oxide-Aluminum Oxide Melts // Science (New York, N.Y.). - 2008. - 322. - 566-70.
[33] Defrain, A., Chim, J. États métastables du gallium. Surfusion et polymorphisme // Journal de chimie physique. - 1977. - 74. - 851-862.
[34] Bosio, L. Crystal structures of Ga(II) and Ga(III) // Journal of Chemical Physics. - 1978. - 68. - 1221-1223.
[35] Soares, B.F., MacDonald, K.F., Fedotov, V.A., Zheludev, N.I. Light-Induced Switching between Structural Forms with Different Optical Properties in a Single Gallium Nanoparticulate // Nano Letters. - 2005. - 5(10). - 2104-2107.
[36] Poloni, R., De Panfilis, S., Di Cicco, A., Pratesi, G., Principi, E., Trapananti, A., Filipponi, A. Liquid gallium in confined droplets under high-temperature and high-pressure conditions // Physical Review B. - 2005. - 71(18). - 184111.
[37] Tien, C., Charnaya, E.V., Wang, W., Kumzerov, Y.A., Michel, D. Possible liquid-liquid transition of gallium confined in opal // Physical Review B. - 2006. - 74(2). - 024116.
[38] Carvajal Jara, D.A., Fontana Michelon, M., Antonelli, A., de Koning, M. Theoretical evidence for a first-order liquid-liquid phase transition in gallium // The Journal of Chemical Physics. - 2009. - 130(22). - 221101.
[39] Zu, F.-Q. Temperature-Induced Liquid-Liquid Transition in Metallic Melts: A Brief Review on the New Physical Phenomenon // Metals. - 2015. - 5(1). - 395-417.
[40] Yu, Q., Wang, X.D., Su, Y., Cao, Q.P., Ren, Y., Zhang, D.X., Jiang, J.Z. Liquid-to-liquid crossover in the GaIn eutectic alloy // Physical Review B. - 2017. - 95(22). - 224203.
[41] Yu, Q., Su, Y., Wang, X., Ståhl, K., Glazyrin, K., Liermann, H., Franz, H., Cao, Q., Zhang, D., Jiang, J. Structural evolution in liquid GaIn eutectic alloy under high temperature and pressure // Journal of Applied Physics. - 2019. - 126(1). - 015902.
[42] Yu, Q., Ahmad, A.S., Ståhl, K., Wang, X.D., Su, Y., Glazyrin, K., Liermann, H.P., Franz, H., Cao, Q.P., Zhang, D.X., Jiang, J.Z. Pressure-induced structural change in liquid GaIn eutectic alloy // Scientific Reports. - 2017. - 7. - 1139.
[43] Bosio, L., Cortes, R., Copley, J.R.D., Teuchert, W.D., Lefebvre, J. Phonons in metastable beta gallium: neutron scattering measurements // Journal of Physics F: Metal Physics. - 1981. - 11(11). - 2261.
[44] Lee, M.K., Tien, C., Charnaya, E.V., Sheu, H.S., Kumzerov, Y.A. Structural variations in nanosized confined gallium // Physics Letters, Section A: General, Atomic and Solid State Physics. - 2010. - 374(13-14). - 1570-1573.
[45] Charnaya, E.V., Tien, C., Lee, M.K., Kumzerov, Y.A. Slowdown of self-diffusion induced by partial freezing in confined liquid indium // Physical Review B. - 2007. - 75(21). - 212202.

[46] Tien, C., Charnaya, E.V., Lee, M.-K., Kumzerov, Y.A. Influence of pore size on the Knight shift in liquid tin and mercury in a confined geometry // Journal of Physics: Condensed Matter. - 2007. - 19(10). - 106217.
[47] Charnaya, E.V., Tien, C., Wang, W., Lee, M.K., Michel, D., Yaskov, D., Sun, S.Y., Kumzerov, Y.A. Atomic mobility in liquid gallium under nanoconfinement // Physical Review B. - 2005. - 72(3). - 035406.
[48] Podorozhkin, D.Y., Charnaya, E.V., Lee, M.K., Chang, L.-J., Haase, J., Michel, D., Kumzerov, Y.A., Fokin, A.V. Diffusion slowdown in the nanostructured liquid Ga-Sn alloy // ANNALEN DER PHYSIK. - 2015. - 527(3-4). - 248-253.
[49] Charnaya, E.V., Tien, C., Lee, M.K., Kumzerov, Y.A. Atomic mobility in nanostructured liquid Ga–In alloy // Journal of Physics: Condensed Matter. - 2010. - 22(19). - 195108.
[50] AG, G.M., Galinstan Safety Data Sheet, 2011.
[51] Knoblauch, M., Hibberd, J.M., Gray, J.C., Bel, A.J.E.v. A galinstan expansion femtosyringe for microinjection of eukaryotic organelles and prokaryotes // Nat. Biotechnol. - 1999. - 17. - 906-909.
[52] Gerald, A.S.F., "Mercury relay," U.S. Patent 1773036, Aug. 12, 1930, 1930.
[53] Fleitman, A.H., Weeks, J.R. Mercury as a nuclear coolant // Nuclear Engineering and Design. - 1971. - 16(3). - 266-278.
[54] Clampitt, R., Jefferies, D.K. Miniature ion sources for analytical instruments // Nuclear Instruments and Methods. - 1978. - 149(1). - 739-742.
[55] Cao, A., Yuen, P., Lin, L. Microrelays With Bidirectional Electrothermal Electromagnetic Actuators and Liquid Metal Wetted Contacts // Journal of Microelectromechanical Systems. - 2007. - 16(3). - 700-708.
[56] Shaikh, K.A., Li, S., Liu, C. Development of a Latchable Microvalve Employing a Low-Melting-Temperature Metal Alloy // Journal of Microelectromechanical Systems. - 2008. - 17(5). - 1195-1203.
[57] Sen, P., Kim, C.J. A Fast Liquid-Metal Droplet Microswitch Using EWOD-Driven Contact-Line Sliding // Journal of Microelectromechanical Systems. - 2009. - 18(1). - 174-185.
[58] Sen, P., Kim, C.J. A Liquid–Solid Direct Contact Low-Loss RF Micro Switch // Journal of Microelectromechanical Systems. - 2009. - 18(5). - 990-997.
[59] Weber, M., Klemm, A., Kimmich, R. Rayleigh-Bénard Percolation Transition Study of Thermal Convection in Porous Media: Numerical Simulation and NMR Experiments // Physical Review Letters. - 2001. - 86(19). - 4302-4305.
[60] Charnaya, E.V., Loeser, T., Michel, D., Tien, C., Yaskov, D., Kumzerov, Y.A. Spin-Lattice Relaxation Enhancement in Liquid Gallium Confined within Nanoporous Matrices // Physical Review Letters. - 2002. - 88(9). - 097602.
[61] Nefedov, D., Antonenko, A., Podorozhkin, D., Uskov, A., Charnaya, E., Kumzerov, Y., Fokin, A., Samoilovich, M., Bugaev, A. Atomic mobility in a ternary liquid Ga–In–Sn eutectic alloy // Physics of the Solid State. - 2017. - 59(2). - 351-356.
[62] Carrington, A., Luckhurst, G.R. Electron spin resonance line widths of transition metal ions in solution. Relaxation through zero-field splitting // Molecular Physics. - 1964. - 8(2). - 125-132.
[63] Rubinstein, M., Baram, A., Luz, Z. Electronic and nuclear relaxation in solutions of transition metal ions with spin S=3/2 and 5/2 // Molecular Physics. - 1971. - 20(1). - 67-80.
[64] Baram, A., Luz, Z., Alexander, S. Resonance line shapes for semi-integer spins in liquids // The Journal of Chemical Physics. - 1973. - 58(10). - 4558-4564.
[65] Poupko, R., Baram, A., Luz, Z. Dynamic frequency shift in the E.S.R. spectra of transition metal ions // Molecular Physics. - 1974. - 27(5). - 1345-1357.
[66] Alexander, S., Luz, Z., Naor, Y., Poupko, R. Magnetic resonance lineshape in the presence of slow motion // Molecular Physics. - 1977. - 33(4). - 1119-1130.
[67] Werbelow, L., London, R.E. Dynamic frequency shift // Concepts Magn. Reson. - 1996. - 8(5). - 325-338.
[68] Tromp, R.H., de Bleijser, J., Leyte, J.C. Nuclear magnetic dynamic shift in an isotropic system // Chemical Physics Letters. - 1990. - 175(6). - 568-574.
[69] Westlund, P.-O., Wennerström, H. NMR lineshapes of I = 52 and I = 72 nuclei. Chemical exchange effects and dynamic shifts // Journal of Magnetic Resonance (1969). - 1982. - 50(3). - 451-466.
[70] Eliav, U., Shinar, H., Navon, G. An observation of 23Na NMR triple-quantum dynamic shift in solution // Journal of Magnetic Resonance (1969). - 1991. - 94(2). - 439-444.
[71] Marshall, A.G., Wang, T.C.L., Cottrell, C.E., Werbelow, L.G. First experimental demonstration of NMR dynamic frequency shifts: dispersion versus absorption (DISPA) line shape analysis of sodium-23

in aqueous sodium laurate/lauric acid solution // Journal of the American Chemical Society. - 1982. - 104(26). - 7665-7666.
[72] Shekar, S.C., Tang, J.A., Jerschow, A. Dynamics of I = 3\2 nuclei in isotropic slow motion, anisotropic and partially ordered phases // Concepts in Magnetic Resonance Part A. - 2010. - 36A(6). - 362-387.
[73] Kurkiewicz, T., Thrippleton, M.J., Wimperis, S. Second-order quadrupolar shifts as an NMR probe of fast molecular-scale dynamics in solids // Chemical Physics Letters. - 2009. - 467(4). - 412-416.
[74] Nefedov, D.Y., Charnaya, E.V., Uskov, A.V., Podorozhkin, D.Y., Antonenko, A.O., Kumzerov, Y.A. Possible liquid-liquid transition in a Ga–In melt introduced into an opal matrix // Physics of the Solid State. - 2019. - 61(1). - 169-173.
[75] Nefedov, D.Y., Podorozhkin, D.Y., Charnaya, E.V., Uskov, A.V., Haase, J., Kumzerov, Y.A., Fokin, A.V. Liquid-liquid transition in supercooled gallium alloys under nanoconfinement // Journal of Physics Condensed Matter. - 2019. - 31(25). - 255101.
[76] Nefedov, D.Y., Charnaya, E.V., Uskov, A.V., Antonenko, A.O., Podorozhkin, D.Y., Kumzerov, Y.A., Fokin, A.V. Atomic mobility in the crystal phase of a nanostructured Ga-In alloy with β-Ga structure // Physics of the Solid State. - 2021. - 63(10). - 1675-1679.
[77] Nefedov, D.Y., Charnaya, E.V., Uskov, A.V., Antonenko, A.O., Podorozhkin, D.Y., Haase, J., Kumzerov, Y.A., Fokin, A.V. Stabilization of β-Ga Structure in Nanostructured Ga–In Alloy // Applied Magnetic Resonance. - 2021. - 52. - 1721-1727.
[78] Uskov, A.V., Nefedov, D.Y., Charnaya, E.V., Podorozhkin, D.Y., Antonenko, A.O., Kumzerov, Y., Fokin, A., Bugaev, A. Dynamic shift of NMR lines in a nanostructured Ga-In-Sn melt // Physics of the Solid State. - 2017. - 59(12). - 2452-2456.
[79] Knight, W.D. Nuclear Magnetic Resonance Shift in Metals // Phys. Rev. - 1949. - 76(8). - 1259-1260.
[80] Slikter, Ch.P., Korst, N.N., Provotorov, B.N., Stepanov, A.P. Fundamentals of the theory of magnetic Resonance, - Mir, 1981.
[81] Mikushev, V.M., Charnaya, E.V. Nuclear Magnetic Resonance in solids, - Autonomous Non-Profit Organization " St. Petersburg University Press ", 1995.
[82] Charnaya, E.V., Michel, D., Tien, C., Kumzerov, Y.A., Yaskov, D. The Knight shift in liquid gallium confined within porous glasses and opals // Journal of Physics Condensed Matter. - 2003. - 15. - 5469-5477.
[83] Nagaev, É.L. Small metal particles // Soviet Physics Uspekhi. - 1992. - 35(9). - 747.
[84] Slichter, C.P. The Knight shift—a powerful probe of condensed-matter systems // Philosophical Magazine B. - 1999. - 79(9). - 1253-1261.
[85] Tong, Y.Y., Wieckowski, A., Oldfield, E. NMR of Electrocatalysts // The Journal of Physical Chemistry B. - 2002. - 106(10). - 2434-2446.
[86] Makowka, C.D., Slichter, C.P., Sinfelt, J.H. NMR of platinum catalysts: Double NMR of chemisorbed carbon monoxide and a model for the platinum NMR line shape // Physical Review B. - 1985. - 31(9). - 5663-5679.
[87] Vuissoz, P.A., Yonezawa, T., Yang, D., Kiwi, J., van der Klink, J.J. 103Rh NMR in small rhodium particles // Chemical Physics Letters. - 1997. - 264(3). - 366-370.
[88] Bercier, J.J., Jirousek, M., Graetzel, M., Van der Klink, J.J. Evidence from NMR for temperature-dependent Bardeen-Friedel oscillations in nanometre-sized silver particles // Journal of Physics: Condensed Matter. - 1993. - 5(44). - L571.
[89] Vuissoz, P.A., Ansermet, J.P., Wieckowski, A. Probing by NMR the Effect of Surface Charges on the Chemisorption Bond // Physical Review Letters. - 1999. - 83(12). - 2457-2460.
[90] Tong, Y.Y., Martin, G.A., Van der Klink, J.J. 195Pt NMR observation of local density of states enhancement on alkali-promoted Pt catalyst surfaces // Journal of Physics: Condensed Matter. - 1994. - 6(36). - L533.
[91] Charles, R.J., Harrison, W.A. Size Effect in Nuclear Magnetic Resonance // Physical Review Letters. - 1963. - 11(2). - 75-77.
[92] Williams, M.J., Edwards, P.P., Tunstall, D.P. Probing the electronic structure of small copper particles: 63Cu NMR at 1.5 K // Faraday Discussions. - 1991. - 92. - 199-215.
[93] Ido, M., Hoshino, R. Surface Effect on NMR of Fine Copper Particles // Journal of the Physical Society of Japan. - 1974. - 36(5). - 1325-1329.
[94] Charnaya, E.V., Tien, C., Kumzerov, Y.A., Fokin, A.V. Influence of confined geometry on nuclear spin relaxation and self-diffusion in liquid indium // Physical Review B. - 2004. - 70(5). - 052201.

[95] Podorozhkin, D.Y., Charnaya, E.V., Michel, D., Haase, J., Tien, C., Lee, M.K., Chang, L.J., Kumzerov, Y.A. Influence of dimensional effects on the Knight shift of NMR lines in a gallium-indium alloy // Physics of the Solid State. - 2012. - 54(5). - 1035-1038.
[96] Ruthven, D.M., Kärger, J., Theodorou, D.N. Diffusion in nanoporous materials, - John Wiley & Sons, 2012.
[97] Kärger, J., Ruthven, D.M. Diffusion in zeolites and other microporous solids, - Wiley New York, 1992.
[98] Konrad, H., Weissmüller, J., Birringer, R., Karmonik, C., Gleiter, H. Kinetics of gallium films confined at grain boundaries // Physical Review B. - 1998. - 58(4). - 2142-2149.
[99] Hubbard, P.S. Nonexponential Nuclear Magnetic Relaxation by Quadrupole Interactions // The Journal of Chemical Physics. - 1970. - 53(3). - 985-987.
[100] Bosse, J., Quitmann, D., Wetzel, C. Mode-coupling theory of field-gradient correlation functions: The quadrupolar relaxation rate in liquids // Phys. Rev. A. - 1983. - 28(4). - 2459-2473.
[101] Abraham, A. Nuclear Magnetism, - Yoyo Media, (Moscow, 1963), 2013.
[102] Suzuki, K., Uemura, O. Knight shift, magnetic susceptibility and electrical resistivity of pure gallium and gallium-indium eutectic alloy in the normal and the supercooled liquid state // Journal of Physics and Chemistry of Solids. - 1971. - 32(8). - 1801-1810.
[103] Baskes, M.I., Chen, S.P., Cherne, F.J. Atomistic model of gallium // Physical Review B. - 2002. - 66(10). - 104107.
[104] Cadien, A., Hu, Q.Y., Meng, Y., Cheng, Y.Q., Chen, M.W., Shu, J.F., Mao, H.K., Sheng, H.W. First-Order Liquid-Liquid Phase Transition in Cerium // Physical Review Letters. - 2013. - 110(12). - 125503.
[105] Wei, S., Yang, F., Bednarcik, J., Kaban, I., Shuleshova, O., Meyer, A., Busch, R. Liquid–liquid transition in a strong bulk metallic glass-forming liquid // Nat Commun. - 2013. - 4. -.
[106] Stolpe, M., Jonas, I., Wei, S., Evenson, Z., Hembree, W., Yang, F., Meyer, A., Busch, R. Structural changes during a liquid-liquid transition in the deeply undercooled Zr58.5Cu15.6Ni12.8Al10.3Nb2.8 bulk metallic glass forming melt // Physical Review B. - 2016. - 93(1). - 014201.
[107] Xu, W., Sandor, M.T., Yu, Y., Ke, H.-B., Zhang, H.-P., Li, M.-Z., Wang, W.-H., Liu, L., Wu, Y. Evidence of liquid-liquid transition in glass-forming La50Al35Ni15 melt above liquidus temperature // Nature Communications. - 2015. - 6. - 7696.
[108] Bogomolov, V., Kurdyukov, D., Parfenyeva, L., Prokofiev, A., Samoilovich, S., Smirnov, I., Ezhovsky, A., Mukha, Y., Miserek, H. Features of thermal conductivity of synthetic opals // Physics of the Solid State. - 1997. - 39(2). - 392-398.
[109] Harutyunyan, L., Bogomolov, V., Kartenko, N., Kurdyukov, D., Popov, V., Prokofiev, A., Smirnov, I., Sharenkova, N. Thermal conductivity of a new type of medium --- nanocomposites with regular structure: PbSe in opal pores // Physics of the Solid State. - 1997. - 39(3). - 586-590.
[110] Bogomolov, V., Kartenko, N., Parfenyeva, L., Prokofiev, A., Smirnov, I., Miserek, H., Mukha, Y., Ezhovsky, A. Thermal conductivity of three-dimensional regular structures of crystalline and amorphous selenium introduced into the pores of synthetic opal // Physics of the Solid State. - 1998. - 40(3). - 573-576.
[111] Anderson, T.J., Ansara, I. The Ga-In (gallium-indium) system // Journal of phase equilibria. - 1991. - 12(1). - 64-72.
[112] Pirozerskii, A.L., Charnaya, E.V., Lee, M.K., Chang, L.J., Nedbai, A.I., Kumzerov, Y.A., Fokin, A.V., Samoilovich, M.I., Lebedeva, E.L., Bugaev, A.S. Acoustic and NMR investigations of melting and crystallization of indium-gallium alloys in pores of synthetic opal matrices // Acoustical Physics. - 2016. - 62(3). - 306-312.
[113] Unruh, K.M., Huber, T.E., Huber, C.A. Melting and freezing behavior of indium metal in porous glasses // Physical Review B. - 1993. - 48(12). - 9021-9027.
[114] Borisov, B.F., Charnaya, E.V., Plotnikov, P.G., Hoffmann, W.D., Michel, D., Kumzerov, Y.A., Tien, C., Wur, C.S. Solidification and melting of mercury in a porous glass as studied by NMR and acoustic techniques // Physical Review B. - 1998. - 58(9). - 5329-5335.
[115] Pirozerskii, A.L., Charnaya, E.V., Latysheva, E.N., Nedbai, A.I., Kumzerov, Y.A., Bugaev, A.S. Acoustic studies of melting and crystallization of indium-gallium alloy in porous glass // Acoustical Physics. - 2011. - 57. - 637-641.
[116] Lu, H., Shuai, J., Meng, X. Size-Dependent Eutectic Temperature of Ag-Pb Alloy Nanoparticles // Journal of Nanoscience and Nanotechnology. - 2013. - 13(2). - 1480-1483.

[117] Yasuda, H., Mori, H. Phase diagrams in nanometer-sized alloy systems // Journal of Crystal Growth. - 2002. - 237-239. - 234-238.
[118] Liu, S., Sweatman, K., McDonald, S., Nogita, K. Ga-Based Alloys in Microelectronic Interconnects: A Review // Materials. - 2018. - 11(8). - 1384.
[119] Chen, C., Lee, J.-G., Arakawa, K., Mori, H. Quantitative analysis on size dependence of eutectic temperature of alloy nanoparticles in the Ag–Pb system // Applied Physics Letters. - 2011. - 98(8). - 083108.
[120] Charnaya, E.V., Tien, C., Lee, M.K., Kumzerov, Y.A. Superconductivity and structure of gallium under nanoconfinement // Journal of Physics Condensed Matter. - 2009. - 21. - 455304.
[121] Tien, C., Wur, C.S., Lin, K.J., Hwang, J.S., Charnaya, E.V., Kumzerov, Y.A. Properties of gallium in porous glass // Physical Review B. - 1996. - 54(17). - 11880-11882.
[122] Giordano, V.M., Monaco, G. Inelastic x-ray scattering study of liquid Ga: Implications for the short-range order // Physical Review B. - 2011. - 84(5). - 052201.
[123] Bizid, A., Defrain, A., Bellissent, R., Tourand, G. Neutron diffraction investigation and structural model for liquid gallium from room temperature up to 1303 K // J Phys (Paris). - 1978. - 39(5). - 554-560.
[124] Kerlin, A.L., Clark, W.G. Nuclear magnetic resonance and relaxation in liquid Ga and GaSb // Physical Review B. - 1975. - 12(9). - 3533-3546.
[125] Segel, S.L., Heyding, R.D., Seymour, E.F.W. Nuclear Electric Quadrupole Resonance in β-Gallium // Physical Review Letters. - 1972. - 28(15). - 970-971.
[126] Valič, M.I., Williams, D.L. A nuclear magnetic resonance study of gallium single crystals—I: Low field spectra // Journal of Physics and Chemistry of Solids. - 1969. - 30(10). - 2337-2348.
[127] Di Cicco, A. Phase Transitions in Confined Gallium Droplets // Physical Review Letters. - 1998. - 81(14). - 2942-2945.
[128] Uskov, A.V., Nefedov, D.Y., Charnaya, E.V., Haase, J., Michel, D., Kumzerov, Y.A., Fokin, A.V., Bugaev, A.S. Polymorphism of Metallic Sodium under Nanoconfinement // Nano Letters. - 2016. - 16(1). - 791-794.
[129] Taneja, P., Banerjee, R., Ayyub, P., Dey, G.K. Observation of a hexagonal (4H) phase in nanocrystalline silver // Physical Review B. - 2001. - 64(3). - 033405.
[130] Ayyub, P., Palkar, V.R., Chattopadhyay, S., Multani, M. Effect of crystal size reduction on lattice symmetry and cooperative properties // Physical Review B. - 1995. - 51(9). - 6135-6138.
[131] Sharma, A., Varshney, M., Saraswat, H., Chaudhary, S., Parkash, J., Shin, H.-J., Chae, K.-H., Won, S.-O. Nano-structured phases of gallium oxide (GaOOH, α-Ga2O3, β-Ga2O3, γ-Ga2O3, δ-Ga2O3, and ε-Ga2O3): fabrication, structural, and electronic structure investigations // International Nano Letters. - 2020. - 10. - 71-79.
[132] Knight, A.W., Kalugin, N.G., Coker, E., Ilgen, A.G. Water properties under nano-scale confinement // Scientific Reports. - 2019. - 9. - 8246.
[133] Titman, J.M. Nuclear magnetic resonance in liquid metals and alloys // Physics Reports. - 1977. - 33(1). - 1-50.
[134] Tokuhiro, T. Nuclear quadrupole relaxation of spin-32 // Journal of Magnetic Resonance (1969). - 1988. - 76(1). - 22-29.
[135] Mehrer, H. Diffusion in solids: fundamentals, methods, materials, diffusion-controlled processes, - Springer Science & Business Media, 2007.
[136] Carter, A., Wilson, C. Self diffusion in gallium // Journal of Physics D: Applied Physics. - 1968. - 1(4). - 515.
[137] Evans, D.S., Prince, A. Thermal analysis of Ga-In-Sn system // Metal Science. - 1978. - 12(9). - 411-414.
[138] Speckbrock, G., Kamitz, S., Alt, M., Schmitt, H., Low melting gallium, indium, and tin eutectic alloys, and thermometers employing same, U.S. Patent No. 6,019,509, 2000.
[139] Liu, T., Sen, P., Kim, C.J. Characterization of Nontoxic Liquid-Metal Alloy Galinstan for Applications in Microdevices // Journal of Microelectromechanical Systems. - 2012. - 21(2). - 443-450.
[140] Abragam, A. The principles of nuclear magnetism, - Oxford university press, 1961.
[141] Podorozhkin, D.Y., Charnaya, E.V., Michel, D., Haase, J., Tien, C., Lee, M.K., Chang, L.J., Kumzerov, Y.A. Influence of size effects on the Knight shift of NMR lines in the gallium-indium alloy // Physics of the Solid State. - 2012. - 54(5). - 1104-1107.